INAUGURAL - DISSERTATION

zur

Erlangung der Doktorwürde

der

Naturwissenschaftlich - Mathematischen

Gesamtfakultät

der Ruprecht - Karls - Universität

Heidelberg

vorgelegt von

M.Sc. Julia Herz

aus Offenbach

Tag der mündlichen Prüfung: 24. Juli 2015

Ultrafast Triplet Formation in N-Substituted Pentacene Derivatives

Gutachter: Prof. Dr. Marcus Motzkus

Prof. Dr. Uwe H. F. Bunz

Für meinen Vater

Contents

Abstract

Higher members of the acene molecule class, like the benchmark compound pentacene, are known to undergo singlet fission (SF). This extraordinary process is attractive regarding its ability of boosting quantum efficiencies in photovoltaic cells and overcoming the Shockley-Queisser limit of single junction devices. There is consensus that in pentacene SF proceeds on an ultrafast timescale (<100 fs), but the details of the process are still subject of debate. Within this work, pump-probe as well as pump-depletion-probe techniques were used in combination with rate model simulations to disentangle the initial steps of SF. In particular, the effect of nitrogen atoms, which were incorporated into the pentacene backbone, on the photoinduced dynamics of TIPS-pentacene was studied. These solution-processable aza-derivatives, called Diaza-TIPS-pentacene and Tetraaza-TIPS-pentacene, are great building blocks for the design of new architectures with optimized electronic properties and represent promising candidates for their use in photovoltaic devices. Measurements in the visible as well as in the near-infrared spectral region were performed in order to get a complete picture of the triplet manifold. This required the design and implementation of a new experimental setup. By applying global target analyses and numerical simulations, a detailed kinetic model of the excited state dynamics of all investigated materials could be established. The experimental observations indicate a participation of the intermediate coupled triplet pair state ^{1}TT, which has become a hot topic regarding its role in mediating SF. The nitrogen substitution in the heteroacenes not only accelerates the formation of the ^{1}TT state compared to TIPS-pentacene, but also the population of the final triplet state T_1 via the ^{1}TT state, implying higher quantum efficiencies. The absorption of all relevant exited states were successfully assigned with regard to their spectral occurence.

1

Kurzzusammenfassung

Die höheren Acene, wie auch das Referenzsystem Pentacen, sind zu einem Prozess befähigt, in welchem unter Einsatz von einem Photon zwei Triplett-Spezies gebildet werden können. Dieser außerordentliche Prozess (engl.: singlet fission (SF)) ist besonders attraktiv im Hinblick auf eine potenzielle Effizienzsteigerung in photovoltaischen Zellen, insbesondere um die Shockley-Queisser Grenze von Solarzellen zu überschreiten. Es herrscht Einigkeit darüber, dass SF in Pentacen auf einer ultraschnellen Zeitskala abläuft (<100 fs), die Details des Prozesses sind jedoch Gegenstand aktueller Diskussion. In dieser Arbeit werden sowohl Pump-Probe als auch Pump-Depletion-Probe Techniken in Kombination mit Ratenmodell-Simulationen angewandt, um die primären Schritte des SF Mechanismus aufzuklären. Speziell wird der Einfluss von Stickstoffatomen, die in das Pentacen-Rückgrat eingebaut wurden, auf die photoinduzierten Dynamiken hin untersucht. Diese löslichen Aza-Derivate (Diaza-TIPS-pentacen and Tetraaza-TIPS-pentacen) bilden hervorragende Grundgerüste für die Konstruktion neuer Materialien mit optimierten elektronischen Eigenschaften und stellen vielversprechende Kandidaten hinsichtlich deren Einsatz in photovoltaischen Zellen dar. Ein neuer Messplatz wurde entwickelt, um Messungen im sichtbaren, sowie im nahinfraroten Spektralbereich durchführen und hierdurch Informationen über die beteiligten Triplettübergänge erhalten zu können. Durch globale Anpassung und numerische Simulation der Messdaten konnte ein detailliertes kinetisches Modell der Dynamiken des angeregten Zustands von allen untersuchten Materialien aufgestellt werden. Die experimentellen Beobachtungen deuten auf eine Beteiligung des kontrovers diskutierten Zwischenzustands ^1TT bei der Tripletterzeugung durch SF hin. Die Stickstoffsubstitution in den Heteroacenen beschleunigt nicht nur die Bildung des ^1TT Zustandes verglichen zu TIPS-Pentacen, sondern auch die Population des T_1 via ^1TT, was eine höhere Quantenausbeute impliziert. Die Absorption aller relevanter angeregter Zustände konnten bezüglich ihrer spektralen Lage erfolgreich zugeordnet werden.

Chapter 1

Introduction

The sun provides 7000 times more energy per day than we can use, in other words the solar energy absorbed by Earth every hour can meet the energy human civilization demands every year.[1] The challenge is now to harness this diffusive resource.
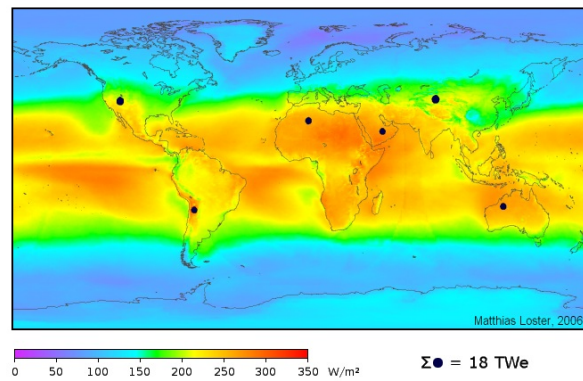

Figure 1.1: Solar irradiation that hits the Earth. Solar panels that cover the black areas could provide the total energy demand of the human civilization.[2]

In the map in Figure 1.1 the solar irradiation that reaches the Earth is presented and in particular the land area, which is required to supply the world's total energy consumption.[2] This is demostrated by the black cycles

that need to be hit by the sunlight in order to power the whole world. Installing solar cells with a conversion efficiency of only 8 % in these areas would produce (on average of solar irradiance, including nights and cloud coverage) 18 TW electrical power.[1] The development of photovoltaic technologies to achieve efficient devices is in the focus of research. State-of-the-art silicon based solar cells exhibit efficiencies of more than 25 %.[3] The drawback of the record-setting designs is their use of high-quality silicon crystals, which is expensive. Organic photovoltaics, though, promise large scale and low cost fabrication, i.e. expensive clean-room procedures are replaced by roll-to-roll processing. If organic solar cell devices would possess efficiencies comparable to other solar cell technologies, they could enable cheap, effective solutions to the solar industry. Organic solar cells have been subject of dramatic increases in performances and the power conversion efficiency has rapidly improved from 2 to over 11 % in the last decade.[4, 5] However, still higher efficiencies will be required for economic implementation on a large scale. In order to further push organic photovoltaics to operate more efficiently, the underlying physics on how the energy of light is converted into electricity are essential. A better understanding of the photophysical processes that govern the operation of organic photovoltaic devices paves the way for optimizing efficiencies. Above all, the vast pool of organic building blocks to develop new materials with tailored properties for the efficient harvesting of the solar spectrum in combination with favorable molecular properties opens new perspectives. Synthesis of new organic compounds to develop materials that show higher efficiencies by an increasing environmental stability is a key to conquer the industrial market of electronic devices. Acenes, which are linearly fused polycyclic aromatic hydrocarbons[6] have been used as hole transporters in thin-film transistors, emitters in light-emitting diodes and donor molecules in organic solar cells for the last years.[7–9] A major drawback of these acenes is, though, their low solubility in organic solvents in combination with low resistance against air and humidity. In 2001 Winkler et al. showed that the incorporation of nitrogen atoms in the acene backbone is a promising approach to produce stable electron transporting materials.[10] On the other hand, the introduction of bulky silyl side groups by Anthony

4

leads to solution processable materials (Tri-*iso*-propylsilyl-pentacene, TIPS-pentacene) with optimized intermolecular interactions.[11] A combination of both approaches, i.e. the introduction of heteroatoms in the pentacene backbone and bulky side groups was done by Bunz et *al.* in 2009.[12] This symmetrical Tetraaza-TIPS-pentacene is the most popular respresentative of the N-heteroacenes. It exhibits lowered frontier orbitals compared to TIPS-pentacene, which results in a changed electronic structure and hence an altered optical behavior.

Most notably, the higher members of the acene family are known to undergo singlet fission, a process where two charges are formed by investing just one photon.[13, 14] This extraordinary process is of particular interest since it has the potential to raise the quantum efficiency above 100 %.[15] As each created exciton contributes one electron to the photocurrent of a photovoltaic device, singlet fission is a key mechanism to improve the performance of organic photovoltaics. A schematic representation of the underlying idea of singlet fission is given in Figure 1.2.
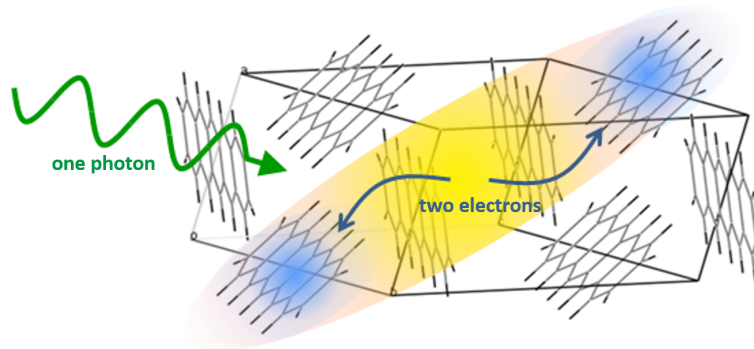
Figure 1.2: In singlet fission one single photon is used to excite a molecule, which interacts with another one creating two charges. Figure adapted from "Applied Physics SuperUROP Projects" by Prof. M. Baldo, MIT.

Singlet fission proceeds on an ultrafast time scale and the physics behind this process are still not well understood. In order to reveal the fate of the acene's excited states, the use of femtosecond time-resolved spectroscopy becomes essential. In particular, transient absorption spectroscopy is a pow-

erful tool to follow the rapid and efficient conversion of a photoexcited singlet into two triplet excitons. The evolution of the photo-induced dynamics can be directly monitored, where rising and decaying signal contributions are assigned to transitions between specific states. A global target analysis helps to further extract information from the two-dimensional data array by reducing the spectrally superimposed signals to several components with their according time constants. Measurements in the visible and near-infrared spectral region provide complementary information on the triplet manifold after photo-excitation. However, this technique is not able to completely explain all experimental obervations and more sophisticated methods, such as pump-depletion-probe, are necessary to disentangle the excited state dynamics of pentacene and its derivatives. The idea of this technique is to change the population after excitation by intercepting the normal relaxation pathway by an additional pulse. The changed population can in turn identify specific states of the energy flow network that are dependent on that additional pulse. Combining this two techniques, i.e. transient absorption and pump-depletion-probe spectroscopy with rate model simulations provides better understanding on how the triplet manifold is populated via singlet fission and furthermore reveal the origin of the observed excited state transitions. Of major significance is the question, if the new air-stable N-heteroacenes are able to perform singlet fission in a similar or even more efficient way compared to the reference coumpound TIPS-pentacene. Information about their relaxation networks allows for studying structure-function relationships, for instance the interplay between the singlet fission process and chemical modifications of TIPS-pentacene. This knowledge helps in a further step to modify special transitions on a molecular level and thus optimize efficiencies by eliminating loss channels to exceed the triplet quantum yield. The potential to enhance and direct the singlet fission mechanism in these new materials is of vital importance in prospect of the design of organic electronic devices.

Outline of this work

In **Chapter 2** the fundamental aspects and properties of organic materials are presented. The basic characteristics of excitons, which play the major role regarding the optical behavior are presented. All possible optical transitions that occur in organic molecules are shown and singlet fission as the most important process within this thesis is introduced. After having provided information on selected photovoltaic applications, the influence of heteroatoms on the electronic properties of pentacene is discussed. **Chapter 3** deals with the experimental methods that were used and implemented within this work. The newly developed transient absorption setup with probing wavelengths between 350-1100 nm is presented and the principle of pump-depletion-probe spectroscopy is elaborated. Additionally, experimental details and the underlying nonlinear processes are described. The investigated samples and how they were characterized is presented in **Chapter 4**. Together with their steady state spectra, the crystal structures of the samples as well as the thin-film preparation techniques are shown. In **Chapter 5** the experimental results are represented and thoroughly discussed. The interpretation of the experimental observations is supported by simulations and at the end a kinetic model of the excited state dynamics of all investigated compounds is established. **Chapter 6** concludes the gained insights into the relaxation network and gives an outlook on future experiments.

Chapter 2

Background

This chapter introduces the fundamental characteristics of organic materials in comparison with inorganic semiconductors. The background of conjugated systems is described and the nature of excitons as the most important quantity elaborated. After discussing the nature of singlet and triplet states, all optical transitions and the underlying photophysical processes (radiative and non-radiative) of conjugated molecules are presented. Singlet fission as the key process in boosting quantum efficiencies is introduced and several theoretical perspectives are discussed. Applications of singlet fission based organic photovoltaics and working principles of novel solar cell architectures are presented as a major motivation for the investigation of new materials. Finally, the effect of heteroatoms on the molecular properties of acenes is presented.

2.1   Organic Electronics

The potential advantage of solution processed organic semiconductors, such as high operating speed, low-cost, easy fabrication and large area flexible circuit, has been receiving a substantial and strongly increasing amount of attention and motivated many studies in this field.[16, 17] Applications related to organic electronics include three major fields, namely organic light emitting diodes (OLEDs), organic field effect transistors (OFETs) and or-

ganic photovoltaic cells (OPVs). The term 'organic' involves molecules that consist of a carbon network. They can be divided into two classes: small molecules (e.g. acenes) and macro molecules or polymers. In order to exhibit semiconducting properties they need to form π-bonds. When two carbon atoms are bond via hybridized orbitals, two different types of bonds exist, depending on their alignment with respect to the bonding direction. σ bonds are symmetrical with regard to the axis between the two nuclei and the electron density is therefore concentrated in the intervening space between the carbon atom centers. These bondings determine the structure of the molecule, however, the electrons are strongly bound and do generally not participate in optical processes. π bonds are constructed from electrons in unhybridized orbitals that are oriented perpendicular to the the axis between the carbon nuclei and the electrons are delocalized. These π-bonds are responsible for the conjugation of a molecule and thus for the strong interaction with electromagnetic radiation in the visible spectral region. The two types of bonds differ significantly by means of their strength. Since the spatial overlap of orbitals with σ-bonding is larger than for the π type, the latter is a lot weaker and the consequently the electronic levels are higher in energy compared to the former one.

By adding more sp_2-hybridized carbon atoms to the bonding network, the π-orbitals delocalize further and form orbitals that can have significant spatial extent. The resulting molecular orbitals (formed by the carbon atomic orbitals) are referred to as bonding and antibonding, also known as highest occupied molecular orbital (HOMO) and lowest unoccupied molecular orbital (LUMO), respectively as shown in Figure 2.1. The energy difference between these states is called *optical gap* and determines the lowest optical transition. Even though an electron is promoted from the bonding to an anti-bonding state via absorption of a photon, the destabilizing effect is not sufficient to overcome the total bonding energy of the remaining σ and π bonds of the carbon-network. These considerations address the conditions within one molecule, when carbon atoms fuse together forming a conjugated system. Moving on to the case where several molecules interact with each other as in a molecular assembly, different forces have to be taken into account. Here,

the molecular bonding occurs via weak intermolecular van-der-Waals bonds, resulting in electronic properties that are largely determined by the molecules themselves. The role of the weak forces is only to hold the organic molecules together within the solid. This is in contrast to crystalline inorganic semiconductors where strong covalent/ionic interatomic bondings throughout the material lead to an occupied valence band separated by an empty conduction band. In that sense, an analogy between the valence band and the HOMO and the conduction band and LUMO is possible, however, the band widths of the formed HOMO and LUMO levels are rather low.
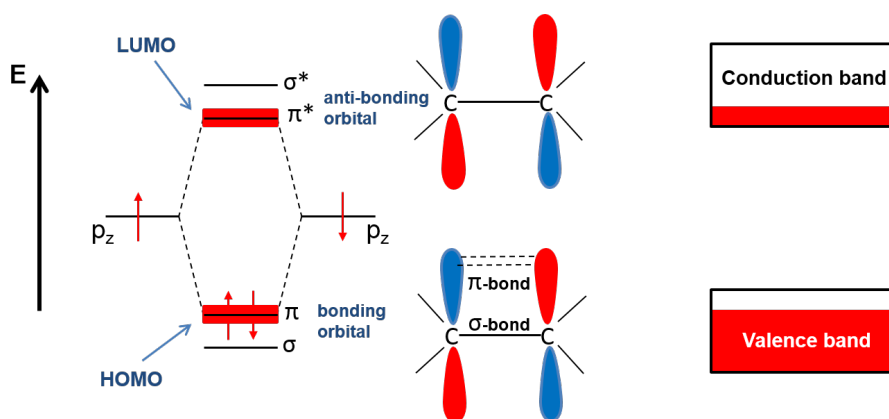

Figure 2.1: Adjacent overlapping p_z orbitals form into bonding (occupied) and anti-bonding (empty) π-states. In the solid state, the resulting HOMO and LUMO orbitals take the form of bands (left), analogous to the valence and conduction band of inorganic semiconductors (right), however, their bandwidths are significantly smaller.

The larger width of the energy bands in inorganic semiconductors has also an impact on the charge transport within the material. Here, transport takes place in a band and the charges are free in form of electrons and holes. The mobility of charge in organic materials is defined by a hopping mechanism of positive and negative polarons. Above all, organic semicondutors form bound electron hole pairs (Frenkel type excitons), which exhibit large binding energies and play the major role in relation to their optical behavior. In their inorganic counterparts excitons (Wannier-Mott type) possess small binding energies and are rarely observed at room temperature.

2.2 Excitons

In a simplified picture, absorption of a photon at the optical band gap causes an electron to occupy the LUMO, while leaving behind a hole in the HOMO. Due to their opposite charges, the electron and hole experience appreciable coulombic attraction. The energy of the Coulomb coupling binds the charges to each other in space, resulting in an electrically-neutral bound state, called exciton.[18] Creation of an exciton involves a reorganization of intermolecular distances and partial polarization of the electronic configuration of the surrounding. In other words, the change of electron density leads to nuclear geometry shifts resulting in a reorganization energy that stabilizes the exciton with respect to ground state molecules. This energy varies in molecules with a different permittivity. For example, inorganic materials have higher permittivities and thus lower exciton stabilization energies, accompanied by stronger lattice interactions and more delocalized and mobile excitons. These Wannier-Mott excitons, which are found in densely packed media, are largely indistinguishable from free charges at room temperature. The atoms mask some of the electron-hole attraction and the excitons have a larger spatial extent as illustrated in Figure 2.2.
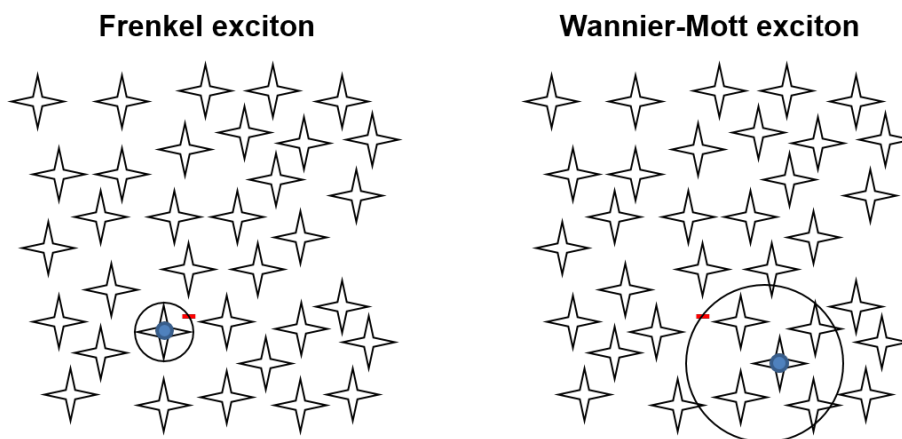

Figure 2.2: Spatial discrimination of a Frenkel exciton (left), which is localized on one molecule and a Wannier-Mott (right) exciton that is more spread out within the solid state network (adapted from Ref.[19]).

In organic materials, in contrast, the intermolecular interactions are much weaker and the exciton is localized at a single conjugated segment. This localization is due to the relatively low dielectric constant of organic molecules resulting in a strong electrostatic attraction between the opposite charges. The limiting case, where the hole and the electron residing on the same molecule is referred to as Frenkel exciton. The regime where the hole and the electron are localized several molecules away from each other, is termed a charge transfer exciton. However, when it comes to the solid state and both inter- and intramolecular coupling are relevant, these different regimes overlap. Hence, an unambiguous differentiation between a charge transfer state, a Frenkel exciton delocalized over a few molecules and a bound Wannier-Mott exciton is challenging.

2.2.1 Spin States

The spin plays an important role in determining the properties of excitons according to their optical activity. The overall spin of an exciton can be determined by the correlative arrangement of the electron spins in the respective orbitals. According to the Pauli exclusion principle, two electrons that occupy the same orbital must be paired, i.e. have opposite spins. Since spin angular momentum is a vectorial quantity and quantized, only two measurable orientations of the the spin are allowed with respect to the magnetic field. When an electron is promoted from the HOMO to the LUMO by absorption of a photon, it can either exhibit the same (parallel) or the opposite (paired) spin as the vacant electron, since they are occupying different orbitals now. Moreover, the spins can precess either in-phase (spins point in the same direction) or out-of-phase (spins point to opposite directions). This leads to four possible spin vector representations to describe a two particle system (see Figure 2.3). The corresponding spin quantum number S can be either 0 or 1. If S equals 0 there is just one possibility for the magnetic quantum number M_s (M_s=0). Thus, the S=0 state has a total angular momentum of zero and is called singlet state. For S=1 there exist three states with a total angular momentum of one and $M_s = (-1, 0, 1)$, which are collectively
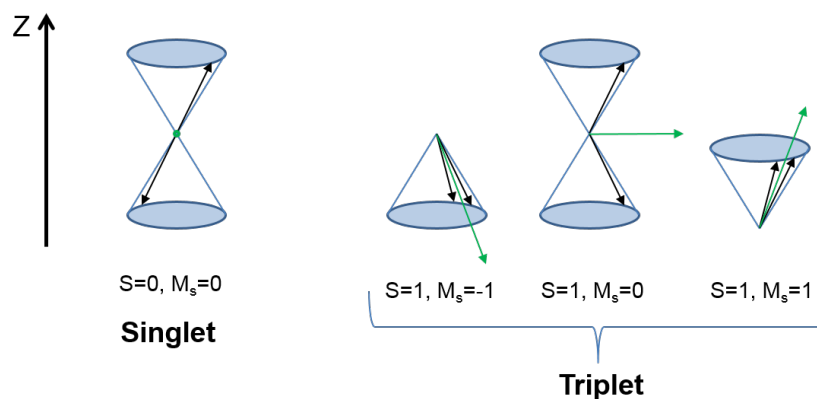
termed triplet state.

Figure 2.3: Vector based diagram of singlet (left) and triplet (right) spin configurations. The electron spins precess around a local magnetic field they experience in z-direction. The out-of-phase configuration results in a singlet state, while the spin vectors have to precess in-phase to yield a triplet state. (Figure according to Ref.[20]).

If we just take the Coulomb interactions between the two spin-half electrons that form the exciton into account, the four distinct spin states should be degenerate in energy. However, if we include the electron exchange energy, which is a consequence of the Pauli exclusion principle, the triplet state is stabilized in energy with respect to the singlet state. This can be explained by assuming that quantum mechanics requires that electrons of the same spin avoid approaching one another, but electrons of opposite spin have the tendency to stick to one another.[21] Accordingly, the electron-electron repulsion is reduced in the case of parallel spins and the energy gap between a singlet and a triplet state of the same electronic configuration is purely the result of electron exchange. As the dielectric constant is low in conjugated organic materials, we have to consider these interactions, which scale with the spatial overlap of the HOMO and LUMO electronic wavefunctions.[13] The result is a triplet state, which is about 0.7 eV below the singlet state in most conjugated polymers and can get even lower in energy for polyacenes.[22] This is important regarding the triplet generation in these materials. In particular,

the fact that for pentacene the singlet state is more than twice as high as the triplet state in energy has a substantial consequence on the singlet fission energetics, which will be discussed in section 2.4.1.
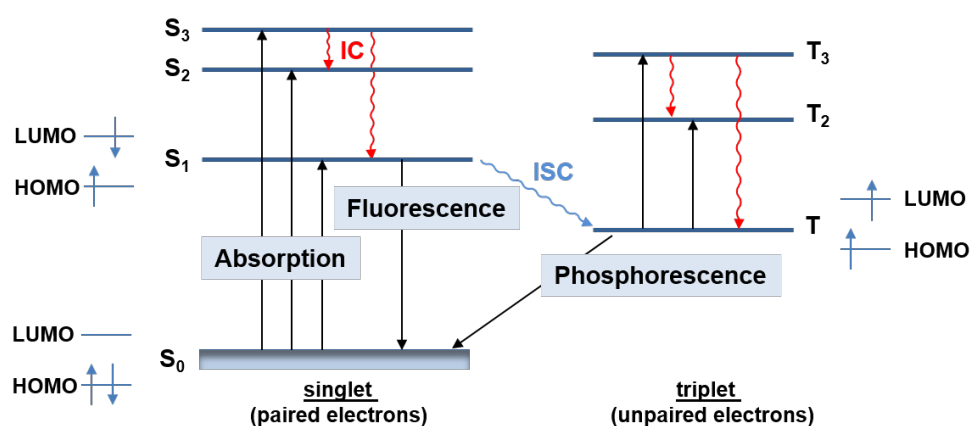
2.3 Optical Transitions

Figure 2.4: The Jablonski diagram illustrates schematically all possible optical transitions of a single conjugated molecule. IC=Internal Conversion (radiationless $S_n \to S_1$ transition), ISC=Intersystem Crossing (radiation-less $S_n \to T$). The corresponding spin states of the transitions are shown on the left and right side, respectively.

All possible optical transitions that occur in an organic molecule are presented in Figure 2.4 within a so called Jablonski diagram. These transitions are divided into radiative and non-radiative ones. The optical absorption promotes the molecule into an excited state. According to the Franck-Condon principle, this transition from the ground to the excited state must occur vertically. This principle provides a selection rule for the relative probability of vibronic transitions. It states that the most probable electronic transition will occur between those states exhibiting a similar nuclear configuration and vibrational momentum. Their vibrational wave functions have to overlap constructively, where the squared of the vibrational overlap integral is

called Franck-Condon factor. The larger this factor, the larger is the overlap of the wave functions and the more probable is the transition. Figure 2.5 shows a schematic representation of the Franck-Condon principle for a radiative transition from an initial ground (S_0) to a final electronic excited state (S_1).
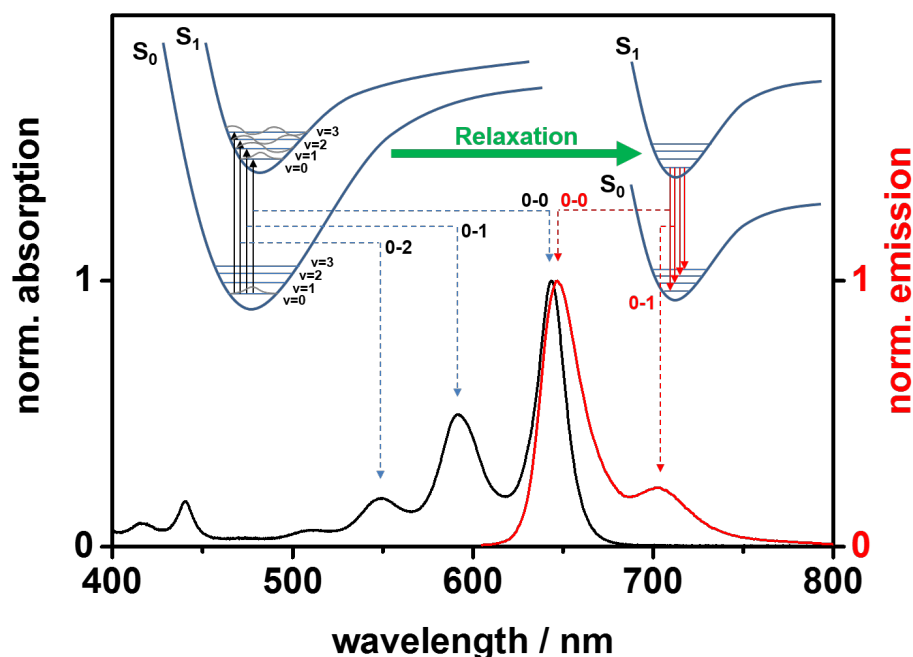

Figure 2.5: Absorption (black curve) and emission (red curve) spectra of TIPS-pentacene in toluene solution. The bands of the spectra correspond to the transitions shown in the potential curves of the respective S_0 and S_1 states. The electronic transitions are strongly coupled to a high vibrational mode resulting in a vibrational progression. The corresponding transitions are labeled by the vibrational indices. After relaxation to the lowest vibrational state v=0 in S_1, fluorescence is observed. The bands can again be related to the transitions of the respective vibrational levels in S_0. The energetic separation between the 0-0 peaks of absorption and emission bands is called Stokes-shift and related to the reorganization energy.

Since rigid aromatic hydrocarbons, such as pentacene, show only a very small vertical displacement of the potential energy curves, the v=0 $\rightarrow$ v=0 transition is most pronounced for both absorption and emission. This situation corresponds to an electronic orbital jump for which the overall bonding is similar for both states (S_0 and S_1) and accordingly their equilibrium geometries. There are several ways to redistribute the created excess energy in the excited state, which are summarized in Figure 2.6.
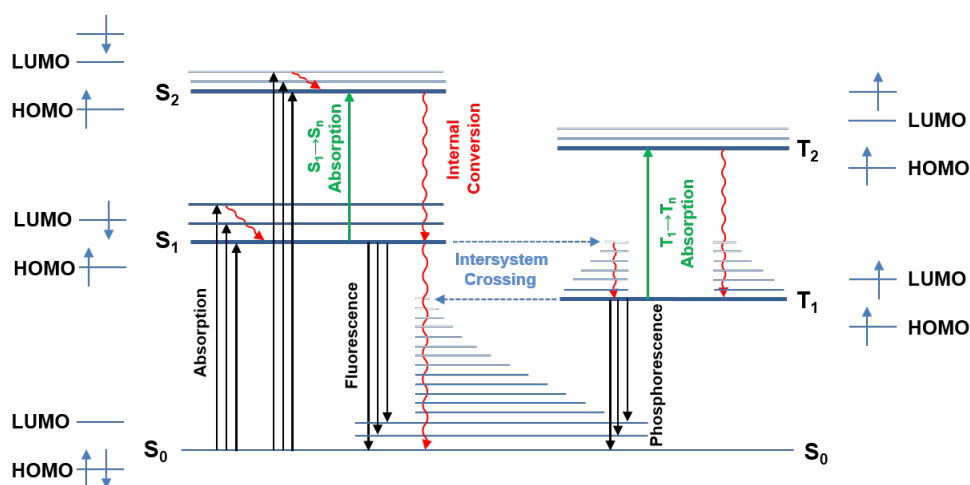

Figure 2.6: Detailed diagram of relevant energy levels including the associated vibrational sublevels in a single conjugated molecule. Absorption to higher states within one spin manifold is called excited state absorption (green arrows). These transitions are most relevant for time-resolved spectroscopy (transient absorption) since they provide insight into the underlying dynamics of a molecule.

The basic ideas for radiative and radiationless transitions are the same, namely a small change in the initial and final nuclear structure, which means that the wavefunctions of these states need to have significant overlap and energy conservation during the transition. Excitation of higher energy states generally results in deactivation to the lowest vibrationally excited state (internal conversion (IC)). IC is defined as the intrinsic radiationless decay of excited electronic states within a spin manifold.[23] As conjugated organic molecules possess closely-spaced electronically and vibrationally ex-

cited states, IC proceeds rapidly from any higher-lying state down to the vibrationally-relaxed lower-lying electronic excited state. The overall IC process is divided into two steps. In the first step, a horizontal (adiabatic), transition from the initially excited electronic state to a vibrationally-excited level of the final electronic state takes place (not shown in Figure 2.6). The subsequent relaxation to the lowest-lying vibrational level occurs along the potential energy curve of high-energy modes by simultaneous emission of multiple phonons.[20, 24] The rate of IC back to the ground state is much slower and fluorescence occurs from the lowest-lying singlet state (Kasha's rule). Accordingly, phosphorescence is also observed from the thermally equilibrated T_1 state, which represents the crucial process in OLEDs.[22] However, conservation of angular momentum implies that radiative decay of the triplet exciton to the singlet ground state is quantum mechanically forbidden. The appearance of phosphorescence requires a mixing of the singlet and triplet states, which can be realized by spin-orbit coupling. This coupling maintains a balance between the change in the angular momentum due to the orientation of the spin by a change in the orbital angular momentum. However, this interaction scales with the atomic number by the power of four (Z^4) and is thus mostly observed in molecules that contain heavy atoms. As a consequence of the spin-forbidden relaxation back to the ground state $T_1 \rightarrow S_0$, the lifetime of triplet excitons exceed the singlet one by orders of magnitude (fs-ns for singlets and ns-s for triplets). The radiationless transition between excited states of different spin is called intersystem crossing (ISC). Due to the small atomic numbers and large differences in reorganization energies (singlet vs. triplet) present in organic materials, the ISC rate is typically in the order of tens of ns.[20] Besides ISC, the spin of an exciton can also change by a process called singlet fission, which will be subject of the next section because of its particular importance.

2.4 Singlet Fission

In singlet fission (SF) one photon-generated singlet exciton shares its energy with a neighboring molecule in its ground state creating two triplet excitons residing on each chromophore in an overall spin allowed process (see Figure 2.7).[13, 14]
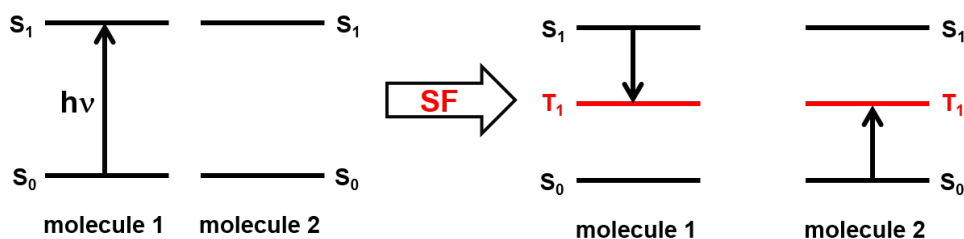

Figure 2.7: Schematic demonstration of the singlet fission process between two chromophores. One molecule is initially excited and a singlet exciton is created. It reacts with a neighbor molecule, which is in its ground state. The energy of the excitation is shared between them and one triplet exciton is formed on each molecule.

A general description of singlet fission that provides insight into the mechanism is presented in Equation 2.1 where S_1 is the singlet excitation state, S_0 the ground state, ^1TT the singlet-coupled correlated triplet pair and T_1 the relaxed triplet exciton. The initial S_0+S_1 state is converted into ^1TT and conservation of angular momentum requires that this pair of local triplet states is coherently coupled into a state of pure singlet character. This first spin-conserving step occurs extremely rapid and is mediated by electrostatic interactions. It represents the internal conversion aspect of SF. The formation of two individual triplet states includes decoherence and relaxation of the ^1TT state as well as diffusive processes. As these proceed relatively slow, the second step of the two artificially separated steps represents the intersystem crossing aspects of SF (see Figure 2.8).
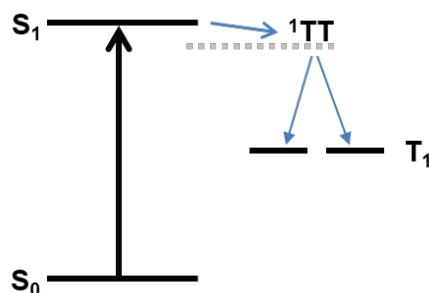
$$S_0 + S_1 \rightleftharpoons {}^1TT \rightleftharpoons T_1 + T_1 \tag{2.1}$$
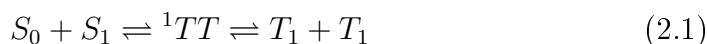
Figure 2.8: Low-lying electronic states that are involved in the singlet fission process. After photo-excitation of the S_1 state singlet fission occurs initially forming a coupled triplet pair (^1TT), which eventually dissociates to form free triplet excitons in the T_1 state.

There is an optimal range for interchromophoric coupling if free triplet excitons are the desired outcome. On the one hand, coupling has to be strong enough to permit rapid SF in order to out-compete events such as fluorescence and on the other hand, a coupling that is too strong keeps ^1TT as a terminal bound state and the triplets cannot separate to diffuse apart. The relative strength of the direct electronic couplings between the first excited singlet state, intermolecular charge-transfer states and the coupled triplet pair state determine the overall SF mechanism.[25–30] There exist several approaches to describe the SF mechanism based on different kinetic models (see Figure 2.9). In the 'direct' model ^1TT is formed by electrostatic couplings and the singlet-to-triplet conversion is accomplished through an avoided crossing or a conical intersection. Within a theoretical study, the reaction path of SF was followed by an *ab initio* quantum mechanical description of ^1TT, which is termed as dark multiexciton state (D).[31, 32] The initially bright delocalized S_1 state is localized onto a pair of monomers (excimer like state). Non-adiabatic coupling mediated by intermolecular motion between the optically allowed S_1 state and D facilitates SF. The population transfer occurs through a narrowly avoided crossing in the limit of near degeneracies between the two adiabatic states where the Born-Oppenheimer approximation is no longer valid. Their studies show that a charge transfer intermediate does not contribute to SF

because it lies too high in energy.[25, 32]. Alternatively, the 'mediated' model suggests that the initially excited singlet state couples to charge-transfer configurations that in turn have a strong coupling to ^1TT and enable SF.[26, 27] In the limiting case, termed as 'coherent' model, a superposition of S_1 and ^1TT is created and the states are linked by electronic coherence.[33] Here, the intermediate state ^1TT is referred to as multiexciton state (ME).
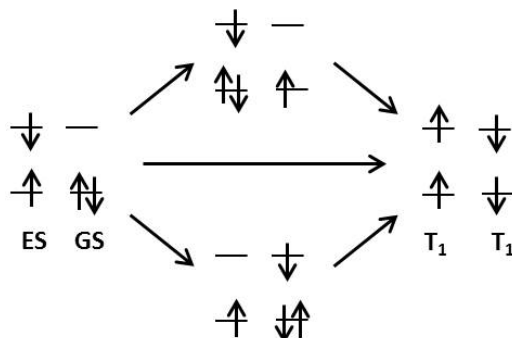

Figure 2.9: Spin states of the molecules connected to the SF process. One molecule is in its excited state (ES) while the neighbor is in its ground state (GS). They share energy and create two T_1 states either via a 'direct' or via a 'mediated' mechanism.

The existence of such a process where a singlet exciton is converted into a triplet pair was first mentioned in a study of crystalline anthracene to explain the origin of delayed fluorescence at high temperatures.[34] Delayed fluorescence appears in an opposite exciton fusion process of two triplet excitons re-forming the singlet exciton, which undergoes radiative relaxation to the ground state. Singh *et al.* found out that the triplet generation was achieved when the energy of the exciting photon was equal to twice that of the triplet exciton and concluded that this mechanism must be rapid in order to compete with IC. The fusion of two triplets can only occur if SF is endoergic, which means that the energy of the relaxed singlet state (S_1) is less than twice of the triplet (T_1) energy and an activation energy is necessary. Thus, in anthracene SF occurs from unrelaxed high-lying vibrational states in S_1 only, what makes the process relatively inefficient.[34] In tetracene $E(2T_1) \approx E(S_1)$ and SF is the dominant relaxation mechanism,

while triplet fusion that results in delayed fluorescence is also present.[35, 36] Pentacene is the first homologue in the acene family where SF is exoergic ($E(2T_1) < E(S_1)$) and proceeds very rapidly making triplet fusion back to the singlet state energetically impossible.

2.4.1 Singlet Fission in Pentacene

In the last decade there was a controversy over the fate of the excited state dynamics of polycrystalline pentacene in experimental as well as in theoretical respect. Marcinak *et al.* stated that the ultrafast component of 70 fs is related to the formation of a doubly excited dimer state rather than a triplet species. They propose that this excimer is stabilized by changes of the local crystal structure and that SF occurs on the picosecond timescale as secondary, thermally activated process with a total yield of only 2 %.[37, 38] Thorsmølle *et al.* claim that triplet formation is suppressed and singlet excitons are quenched by charge transfer to electron traps instead.[39] Theoretical approaches, such as QM/MM simulations, in turn predict that the photoexcited singlet relaxes to a non-emissive intermolecular doubly-excited-state.[40] A dark doubly-excited state that is lower in energy compared to the optically-bright S_1 state was suggested even for the pentacene monomer.[25] However, this is inconsistent with the experimental observation of fluorescence in pentacene dissolved in cyclohexane.[41] On the other hand, SF was predicted to proceed ultrafast and as major relaxation channel in pentacene.[33, 42, 43] These studies were confirmed by experiments on pentacene/C_{60}-bilayers that convincingly demonstrated the generation of multiple charge carriers by obtaining quantum efficiencies above 100 %.[9, 43, 44] However, there is an ongoing debate, whether charge transfer states are involved in the ultrafast dynamics of pentacene or not.[38, 40, 45] Zeng *et al.* applied multireference calculations on a pentacene dimer to investigate low-lying adiabats in the process of SF. They claim that there is weak direct interaction between the multi- and single-exciton states and that they are indirectly coupled through a charge transfer state. Thus, the involvement of charge transfer states in-

duces effective mixing between them and need to be considered in the general model of SF.[45] An excimer-like state (EX) was recently found to be involved in the SF dynamics of the model system perfluoropentacene. This EX state evolves after ^1TT formation as an intermediate rather than a competitive state.[46] Lately, Musser *et al.* showed that SF proceeds via a conical intersection in agreement with former calculations.[30, 31] Their results can be explained by the 'direct' model, however, charge-transfer contributions to the S_1 and ^1TT, respectively may also play a role resulting in a superexchange-type 'mediated' model. This survey of experimental as well as theoretical studies emphasizes the controversy in this field and that the fate of SF is not well understood so far. Gaining new insight into the fundamental process, based on more sophisticated experiments and theoretical approaches, is essential. Moreover, these results motivate to more intensively study the incorporation of pentacene-based materials into organic solar cells in order to raise quantum efficiencies.

2.5 Influence of Nitrogen Atoms

Pentacene is an attractive starting compound to develop new chromophores with promising photo-physicochemical qualities. Due to its high charge carrier mobility, pentacene is also the benchmark p-type semiconductor in organic field effect transistors.[47–49] Besides, it exhibits long diffusion lengths, which is favorable for its application in photovoltaic devices.[9, 39] One major drawback of pentacene itself is its poor oxidative stability against light and oxygen leading to linked dimers or oxidized species. This tendency can be attenuated by derivatization at the positions 6 and 13 of pentacene, which can in turn change the overall structure and accordingly its electronic properties. Specific modifications like the addition of bulky side groups such as tri*iso*propylsilylethynyl (TIPS) strongly improved the solubility of pentacene, thus simplifying its purification and processing.[11, 50] Above all, this functionalization prevents pentacene's oxidation and π-stacking between neighboring molecules becomes relevant, resulting in strong intermolecular

"face-to-face" interactions. The possibility to adjust the electronic behavior required for a particular device by tuning the electronic structure, stability, solubility and molecular packing is of particular interest for applications in organic electronics. For instance, the intermolecular structure has proven to be of critical importance for the performance of an organic material in an electronic device.[51, 52] Favorable intermolecular orientations within the two-dimensional π-stacked array leads to high hole mobilities in the solid state due to enhanced orbital overlap.[53] Further, the substitution of carbon by heteroatoms in the acene core represents an attractive approach to change the overall chemical and physical properties of a material. More precisely, the incorporation of nitrogen atoms into the pentacene backbone results in an energetically stabilized acene with lower lying frontier orbitals.[12, 54, 55] The nitrogen atoms reduce the electron density within the ring structure what makes them to electron poor systems. Since large overlap of frontier orbitals to neighbor molecules in the solid is mandatory to achieve high charge carrier mobilities, their π-stacked structure is beneficial. Such heteroacenes are electron transporters (or ambipolar), that work well in thin-film transistors with high charge mobilities using simple solution processing.[56–59]

Within this thesis, two different aza-derivatives of TIPS-pentacene are studied. In Diaza-TIPS-pentacene (Diaza) one pyrazine unit is inserted into the backbone of TIPS-pentacene, whereas Tetraaza-TIPS-pentacene (Tetraaza) exhibits two pyrazine units symmetrically incorporated. The chemical structures are shown in the following Figure 2.10, whereas the influence of the nitrogen atoms on the energetic levels of the frontier orbitals is illustrated in Figure 2.11. In principle, both the HOMO and the LUMO are lower in energy when carbon is substituted by nitrogen, whereas the LUMO is even more stabilized resulting in a smaller band gap for the heteroacenes. Interesting to note is the further stabilization of Diaza, which has an even smaller gap compared to TIPS-pentancene and Tetraaza. This is related to the broken symmetry, which will be discussed in section 4.2.
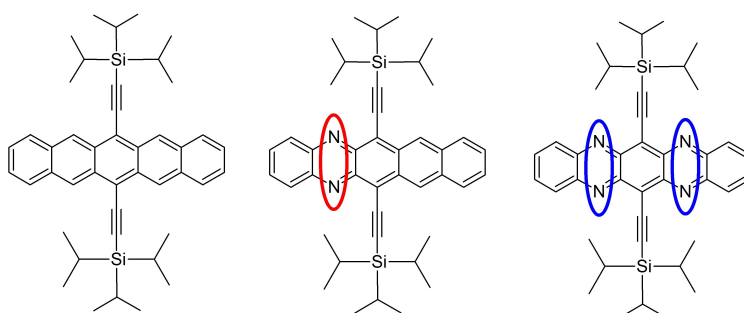
Figure 2.10: Chemical structures of TIPS-pentacene (left), Diaza (center) and Tetraaza (right).
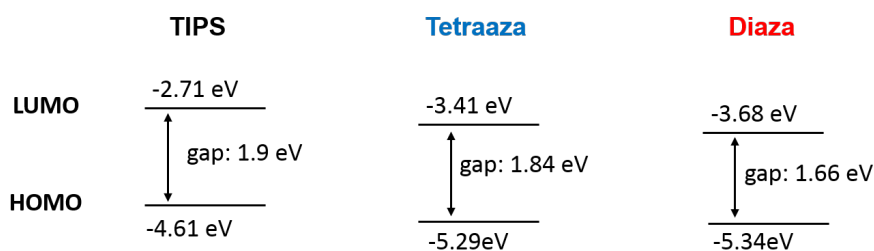

Figure 2.11: Energy levels of the frontier orbitals of TIPS-pentacene, Tetraaza and Diaza.

Due to their lower lying LUMO, they are also promising regarding their application as acceptors in OPVs. A key challenge is to find substitutes for fullerene-based acceptors with suitable LUMO energies, because fullerenes are the main source of instability in life time test of solar cells and very costly.[60] From this point of view it would be highly valuable to use an acceptor material that is also capable of performing SF. In that way, solar cells could be designed that use a donor that transfers the excited electrons to the acceptor, which itself provides additional charges via the SF process. In order to develop this idea, the fundamental excited state dynamics of these new air-stable azaacenes need to be studied first.

2.6   Photovoltaic Applications

Organic photovoltaics, although it is still in its start-up stage, receives a strongly increasing amount of attention. Organic solar cells show a lower efficiency compared to their silicon-based counterparts, however, they offer numerous advantages, such as[61, 62]:

- low weight and flexibility

- semitransparency

- large area production

- low cost fabrication - low temperature manufacturing in a continuous process using state-of-the-art printing tools

- wearable OPVs - printed on clothes, umbrellas, windows,...

- short energy payback times and low environmental impact during operations

There are several research and development activities and a lot of progress has been made in increasing the power conversion efficiency in order to get closer to the Shockley-Queisser limit of 34% for single junction solar cells.[63] The most widely studied OPV contains the conjugated polymer P3HT (poly-3-hexyl thiophene) as donor and a fullerene derivative PCBM (phenyl-C_{61}-butyric acid methyl ester) as acceptor molecule. They form a bulk heterojunction, where the two components interpenetrate each other in a way that the regions of each material are separated only by several nanometers. Consequently, an exciton will never be far away from the interface and the diffusion length can be short. This, however, puts many constraints on how to manage the morphology of the interpenetrating network in terms of solvents and donor-acceptor weight ratio.[64]

The limit of 15 % efficiency should be reachable by optimizing energetic levels, optical and electrical properties of the absorber layers and the device arrangement. New designs to overcome that barrier would require an
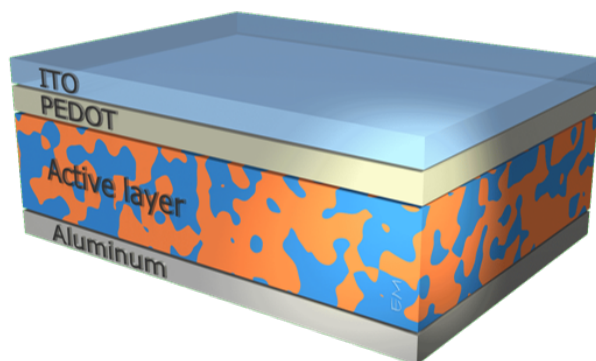
Figure 2.12: Scheme of a OPV multilayer device made of a bulk heterojunction (active layer that contains the organic donor and acceptor materials). ITO= conductive indium tin oxide, PEDOT=transport layer, aluminum=metal electrode. (Thanks to Nanochemistry.it for providing the picture.)

elimination of the most dominant loss channel, namely non-radiative recombination of charges. Another approach to boost quantum efficiencies is to use materials that are capable of doing SF. As motivated before, SF is a type of multiple exciton generation mechanism promising for photovoltaic applications. Pentacene as donor combined with C_{60} as acceptor was studied within a bilayer, in order to confirm enhanced quantum efficiencies and efficient charge separation at the junction.[9, 43] It was shown that triplets are present from the beginning on ($\leq$200 fs) created via SF while charge generation occurs primarily 2-10 ns after photo excitation. The triplet excitons diffuse slowly to the heterojunction where they can dissociate. A great advantage of SF as a carrier multiplication technique is the formation of long-lived triplet excitons, which are the dominant relaxation channel for the photogenerated singlet. Since two triplets do not have enough energy to recombine, triplet-triplet annihilation is energetically suppressed. Therefore, issues like limited exciton lifetimes and (triplet) exction-exciton annihilation as found in inorganic nanocrystals are irrelevant. Recently, external quantum efficiencies above 100 % could be achieved in a pentacene-based OPV cell using a fullerene acceptor and a P3HT exciton confinement layer.[15] The idea is to

combine SF with a conventional material that fills the spectrum above the ^1TT state, in order to minimize triplet exciton losses. The exciton blocking P3HT layer was placed between pentacene and the anode. Due to the wide energy gap and suited triplet energy, P3HT can confine triplet excitons and additionally, its high lying HOMO helps to extract holes from pentacene. In practice, singlet excitons generated in P3HT are transferred to pentacene and then split into triplets. The loss pathway of the generated singlet excitons is the direct dissociation into charge instead of SF. In a further work, the generation and diffusion of excitons in this SF sensitized pentacene based solar cell was modeled.[65] Tabachnyk *et al.* showed that the lower bound for the SF quantum efficiency is 180±15%. The diffusion length of pentacene was calculated to be around 40 nm and the absorption-to-injection (from pentacene to P3HT) efficiency about 30±10%. An alternative route to create SF-sensitized solar cells, is an organic/inorganic hybrid OPV device architecture. In this way, pentacene absorbs high-energy photons while simultaneously low-energy photons are harvested. This can be realized either by lead sulfide[66] or lead selenide[67] nanocrystals, which both absorb infrared photons. Within their studies, it has been demonstrated that the triplet excitons can be dissociated at the organic-inorganic interface with quantum efficiencies greater than 50 %. Yang *et al.* showed very recently the incorporation of the solution-processable material TIPS-pentacene into a OPV cell (architecture is shown in Figure 2.13). TIPS-pentacene absorbs in the visible range and the photo-generated charges (via SF) are transferred to the colloidal nanocrystals, which capture the low energy photons. In other words, they are ideal electron acceptors for low energy TIPS-pentacene triplet excitons.[68] The electrons are transported through the titan oxide (TiO_2) layer and extracted from conductive indium tin oxide (ITO), while holes are withdrawn through the gold top contact (see Figure 2.13).
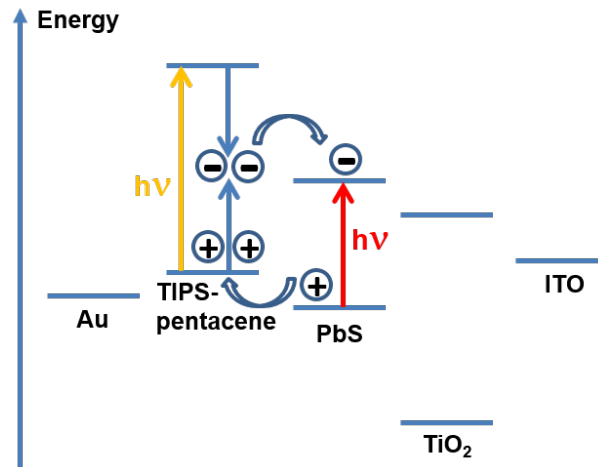
Figure 2.13: Device architecture of a nanocrystal/TIPS-pentacene photo-voltaic device according to Yang *et al.*[68].

The field of designing new, more efficient OPV architectures is continuously growing. Besides improving the arrangement of the solar cell itself, it is of particular importance to elaborate electronic properties on the molecular level. There exist a variety of new materials showing higher resistance against air and humidity by promising high-performances within the device. Studying structure-function relationships in these materials paves the way for novel OPV designs.

Chapter 3

Experimental Methods

This chapter addresses the experimental techniques that were implemented within this thesis. In particular, the details of the newly designed transient absorption setup are described and principles of pump-probe as well as pump-depletion-probe spectroscopy presented. The essential aspects of nonlinear optics and underlying physics, which are crucial in the field of ultrafast spectroscopy are touched on and further elaborated in the appendix. In the end, the important and challenging steps of data processing are elucidated.

3.1   Transient Absorption Experiment

The advent of Femtochemistry in the 1990s has opened up new perspectives in the field of optical spectroscopy.[69] The possibility to monitor molecular dynamics on an ultrafast time scale provides essential information on the photochemical properties of a system. In particular, intra- and intermolecular vibrational energy redistribution and relaxation processes of excited states are directly accessible.
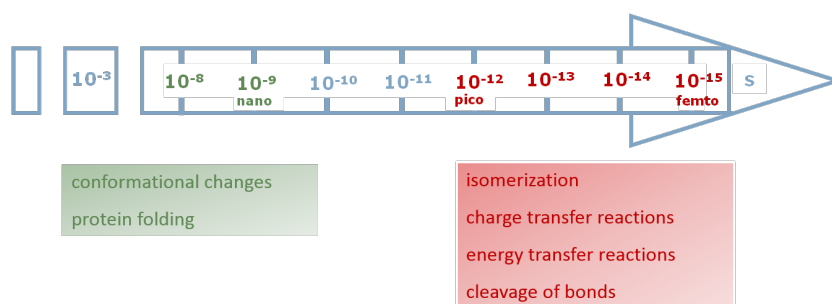
Figure 3.1: The arrow demonstrates the relevant time ranges of fundamental biological and chemical processes.

Femtosecond absorption spectroscopy probes the dynamics of a system in response to a so called pump pulse, allowing the observation of the population evolution in the excited state (see Figure 3.2). Regarding charge generation processes in organic molecules, as in pentacene, it is of vital importance to understand the underlying dynamics in order to exploit their full potential. Above all, revealing the rapid process of SF requires more sophisticated techniques that allow for the investigation of the photo-induced dynamics directly after photo excitation with high temporal resolution.
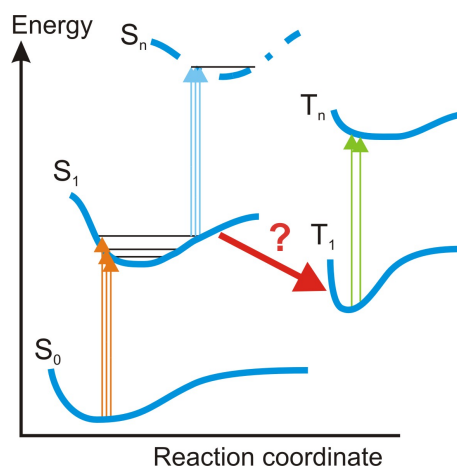

Figure 3.2: Energy level diagram representing the excited states dynamics of a conjugated system. Pump-probe-spectroscopy provides information about how the states are populated and can reveal relaxation processes and their corresponding kinetics.

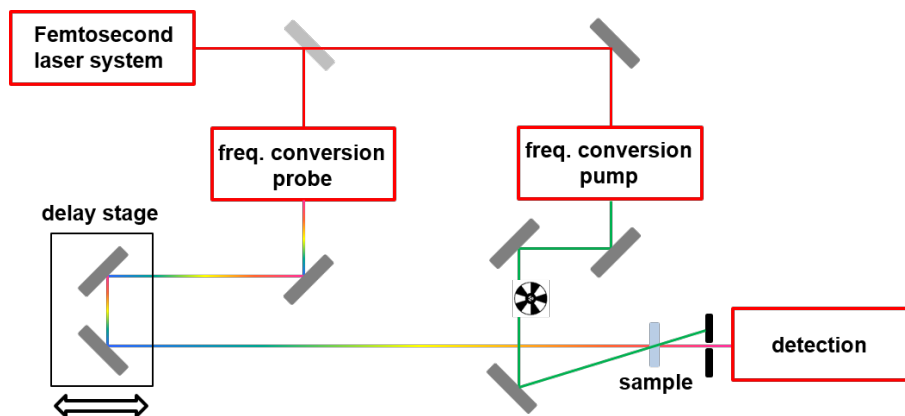The principle of pump-probe spectroscopy is shown in Figure 3.3.

Figure 3.3:   Principle of pump-probe-spectroscopy.   Every second pump pulse is blocked by a chopper wheel. A broad white light continuum acts as a weak probe field, which travels through the sample and reaches the detector either unchanged or changed dependent on the pump interaction.

A fraction of molecules is promoted into the first allowed excited state by the pump pulse. This pump pulse is created by means of a noncollinear optical parametric amplifier (nc-OPA).[70–73] The underlying nonlinear process allows for the generation of broad excitation pulses in the whole visible range from 480 nm to 680 nm at adequate intensities (further explanation is given in the appendix). After a set time delay, a weak probe pulse with low intensity in order to avoid multiphoton processes is sent through the sample. A synchronized mechanical chopper blocks every second pump pulse and thus, alternately the sample is being excited or not. This leads to two scenarios; either the chopper is on (absorption spectrum of the sample in the ground state reaches the detector) or off (absorption spectrum of the excited sample reaches the detector). According to Lambert Beer's law:

$$A = \log\left(\frac{I_{in}}{I_{out}}\right) = c \cdot \epsilon \cdot d \tag{3.1}$$

the difference absorption spectrum can be calculated as follows:

$$\Delta A = \log \left(\frac{I_{probe}^{pump\ off}}{I_{probe}^{pump\ on}} \right) = \Delta c \cdot \epsilon \cdot d \qquad (3.2)$$

By scanning the delay stage, i.e. setting different time delays between the pump and the probe beam, a ΔA profile as a function of time τ and wavelength λ can be obtained ($\Delta A(\tau, \lambda)$). The transient data contain information on the excited state dynamics, such as charge transfer or energy transfer reactions, conformational changes, as well as spin flip reactions and many more. The beauty of transient absorption is that also inaccessible states like symmetry forbidden states, dark states or states of different multiplicity can be revealed. This can be realized due to the fact that after photoexcitation the population is evolving to lower energy states of different character and symmetry, what is catched by the probe pulse. In the case of pentacene, for example, a triplet state is populated, which cannot be photo-excited directly. In the following, the contributing signals to ΔA that occur after population has been transferred to the excited state are explained.
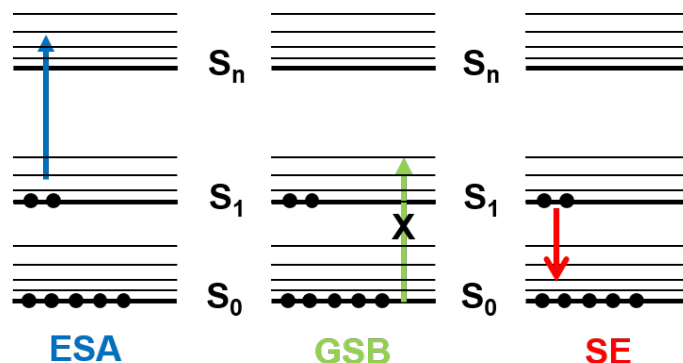

Figure 3.4: Different contributions to the transient absorption signal: excited state absorption (ESA), ground state bleach (GSB) and stimulated emission (SE).

The first contribution represented in Figure 3.4 is the ground state bleach (GSB). As a consequence of the pump beam, the number of molecules in the ground state has decreased. Hence, the absorption from the ground state to the excited state is less than in the non-excited sample. This leads

to a negative signal in the ΔA spectrum in the region of the ground state absorption of the molecule (see Figure 3.5 from 560-700 nm).
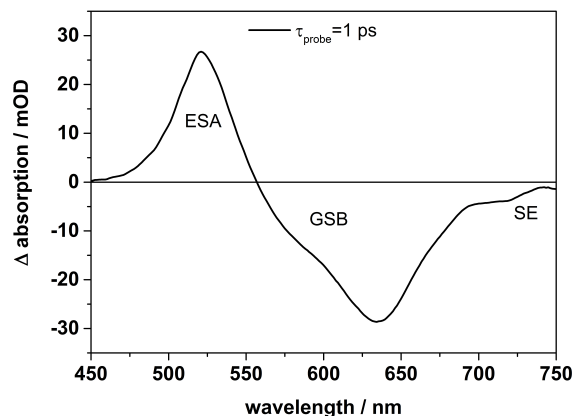

Figure 3.5: Transient absorption spectra of nile blue at 1 ps delay time. The negative signal is assigned to the GSB (560-700 nm) overlapped with the SE signal (>700nm). The positive contribution corresponds to the ESA.

Another negative signal is called stimulated emission (SE), which occurs upon excitation when the probe pulse passes through the excited volume. This will only happen when this transition is optically allowed and typically it shows a spectral profile that follows the fluorescence spectrum (see Figure 3.5 >700 nm). In general, a probe photon induces emission of another photon from the excited state back to the ground state, which leads to a negative signal since more light reaches the detector. A positive ΔA signal results from the excited chromophore, which is promoted to higher excited states. Absorption of the probe pulse at wavelengths where these optically allowed transitions occur is called excited state absorption (ESA, see Figure 3.5 450-560 nm). The intensity of the probe pulse is so weak that the excited state population is not affected. Taking cuts at specific wavelengths of the GSB and ESA signal the temporal evolution of the signals can be followed (see Figure 3.6). By fitting these transients with exponential functions the resulting time constants give information about the overall kinetics of the system.
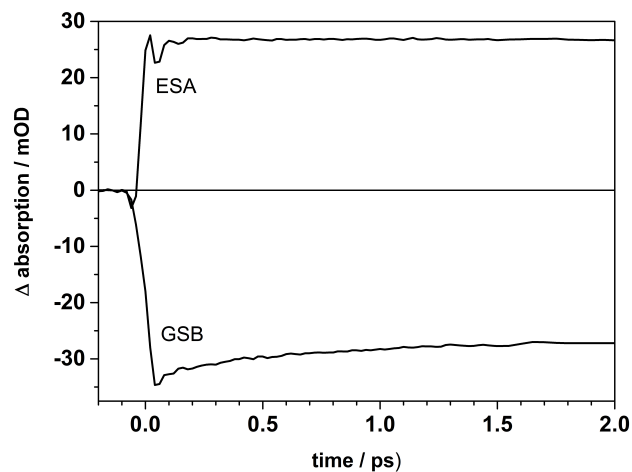
Figure 3.6: Evolution of the GSB and ESA signals in nile blue within the first 2 ps. The sharp decrease of the signal after temporal overlap between pump and probe (delay time zero) represents the de-population of the ground state, whereas the immediate rise identifies the ESA.

3.1.1   Experimental Realization

The ultrafast time-resolved absorption measurements were performed using a regeneratively amplified Ti:Sa laser generating 100 fs pulses with a repetition rate of 1 kHz at 800 nm central wavelength. As the pump-probe technique requires at least two beams in order to realize time-resolved measurements, the fundamental laser output is split into two parts. 99% of the intensity is guided to a nc-OPA in order to create the pump pulse at the required excitation wavelength. Thereafter, the excitation beam travels through a prism compressor in order to compensate for chirp effects and reduce the pulse length (further information is given in the appendix). The other 1% of the intensity is used to generate white light serving as probe beam. The white light continuum is done by focusing the 800 nm beam either in a 2 mm Sapphire crystal (450-750 nm) or in a 3 mm yttrium aluminium garnet crystal (830-1030 nm). The former is collimated using a achromatic lense as it corrects for chromatic as well as spherical aberration. In the latter, a

36

CaF_2 lense is used, due to its high transmission in the near-infrared (NIR) region combined with a low chromatic aberration.
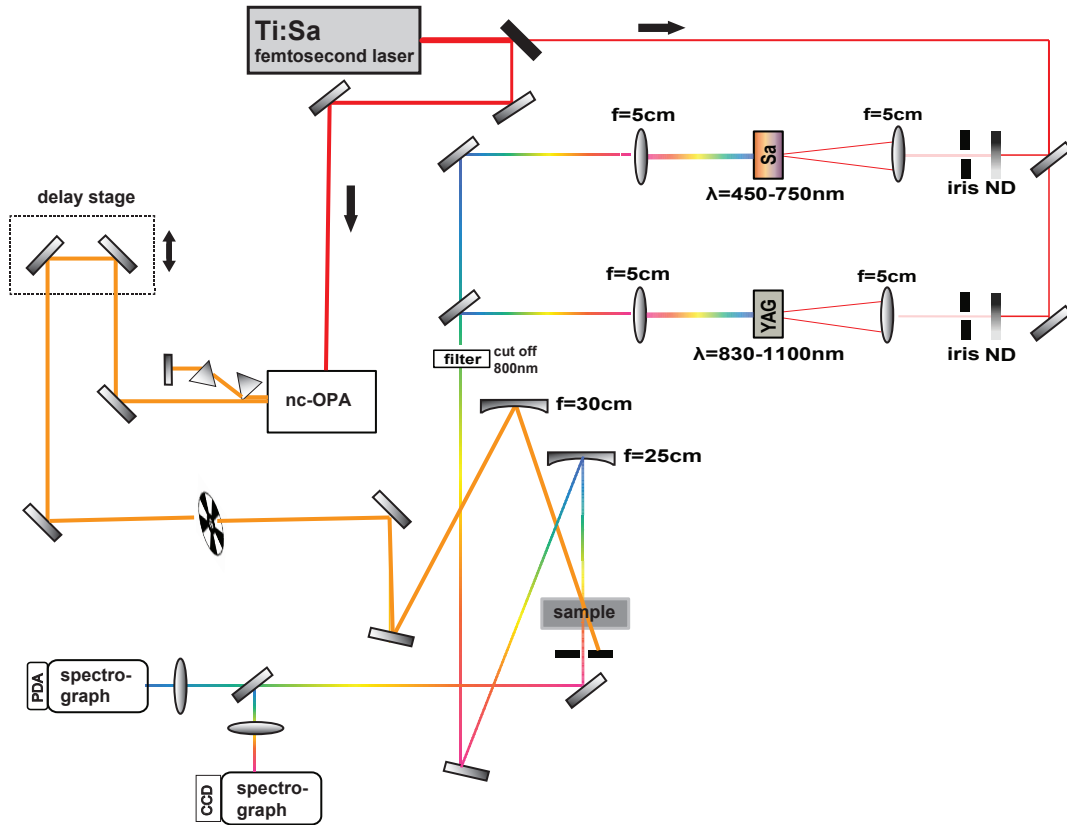

Figure 3.7: Experimental setup of the newly designed transient absorption experiment. 99% of the fundamental laser intensity is used to create the pump beam in the nc-OPA. Before it is sent to the delay stage, the nc-OPA output travels through a prism compressor. After passing the chopper wheel the excitation beam is focused onto the sample. The other 1% of the intensity is used to generate white light either in a Sa or a YAG substrate. The collimated white light is also focused onto the sample and afterwards sent to the detector.

There is also the possibility to probe in the UV range ($\leq$ 450 nm) generated in a CaF_2 substrate that is mounted in a rotating holder. This is necessary due to the low damage treshold of this material. By rotating the CaF_2 substrate at a moderate frequency the focused laser hits every time another position of the material. The generated white light continuum has an intrinsic group velocity dispersion (GVD, see appendix). After traveling through optically dense materials, this dispersion readily increases. It is necessary to consider this effect in the data analysis. In principle, the dispersion can be described by a polynomial function, which was applied to the raw dataset. This dispersion correction is necessary in a sense that all wavelengths share the same time zero. To get rid of the 800 nm beam before the sample and the detector, a 800 nm edge filter in the visible and a long pass filter in the NIR was used, respectively. The desired probe light can be chosen by flipping two mirrors and aligning the beam into the appropriate detector. Both beams, the pump and the probe are focused with a 30 cm and 25 cm focusing lense, respectively, onto the sample leading to spot diameters of approximately 200 μm. The energy of the excitation beam was between 60 and 120 nJ per pulse what corresponds to 6×10^{14}-1.2×10^{15} photons/cm^2. The polarization of the pump beam is parallel with respect to the probe beam when measuring thin-films and set at the magic angle (54.7°) when measuring in solution to eliminate anisotropy.[74] The pump beam is blocked after the sample with an iris and the signal beam is focused on a silicon (visible) or InGaAs (NIR) photodiode array multichannel detector (256 pixels with a resolution of 1.32 nm per pixel). Every second pump beam is blocked with a synchronized chopper wheel in order to get difference spectra, i.e. with and without excitation, according to equation 3.2. The absorbance change is calculated at a set time delay. This is realized by delaying the pump beam with respect to the probe beam. In other words, the pump beam travels through a high-precision motorized computer-controlled translation stage while the probe beam is kept constant. All samples were measured under normal air conditions.

In order to generate white light in the UV spectral region (below 400 nm), a CaF_2 substrate is used. Since this material has a very low damage threshold, it needs to be rotated to minimize crystal damage. A motor-driven stage was designed and constructed, together with the mechanical workshop, to realize this demand (see Figure 3.8).
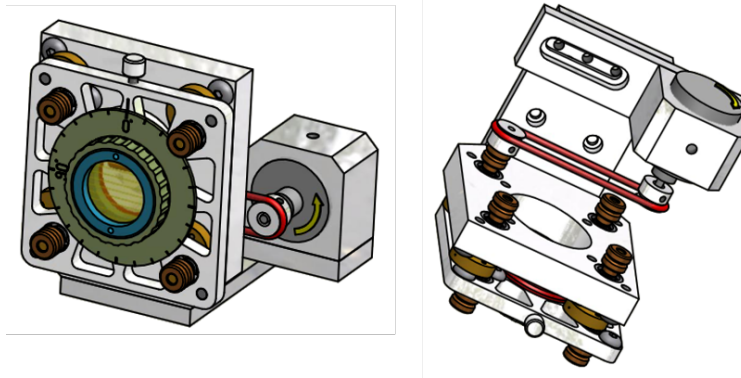

Figure 3.8: Schematic representation of the constructed rotating holder for CaF_2 to generate white light in the ultraviolet inspired by the group of Prof. Riedle[75].

The implementation of this holder to drive a CaF_2 substrate is shown in Figure 3.9. The collimation of the white light after generation is done with a spherical mirror. The angle between incoming white light and the outgoing beam after the spherical mirror has to be as small as possible. In order to realize this, a D-shaped mirror is used before the beam is guided to the experiment.
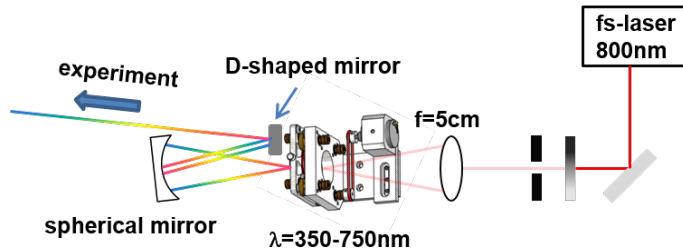

Figure 3.9: Experimental setup of the white light generation in the ultraviolet.

3.1.2   Experimental Response Time

The temporal resolution of the transient absorption experiment depends on the pulse duration of the pump beam (in combination with a spectrally broad probe beam) and the accuracy of the delay stage. However, a short pulse duration Δt implies a large spectral bandwidth $\Delta \nu$ according to the time-bandwidth product. A 10 fs pulse, for example at 600 nm corresponds to a bandwidth of 100 nm full width at half maximum (FWHM), which means a high temporal resolution at the expense of spectral selectivity. Therefore, a compromise between a selective excitation and high temporal resolution has to be made. The use of chirped pulses (frequencies possess different velocities when travelling through a material) in the transient absorption experiment leads to non-resonant contributions to the signal. Accordingly, light interactions of the pump and probe beams in a substrate, for example, do not represent population dynamics of electronic states, but rather cross-phase modulation (XPM) effects known as coherent artefact (see appendix). XPM becomes higher with increasing chirp of the probe pulse, which is the case for a supercontinuum as used in ultrafast absorption measurements. Accordingly, at temporal overlap between the pump and probe pulse (delay time zero) a huge coherent spike appears. This undesired contribution highly complicates data interpretation and analysis of the initial dynamics. A simple subtraction is commonly not possible, since the amplitude of the coherent artefact changes from the sample to the pure substrate or solvent. Nevertheless, the interaction of pump and probe beam in a pure substrate can be utilized to calculate the experimental response time. By fitting the coherent artifact using the following equation[76, 77]:

$$CS = A \left(te^{-2\left(\frac{t}{\tau}\right)^2} \right) - (t - T_{gvd})\, e^{-2\frac{\left(t - T_{gvd}\right)^2}{\tau^2}} \qquad (3.3)$$

where T_{gvd}=group velocity dispersion, A=amplitude of the coherent artefact and τ=shape factor of the Gaussian envelope, the FWHM and therefore the time resolution of the experiment can be determined by the following relation: $\tau_{FWHM} = \frac{\tau}{0.849}$. In Figure 3.10 the charateristic coherent artefact at 500 nm is shown where τ=34 fs, T$_{gvd}$=51 fs. The FWHM of the coherent

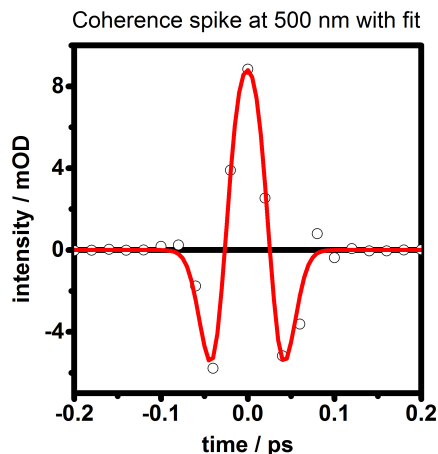spike is 38 fs representing the experimental response time.

Figure 3.10: Fit of the coherent artefact at 500 nm giving a time resolution of 38 fs.

3.2 Pump-Depletion-Probe Experiment

Femtosecond pump-depletion-probe experiments are highly useful techniques to control the evolution of excited species.[78–81] The idea of this method is to set a specific marker within the kinetic network on a preselected state which intercepts the normal relaxation dynamics. Experimentally this is realized by introducing a second, depletion or dump pulse which modifies the population after the initial excitation. The changed population pathway can in turn identify specific states of the energy flow network that are dependent on the additional pulse. This information is important for revealing new relaxation pathways and thus to gain more insight into underlying dynamics. Related to the excited state dynamics of TIPS-pentacene, this technique can provide a deeper insight into relaxation pathways and thus the formation of triplet states (see Figure 3.11). Experiments in different spectral regions can reveal the origin of excited state transitions and furthermore the interplay between them. A better understanding on how the triplet manifold is populated via SF helps, in a further step, to modify special transitions on a molecular level.

In that way, namely by avoiding or activating transitions, the SF process can be optimized.
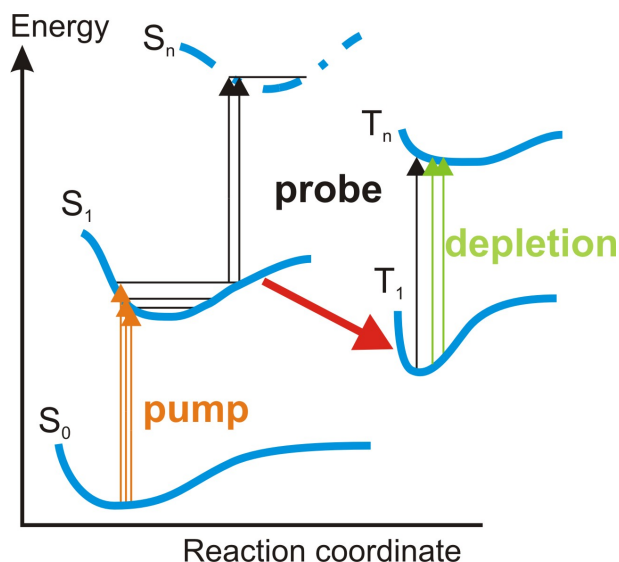

Figure 3.11: Schematic representation of the pump-depletion-probe experiments in a energy level diagram. After the excitation pulse (orange arrows) a second depletion pulse (green arrows) is applied, which is resonant with the triplet transition. The distrurbed relaxation pathway is finally recorded by the probe pulse (black arrows).

3.2.1 Experimental Realization

For the pump-depletion probe technique the fundamental laser is again divided into two parts. As for the conventional pump-probe setup 1% of the intensity was used to generate white light. The remaining 99% are further spitted into a pump and a depletion beam (see Figure 3.12). Both pulses are created in nc-OPAs and compressed to pulse durations of ≤ 20 fs using prism compressors. All three beams are focused onto the sample under normal air conditions. The signal beam is directed to a silicon (visible) or InGaAs (NIR) photodiode array multichannel detector as in the pump-probe setup. The pulse sequence is shown together with the beam geometry of the pump-depletion-probe experiment in Figure 3.13.
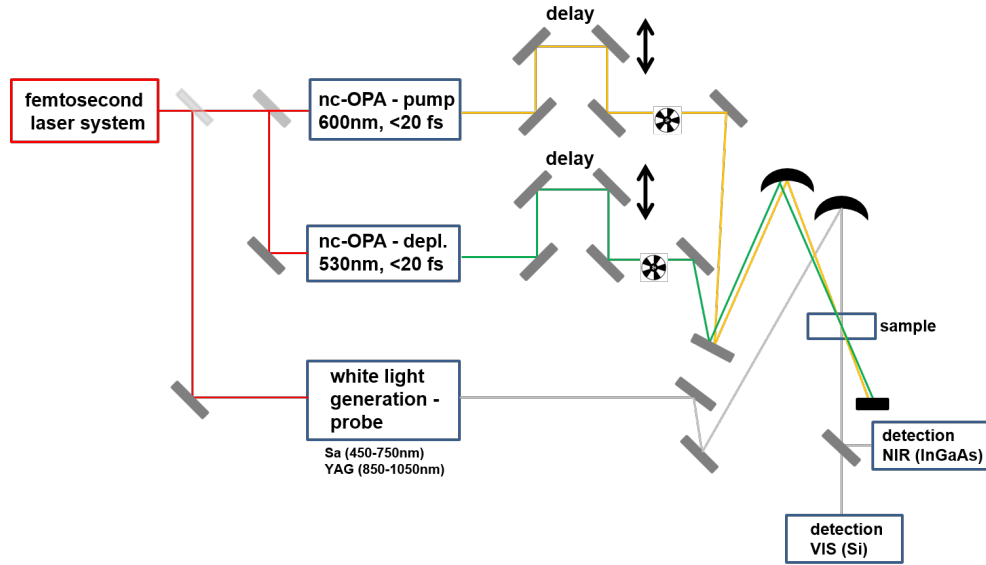
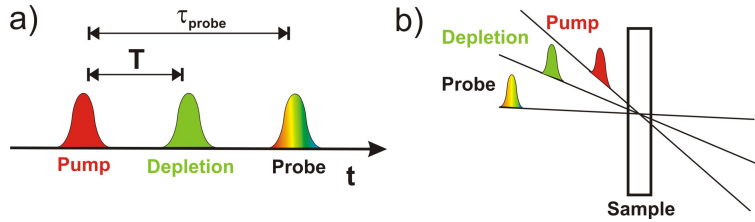**Figure 3.12:** Simplified scheme of the pump-depletion-probe setup.

Figure 3.13: a) Pulse sequence of the pump-depletion-probe technique and b) geometry of the three beams in the experiment.

After the pump pulse has promoted population into the excited state, the depletion pulse is applied with a variable delay T. The pump-probe delay is defined as τ_{probe}. Due to the fact that the depletion pulse is also partly resonant with the $S_0 \rightarrow S_1$ transition in the case of TIPS-pentacene and its derivatives, we could find temporal overlap using the depletion as excitation pulse. The time between the pump and depletion pulse was set indirectly after defining the temporal overlap first between the pump and the probe and second between the depletion and the probe pulses. The spatial overlap between all three beams was optimized by maximizing the depletion effect

at fixed T=1 ps and fixed τ_{probe}=2 ps. The pump beam centered at 600 nm shows a pulse duration of 14 fs and the depletion pulse around 530 nm has a pulse duration of 18 fs. Both beams were attenuated to pulse energies of 40 nJ with a focal spot diameter of approximately 200 μm (ca. 4×10^{13} photons/cm^2) in order to minimize exciton-charge and exciton-exciton annihilation reactions. The temporal resolution of the experiments was calculated to be 40 fs in the visible and 100 fs in the NIR. The principle of the pump-depletion-experiment, such as signal generation, time ordering of the beams and origin of the observed singal evolution, is demonstrated by means of a laser dye. Nile blue is perfectly suited, since it absorbs at 600 nm and shows an ESA at 530 nm (transient absorption data of nile blue are shown in the previous section).[82–84] There are different ways to generate signals, dependent on the experimental settings. By chopping the pump beam, only the effect of the depletion pulse on the pump pulse is recorded. If the time between the pump and depletion pulse (T) is fixed, the probe beam is scanned (τ) and three possible cases arise, which are presented in Figure 3.14, where T=1 ps. Before delay time zero, the probe arrives first and therefore no signal is recorded (see Figure 3.14 I). The temporal overlap between pump and probe creates the coherent spike. When the probe beam is between the pump and the depletion pulse the usual transient absorption signal is detected where the depletion pulse has no effect on the dynamics (see Figure 3.14 II). At the time point when the probe and depletion pulses overlap in time, the signal gets depleted (sharp signal decay). Afterwards, the signal recovery is monitored, here the probe pulse arrives after the depletion pulse and tracks the depletion action (see Figure 3.14 III).
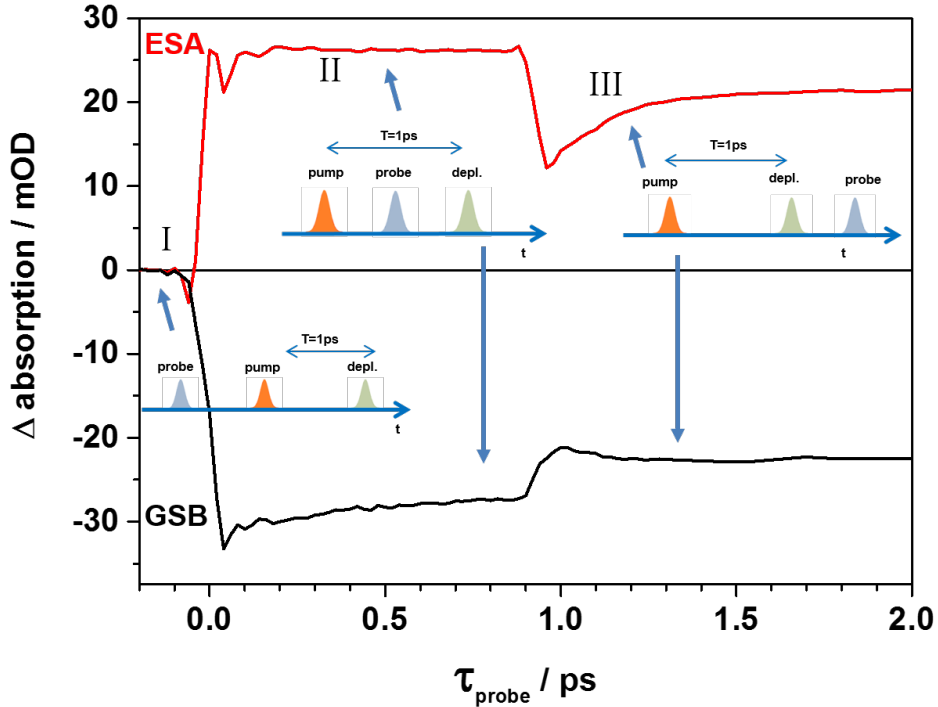
Figure 3.14: Pump-depletion-probe data of nile blue in ethanol for two wavelengths (ESA and GSB). The pump pulse is chopped and the probe pulse is delayed. The time delay between the pump and depletion pulse is T=1 ps.

If the pump and probe pulses are fixed and the depletion pulse is scanned, a so called action trace can be recorded. In this way, the depletion effect can be monitored in time and the point of its maximum impact determined. This is demonstrated in Figure 3.15 where τ_{probe} is fixed at 1 ps. When the depletion pulse arrives after the probe pulse it has no effect and the signal corresponds to the conventional pump-probe signal at a delay time of 1 ps (see Figure 3.15 I). When the depletion pulse overlaps with the probe pulse a sharp increase of the ESA and GSB signals is observed. After the temporal overlap the depletion pulse is scanned between the pump and probe pulses (see Figure 3.15 II). The deletion effect is most pronounced around 1 ps, where the pump and depletion pulse overlap in time (step in signal

at T=1 ps). The remaining signal (see Figure 3.15 III) should be again the conventional pump probe signal because the depletion pulse arrives first. However, this is only valid if the depletion pulse does not contribute to the signal at all. In the case of nile blue the depletion pulse is also resonant with the inital $S_0 \rightarrow S_1$ transition. Hence, the depletion pulse itself acts as an excitation pulse and its contribution is reflected in an increase of ESA and GSB signal after the depletion action (see Figure 3.14 in the recovery of transient signal).
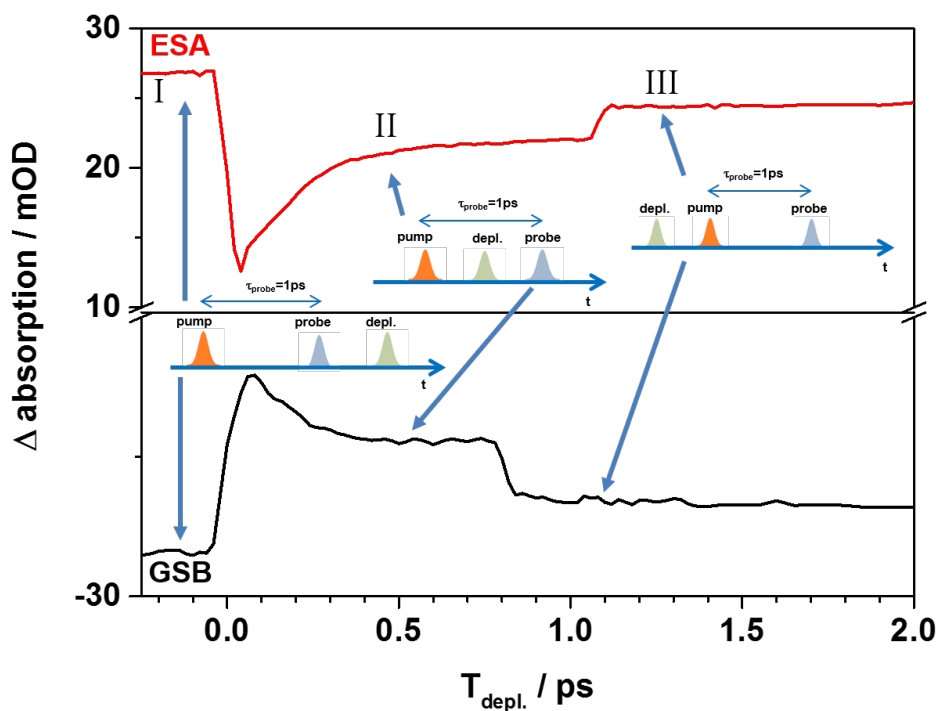

Figure 3.15: Pump-depletion-probe data of nile blue in ethanol for two wavelengths (ESA and GSB). Pump pulse is chopped and depletion pulse is delayed. The time delay between the pump and probe pulse is τ_{probe}=1 ps. The measured action trace determines the effect of the deletion pulse on the dynamics in time.

The amount of the depletion contribution to the conventional pump-probe signal can be determined by recording a signal, where the depletion pulse is chopped and delayed. This scenario is demonstrated in Figure 3.16. When the depletion arrives before the pump pulse the recorded signal arises from the depletion pulse only.
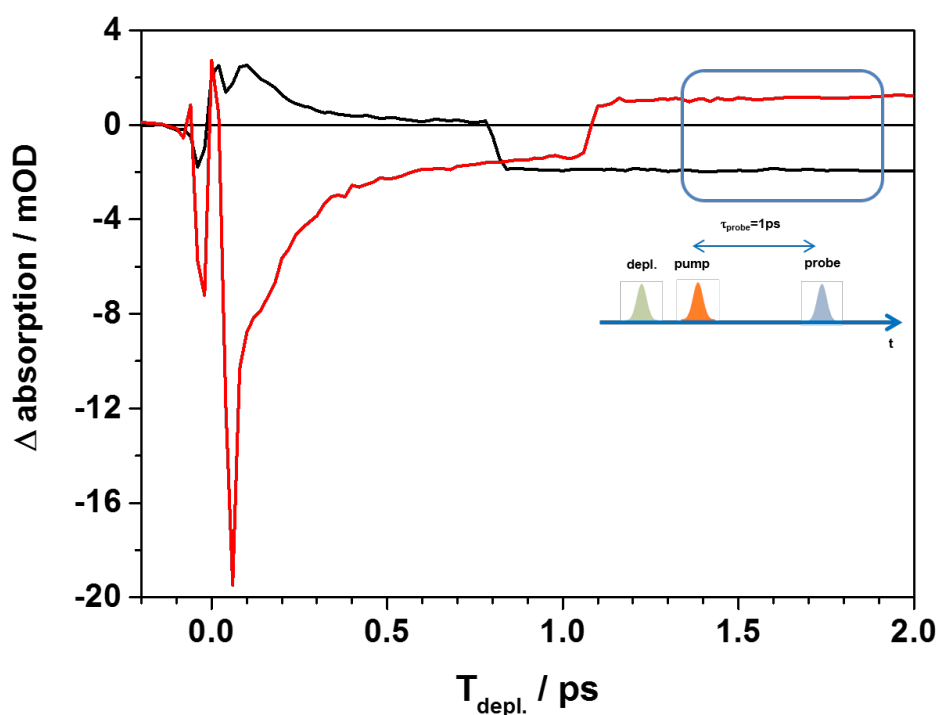

Figure 3.16: Pump-depletion-probe data of nile blue in ethanol, where the depletion pulse is chopped and delayed. The amount of population that is created by the depletion pulse itself can be determined when the depletion pulse arrives first, which is shown in the square.

The total amount of population which is affected by the depletion pulse can be obtained by taking the difference between the signal with and without depletion action. This is schematically shown at τ_{probe}=2 ps (see Figure 3.17). It is important to note, that a direct determination is only possible in solution if the sample volume is exchanged between two subsequent pump-depletion-probe experiments. In this case, several data sets can be taken right after one another and a direct comparison is easily possible. Since measurements performed on thin-films only take one sample position for a whole dataset, photo bleaching effects has to be taken into account. The overall dynamics are not changed during one measurement, hence, the amount of the depletion effect can be determined indirectly by normalizing the data before the depletion pulse is applied.
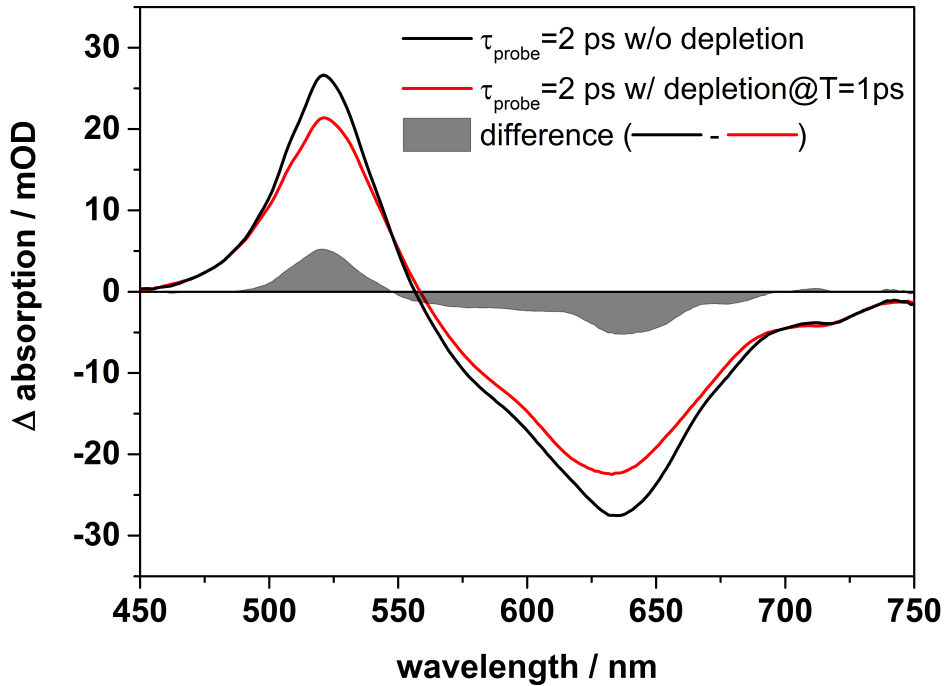

Figure 3.17: Spectrally resolved amount of depletion effect at τ_{probe}=2 ps. The difference of the transient absorption signal is shown with and without presence of the depletion pulse at T=1 ps.

3.3 Data Processing

The obtained experimental data contain substantial dynamical information, which needs to be thoroughly analyzed. First, time constants have to be extracted from the transient data, before a kinetic model can be developed. This model explains the overall dynaimcs and is essential for a global fitting procedure. The global target analysis in turn can give a detailed picture on the underlying photochemical processes, i.e. the assignment of spectral features to specific species, both time and wavelength dependent.

In order to extract initial information on the kinetics transients need to be fitted by an appropriate multiexponential function. The obtained rise and decay times can help to describe the underlying dynamics. By gaining a better understanding of the experimental observations, a first interpretation of the data can be made. Fitting of selected transients was carried out using an evolutionary algorithm.[85, 86] The applied function contains rising and decaying contributions as shown in the following equation.

$$S = A \left[ae^{\left(-\frac{t}{\tau_{decay1}}\right)} + (1-a)\left(e^{\left(-\frac{t}{\tau_{decay2}}\right)}\right)\right] \times \left(1 - e^{\left(-\frac{t}{\tau_{rise}}\right)}\right) \quad (3.4)$$

with: A=amplitude, a=scaling factor, t=time, $\tau_{decay1,2}$=decay times, τ_{rise}=rise time, T_{gvd}=group velocity dispersion.

The approach of fitting selected single transients helps, in a first step, to get a rough estimate of the observed kinetics. However, there is a general problem when it comes to signals that are spectrally not well separated. Regarding TIPS-pentacene, the singlet and triplet bands are superimposed what makes fitting of single transients challenging. Hence, the assignment of these species to specific wavelengths and extracting independent time constants in a further step is problematic.
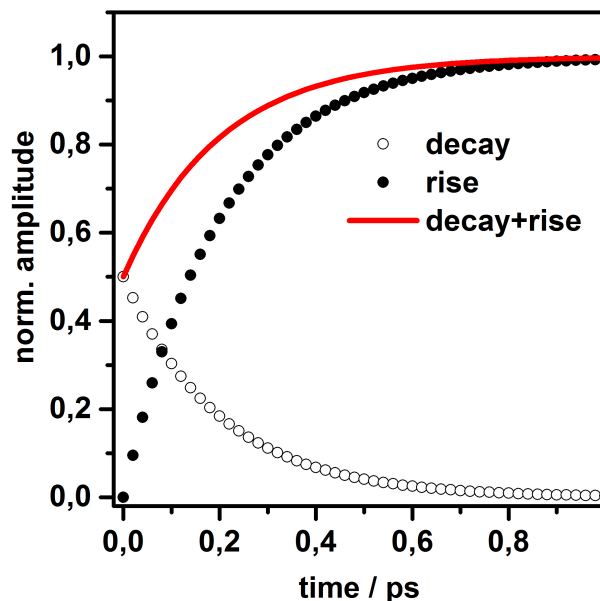
Figure 3.18: Result of superimposed transient absorption signals; triplet rise (black dots), singlet decay (transparent dots) and their sum (red curve).

A signal that contains a certain amount of decaying character overlaid by a rising component represents a combination of both. Figure 3.18 shows the case where 50 % singlet decay is overlaid with a triplet rise. Fitting of this single transient leads to a shorter time constant and thus to an apparent faster triplet formation, which is actually not the case. This fact makes fitting of single wavelengths very difficult and more sophisticated methods have to be applied to gain information about the intrinsic kinetics of a system. The idea of a global fitting procedure is presented in the following.

3.3.1 Global Target Analysis

In order to manage the overwhelming amount of data obtained by time re-solved transient absorption measurements, a global target analysis (GTA) was carried out.[87–89] ”Global” in that sense means a simultaneous analysis of all measurements (the whole dataset) while target is referred to the appli-cability of a particular target model. A time-resolved spectrum is a collection of measurements in two dimensions; the first spectral parameter is wavelength

(λ) and the second variable to monitor the spectral changes is time (t). The interpretation of transient absorption data poses a big challenge due to largely superimposed signals. This means that at any wavelength a mixture of several signals from different contributions is present. This emphasizes the need for compensating the data to a relatively small number of components and spectra, which is done within a global analysis. It is based on a deconvolution of the measured data array $\Delta A(\lambda, t)$ into time-independent spectra and wavelength-independent kinetics. The goal is to convert raw kinetic data into intrinsic properties of the involved components. The derivation of a complete kinetic model and thus extraction of intrinsic rather than apparent time constants as well as pure intermediate spectra, is desirable. In a first step, the number of transient states, which give rise to the observed kinetics are defined. This is based on *a priori* assumptions on the mechanism of the involved intermediates. $\Delta A(\lambda, t)$ at each measured wavelength can be expanded into a sum of time-dependent (wavelength-independent) functions $f(j, t)$ and their amplitudes $B(j\lambda)$ (wavelength-dependent) $\sum \{B(j, \lambda)f(j, t)\}$, where j is the final state of a transition. The time-dependent factors are mostly exponentials resulting in the following global fitting expression:

$$\Delta A(\lambda, t) = \sum B(\lambda, j)e^{-\frac{t}{\tau(j)}} \tag{3.5}$$

The second step is to find a phenomenological description of experimentally measured data by approximating the apparent kinetics with time constants and amplitudes. The final step is to extract the intrinsic rate constants of the pure states with according amplitudes. Within this work, a sequential model $1 \to 2 \to 3 \to ...$, in which the arrows indicate successive monoexponential decays of increasing time constants, was applied to describe the obtained transient data of TIPS-pentacene and its derivatives. Following this target model, the evolution of the excited states can be visualized. In this way, it is possible to disentangle the contributions and extract spectrum signatures of pure excited state intermediates, so called species associated spectra (SAS).

Chapter 4

Sample Characterization

4.1   Sample Preparation

The investigated heteroacenes (chemical structures see in 2.5) were synthe-
sized by Dr. Jens Engelhart from the group of Prof. Bunz of the OCI,
Organisch-Chemisches Institut. The synthesis has been recently developed
and is described in detail in Engelhart *et al.*[90] and Miao *et al.*[12], respec-
tively. Both compounds were purified through recrystallization from hexane
and ethanol. TIPS-pentacene was obtained from Sigma-Aldrich and used
as received without further purification. The concentration of the molecules
in toluene was approximately 1 mmol/L depending on the slightly different
extinction coefficients (ϵ=10000 L/mol· cm for TIPS-pentacene and ϵ=8000
L/mol· cm for Diaza and Tetraaza, respectively). Thin films of ca. 100
nm thickness were prepared on either pure or polyimide coated 1737F glass
substrates (PGO, Iserlohn, Germany) via spin coating performed by Dipl.
Chem. Fabian Paulus from the group of Prof. Bunz. An approximately 30
nm thick Polyimide interlayer (diluted PI-2525, Hitachi Chemical DuPont
MicroSystems GmbH, Neu-Isenburg, Germany) was used to achieve a good
wettability of the organic solution and to provide a homogenous film forma-
tion and crystallization. After cross linking the polyimide film at 300 °C
for 3 hours, all substrates were rinsed in acetone and isopropyl-alcohol in
an ultrasonic bath for 5 minutes and dried with compressed air. The small

molecules were dissolved in anhydrous toluene (20 mg/ml, 10 mg/ml for Tetraaza-TIPS-pentacene) and filtered through 0.45 PTFE filters prior to spin-coating. Films were spin cast at 1500 rpm, followed by annealing (drying) at 40 °C for 30 minutes under nitrogen atmosphere (O_2 and H_2O < 1 ppm).

4.2 UV-VIS and Fluorescence Spectroscopy

Steady state optical VIS absorption spectra were recorded with a commercial UV-VIS spectrometer (Shimadzu 1800). Stationary fluorescence spectra as well as time-resolved spectra with 1 ns temporal resolution were measured with a commercial time-resolved fluorescence spectrometer (Fluorocube NL, Horiba, equipped with a NanoLED-375L). The lifetime of the fluorescence was determined for each molecule after excitation at 376 nm.

In Figure 4.2a) the steady state UV-VIS absorption spectra of TIPS-pentacene, Diaza and Tetraaza in toluene solution are shown. The HOMO-LUMO transition is accompanied by a vibrational progression for all molecules. The distance between the absorption peaks is 50-57 nm for all molecules and corresponds to a vibrational progression of approximately 1400 cm^{-1}, assigned to a vinyl stretching mode. This mode is also observed in Fourier-transform infrared measurements of TIPS-pentacene (see Figure 4.1).
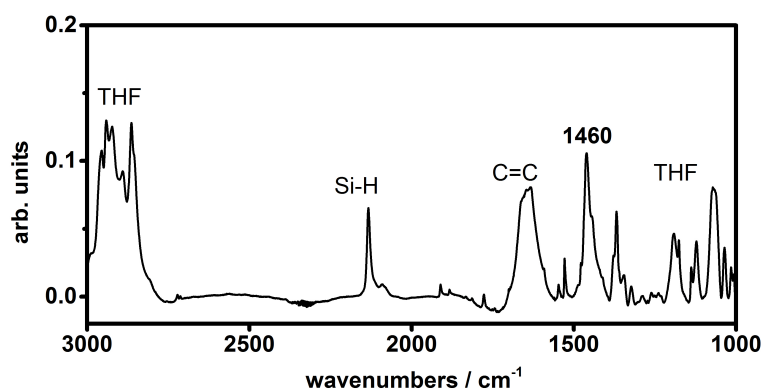

Figure 4.1: FTIR spectrum of TIPS-pentacene showing a peak at 1460 cm^{-1} corresponding to the vinyl stretching mode.
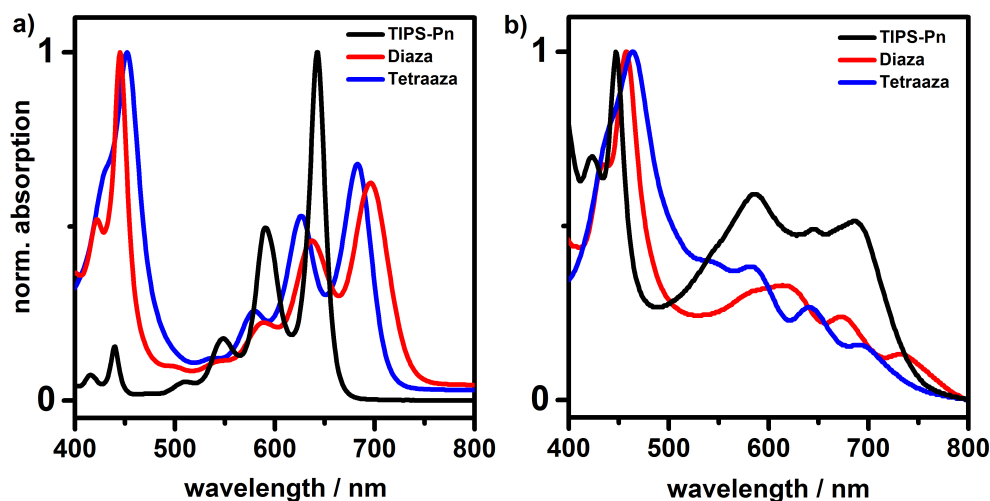
Figure 4.2: Steady state absorption of a) TIPS-pentacene (black curve), Diaza (red curve) and Tetraaza (blue curve) in toluene solution and b) as thin-films. The spectra of TIPS-pentacene [51, 91] and the two aza-derivatives [54] are in good agreement with literature.

The nitrogen substitution causes a red shift of the HOMO-LUMO transition compared to TIPS-pentacene (53 nm for Diaza, 40 nm for Tetraaza). The free electron pairs are localized on the nitrogen atoms and do not contribute to the system, resulting in an electron deficient system. The nitrogen atoms lower the frontier orbitals, however, the HOMO experiences less stabilization than the LUMO in comparison to the unsubstituted TIPS-pentacene. This causes a red shift in the visible spectra as a consequence of a changed electronic structure. Remarkable is the larger red shift of Diaza compared to Tetraaza. This is related to the disjoint charge distribution over the molecule due to the broken symmetry of Diaza. The induced dipole leads to an unequal charge distribution over the molecule, i.e. different parts of the molecular orbitals are occupied.[54, 92, 93] Another interesting observation is the different absorption contribution around 450 nm for the molecules, which exceeds the $S_0 \rightarrow S_1$ transition of Diaza and Tetraaza in intensity and is almost absent in TIPS-pentacene. These finding suggests that different states are involved, which are stabilized or destabilized in solution of particular polarity.

In the solid phase, the molecules are in close vicinity and interact with each other building a two-dimensional π-stacked structure (see Figure 4.4). Figure 4.2b) presents the according absorption spectra of the molecules on spin-coated thin-films. The lowest electronic transition is shifted to higher wavelengths in all molecules, due to enhanced Coulomb interaction of the molecule with its surrounding and exchange interactions between translationally equivalent molecules.[94] Additionally, the bands become broader and the intensity of the individual bands changes in the solid compared to solution. These band shifts and broadening are a result of vibronic coupling, which has a major impact on the Davydov splitting, and the coupling to intermolecular charge-transfer excitons.[95] The enhanced intermolecular interaction has also a consequence on the symmetric vinyl stretching mode, which is distorted going from the isolated molecule to a molecular assembly. For TIPS-pentacene the contribution in the UV at 447 nm gained much intensity and is also slightly red shifted compared to the signal in toluene. The red shift of the HOMO-LUMO transition between solution and thin-film is with 43 nm most pronounced for TIPS-pentacene. A splitting of this lowest energy transition is observable and two peaks appear. For Diaza the red shift in the solid state compared to solution is 36 nm, whereas Tetraaza shows only a shift of 12 nm. The band intensities increase with lower wavelengths and the splitting does not become apparent for both Diaza and Tetraaza. In Figure 4.3a) the steady state fluorescence spectra of TIPS-pentacene, Diaza and Tetraaza in toluene solution are illustrated. The expected shift to higher wavelengths, as a consequence of the changed charge distribution over the molecules in the order TIPS-pentacene, Tetraaza, Diaza, is conserved in the fluorescence measurements. The fluorescence bands of TIPS-pentacene and Diaza exhibit a shoulder shifted to the red, however, the underlying vibration of this progression has a lower frequency compared to the vibration observed in the absorption spectra. The Stokes shift in TIPS-pentacene is 13 nm and gets with 22 nm larger in Tetraaza. For Diaza the shoulder lies out of the observed spectral range and the Stokes shift is with 35 nm most pronounced. Fluorescence transients of all compounds are determined with the time correlated single photon counting method in toluene solution. TIPS-pentacene

shows the longest lifetime of 12 ns. The fluorescence decay of Tetraaza has a time constant of 7.5 ns and the shortest fluorescence lifetime of 5 ns is found for Diaza (see Figure 4.3b)). In the solid state, fluorescence is not observable due to the ultrafast exoergic singlet fission process that out-competes all slower transitions.
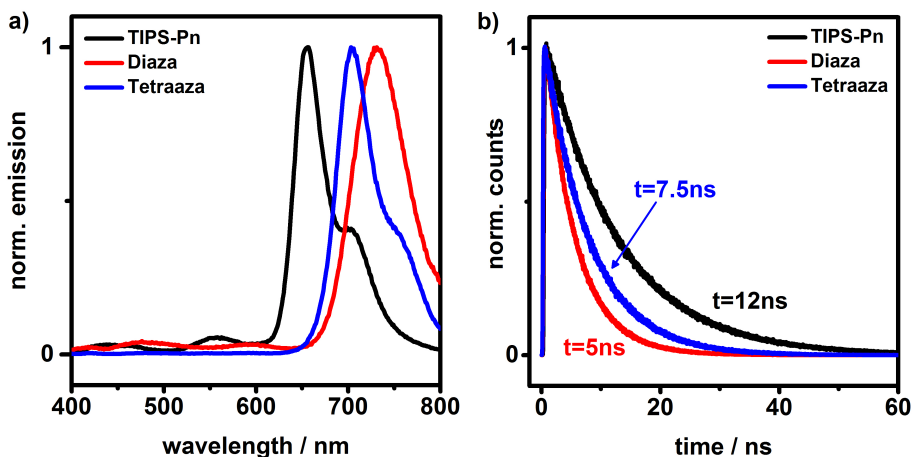

Figure 4.3: a) Steady state fluorescence spectrum and b) time-resolved fluorescene of TIPS-pn (black curve), Diaza (red curve) and Tetraaza (blue curve) in toluene solution. The steady state spectrum of TIPS-pentacene is in accordance to literature.[96]

Table 4.1: Summary of the solution-to-solid shift, Stokes shift and fluorescence life time of TIPS-pentacene and its aza-derivatives for comparison.

	solution-to-solid shift	Stokes shift	fluorescence life time
TIPS-pentacene	43 nm	13 nm	12 ns
Diaza	36 nm	35 nm	5 ns
Tetraaza	12 nm	22 nm	7.5 ns

4.3   Crystallinity of Pentacene-Derivatives

In the following, the crystal structures of all investigated pentacene-derivatives are presented (see Figures 4.4, 4.5, 4.6). Knowledge of their crystal packing is important regarding the intermolecular interactions of the molecules and thus their singlet fission performance. As the distance between the π-systems determine the intermolecular coupling, SF may alter in compounds with different crystal packing architectures. A comparison to the solid-state structure of TIPS-pentacene with the unsubsituted pentacene reveals striking differences. TIPS-pentacene does not adopt the herringbone pattern, but rather stacks in a two-dimensional columnar array with significant overlap of the pentacene rings in adjacent molecules.[7] Due to this arrangement, the interplanar spacing of the aromatic rings is significantly smaller in TIPS-pentacene.[7, 97] While the herringbone packing motif represents a simple combination of edge-to-face and face-to-face interactions, TIPS-pentacene favors a face-to-face orientation and crystalizes in a π-stacked array.[50]
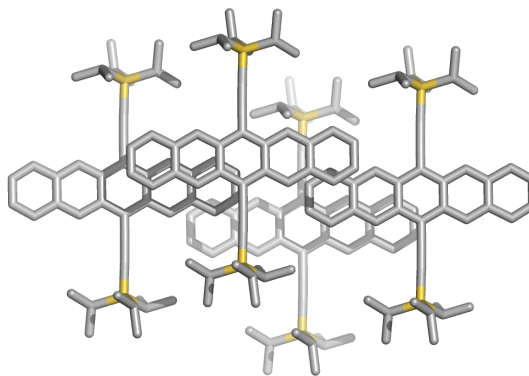

Figure 4.4: Crystal structure of TIPS-pentacene.[11]

In the case of Diaza, the unsymmetrical substitution leads to an alternating arrangement of the π-systems resulting in a closer packing compared to TIPS-pentacene. The smaller distance of the π-systems and hence the stronger intermolecular coupling is manifested in the more J-aggregate type static absorption spectrum of Diaza.[94, 95] Tetraaza in comparison has the

smallest cell unit and the shortest π distance, suggesting that it exhibits the closet packing.[57]
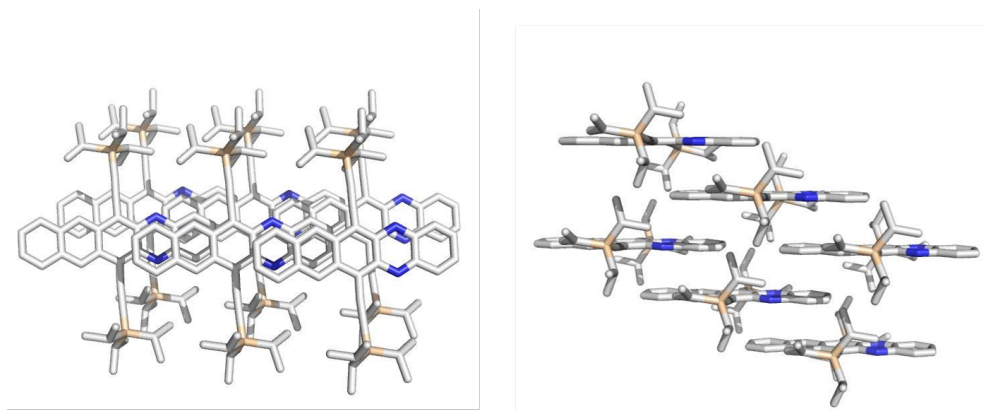

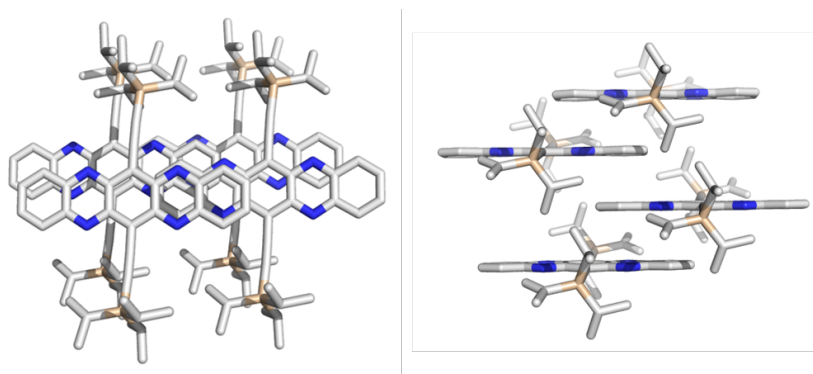**Figure 4.5:** Crystal structure of Diaza.[57]

Figure 4.6: Crystal structure of Tetraaza.[57]

Polarized microscope images were taken on a Nikon LV100-50i-pol under crossed polarizers indicating polycrystalline films in cooperation with Dipl. Chem. Fabian Paulus.[98] It is clearly visible that the thin-films show large polycrystalline domains (see Figure 4.7). The morphology of the films seems to be different comparing TIPS-pentacene and its aza-derivatives. The domain sizes are remarkably larger in the azaacenes resulting from a different crystallization growth. However, all films show a constant homogeneity within the excitation volume (200 μm).
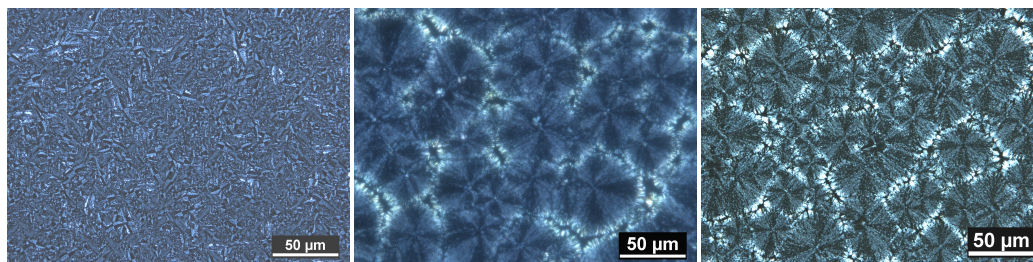
Figure 4.7: Polycrystalline Films of TIPS-pentacene (left), Diaza (center) and Tetraaza (right) on polyimide coated glass substrates.

In order to get quantitative information about the film crystallinity, X-ray diffraction measurements were carried out. The XRD pattern of TIPS-pentacene, Diaza and Tetraaza are shown in Figure 4.8 and show clear diffraction peaks. The Bragg reflections of TIPS-pentacene are in good agreement with previous studies.[99, 100]
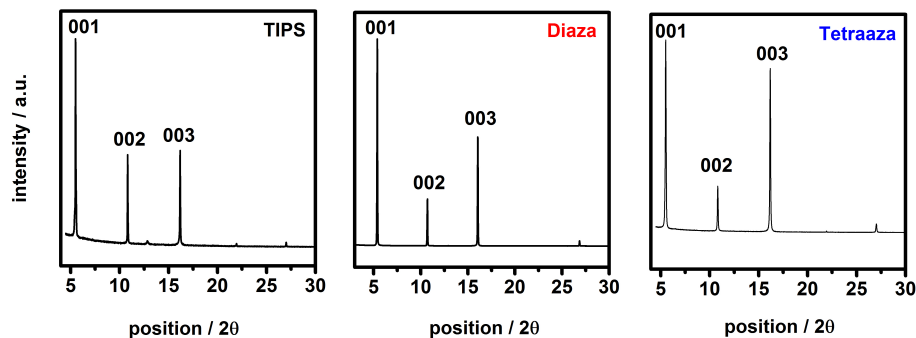

Figure 4.8: X-ray diffraction peaks of TIPS-pentacene (left) Diaza (center) and Tetraaza (left). The measurements were done by Dr. Andreas Leineweber at the Max-Plack-Institute in Stuttgart.

The height of the thin-films was determined by means of atomic force microscopy (atomic force microscope, Dimension^{TM} 3100, Digital Instruments). By removing a fraction of the thin-film, a substrate/film interface was created. The material was wiped off with solvent leading to an accumulation of material, which can be seen in Figure 4.9. Following the AFM trace from glass to film there is peak at the border (from approximately 25 μm-40 μm),
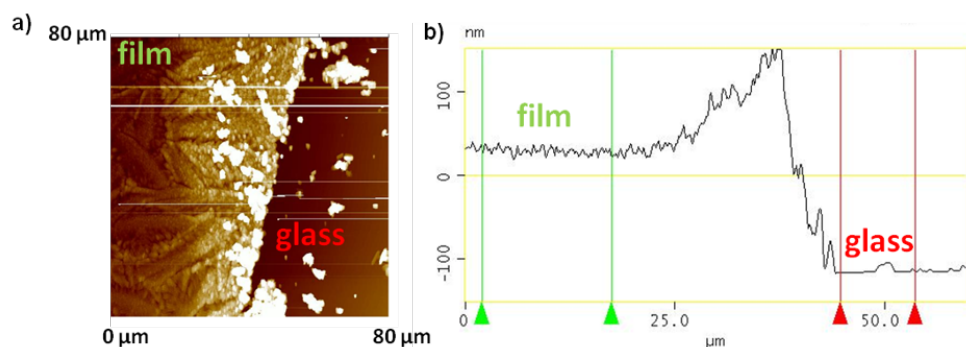
which represents exactly this accumulation.

Figure 4.9: a) AFM image of the TIPS-pentacene/glass interface, b) AFM trace shows the boundary of glass and film in order to determine the height of the film. The cursor positions indicate the area that is averaged to determine the height of the film.

The cantilever scans over the created boundary and the integration of the different areas (glass and film) gives the according height. AFM images of TIPS-pentacene in comparison to the two aza-derivaties are shown in Figure 4.10. For TIPS-pentacene the surface looks homogeneous and smooth, whereas for Diaza the domains are larger and the surface is rough. In the AFM image of Tetraaza there is a large domain observable (upper left), as a consequence of the spherulite growth.
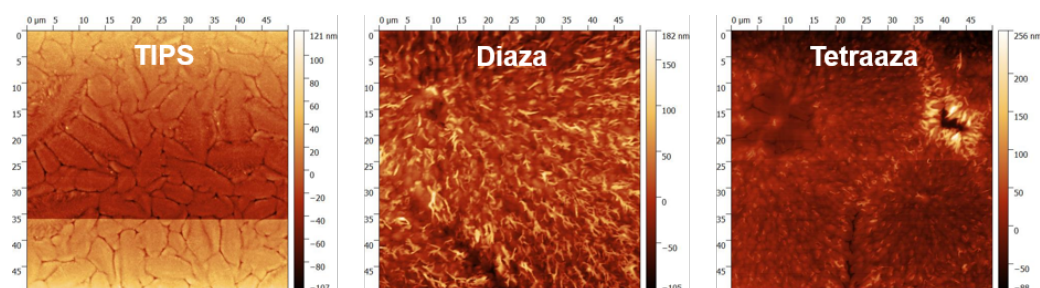

Figure 4.10: AFM image of TIPS-pentacene (left) Diaza (center) and Tetraaza (left).

Chapter 5

Ultrafast Dynamics of TIPS-Pentacene and its Aza-Derivatives

The overall goal in designing new organic based photovoltaics is to reduce loss channels on the one hand and raise quantum efficiencies on the other. One possibility to realize this desire is to use materials that undergo SF. This profitable process, where two triplet states are generated by investing one photon to excite a singlet molecule, is described in detail in section 2.4.1. In the following, the ultrafast photo-induced dynamics of TIPS-pentacene are described, elaboratively discussed and compared to those of its aza-derivatives. The objective of these time-resolved experiments is to unravel the ultrafast triplet formation in these materials in order to gain insight into their structure-function relationships. First, the outcome of the transient absorption measurements is presented. Taken the outcome of the global target analyses for TIPS-pentacene and the azaacenes together, a first summary of the excited state dynamics is given and open questions are raised. Subsequently, the results of the pump-depletion-probe experiment combined with a kinetic rate model simulation, as a complementary study, are shown, which is the core of this thesis. Finally, the experimental observations are successfully described in a qualitative and quantitative way. A kinetic model of the excited state dynamics of TIPS-pentacene and accordingly of the heteroacenes is established, which summarizes all the obtained information.

5.1 Transient Absorption in Solution

First, the transient absorption measurements in toluene solution are shown. Since the ability of the compounds to undergo SF is in the focus of this work, the experiments in thin-films are discussed in more detail afterwards.

5.1.1 Ultrafast Dynamics of TIPS-Pentacene

Figure 5.1 shows the absorbance changes of TIPS-pentacene at several times after photoexcitation at 600 nm. The excited state absorption (ESA) signal ranges from 430 nm up to 600 nm and can be assigned to the singlet $S_1 \rightarrow S_n$ transition. The ground state bleach (GSB) peaks at 645 nm and exhibits almost twice the intensity compared to the ESA signal, indicating a larger extinction coefficient for this transition. Around 710 nm the SE is visible, which reflects the fluorescence band. The ESA signal does not decay significantly in 1 ns underlined by the fluorescence decay of 12 ns (see section 4.2), in other words the ground state is repopulated with a time constant of 12 ns. The triplet ESA $(T_1 \rightarrow T_n)$ is not visible in solution, since the intersystem crossing rate is negligible.
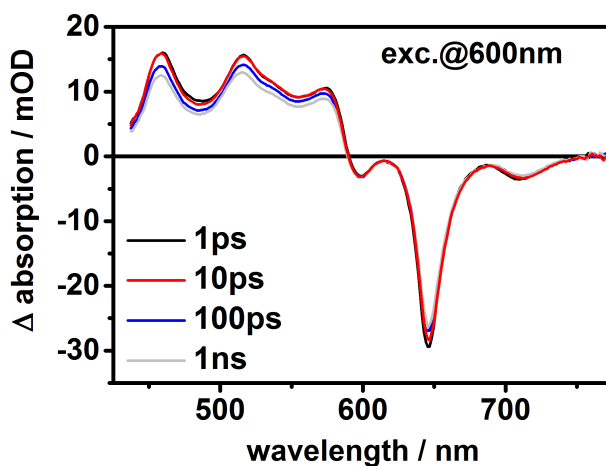

Figure 5.1: Transient absorption data of TIPS-pentacene in toluene solution at several time delays after excitation at 600 nm. The measurements are in good agreement with former experiments.[91]
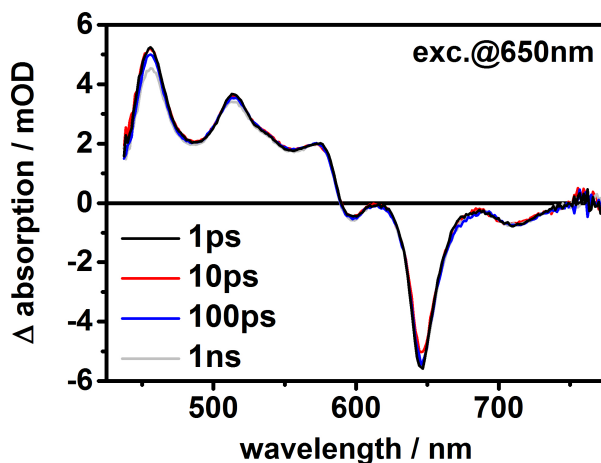
Figure 5.2: Transient absorption data of TIPS-pentacene in toluene solution at several time delays after excitation at 650 nm. The measurements are in good agreement with former experiments[101].

In Figure 5.2 the transient absorption data of TIPS-pentacene after excitation at 650 nm are presented. The overall spectral distribution looks almost the same compared to the data excited at 600 nm (5.1). However, the signal intensity of the ESA and the GSB bands are in the same order (ca. 5 mOD), which was not the case when excited at 600 nm (15 mOD for ESA and 30 mOD for GSB). Being resonant with the TIPS-pentacene's absorption maximum in toluene, the ESA and GSB contributions are of equal intensity. Excitation at lower wavelengths (higher energies) leads to a significant increase of the GSB signal with regard to the ESA band. In Figure 5.3 transients at specific wavelengths of the ESA and the GSB are shown. Measurements with parallel polarization of the pump with respect to the probe beam clearly demonstrate the effect of rotational diffusion. The absorbance changes are due to rotational relaxation of the oriented fraction of chromophores. This is a consequence of the excitation beam, which is linearly polarized. By using a probe pulse that is 54.7°(magic angle) relative to the pump beam, the intrinsic rotational diffusion of the molecules will average all anisotropic interactions to zero. Hence, the magic angle can eliminate the absorbance changes due to rotational diffusion.[102] At very early delay

times (in the first picoseconds) the ESA contributions exhibit low-frequency oscillations (see Figure 5.4).

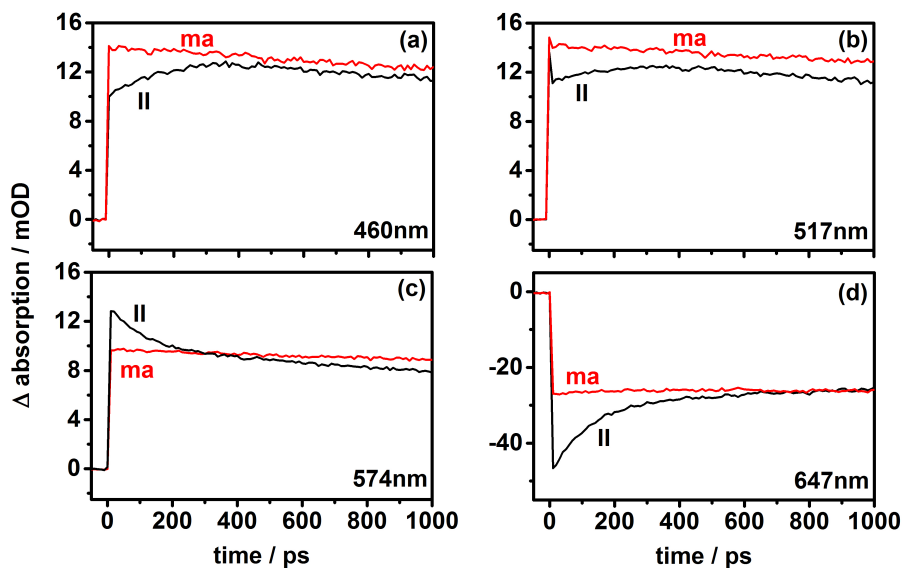**Figure 5.3:** Transients of TIPS-pentacene in toluene solution with parallel and magic angle configuration at specific wavelengths. The time cuts at 460 nm, 517 nm and 574 nm belongs to the ESA, whereas the GSB is represented by the transient at 647 nm.
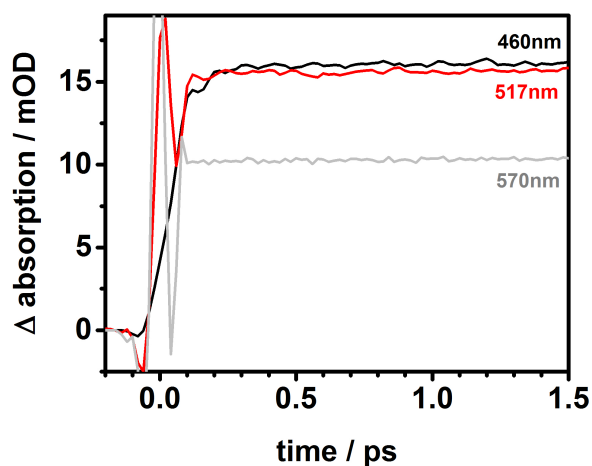

Figure 5.4: Zoom into the first 1.5 ps after excitation of TIPS-pentacene at specific wavelengths illustrating the fast oscillations of the signal.

Most pronounced are the oscillations obtained for the GSB signal for parallel as well as for magic angle polarization. Therefore, exemplary the first 1.5 ps of the GSB signal together with its Fourier transform is illustrated in Figure 5.5. The corresponding vibrational mode (for all the contributions) is 260 cm^{-1} and its origin will be discussed together with the azaacenes in the end of this section.
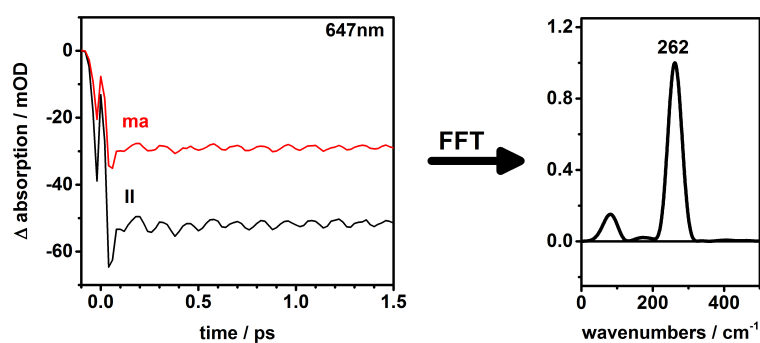
Figure 5.5: The first 1.5 ps of the TIPS-pentacene GSB signal shows a pronounced oscillation (left) and its Fourier transform (right) gives a vibrational mode of 260 cm^{-1}.

5.1.2   Ultrafast Dynamics of Diaza-TIPS-pentacene

In Figure 5.6 transient absorption spectra of Diaza dissolved in toluene are illustrated at different time delays. A broad and very intense ESA signal from 450 nm to 600 nm covers the spectrum. Only a small GSB signal is detected, which is superimposed by the SE around 700 nm. In the first 100 ps a small blue shift of the ESA maximum is observed, which can be attributed to vibrational relaxation in the excited state.

Figure 5.6: Transient absorption data of Diaza in toluene solution at several
time delays after excitation at 620 nm.
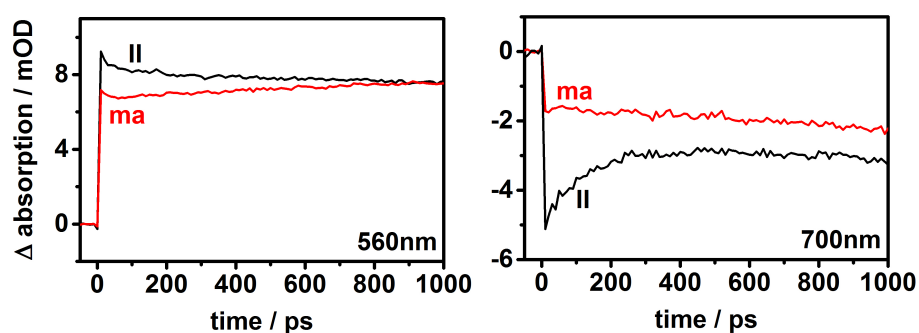
Figure 5.7: Transients at 560 nm=ESA (left) and 700 nm=SE/GSB (right)
of Diaza in toluene solution with parallel and magic angle polarization.

As for TIPS-pentacene, the absorbance changes at perpendicular polariza-
tion of the pump relative to the probe beam are a consequence of rotational
diffusion (see Figure 5.7). The low-frequency oscillations at very early delay
times found for TIPS-pentacene are also present in the ESA and GSB sig-
nal of Diaza, but less pronounced (see Figure 5.8 (left)). The corresponding
frequency mode is same as observed for TIPS-pentacene (260 cm^{-1}).
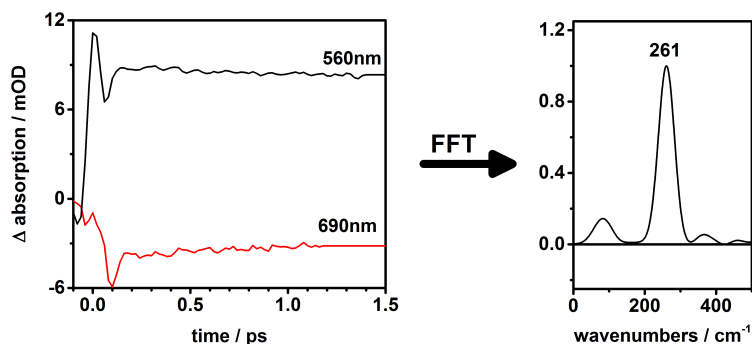
Figure 5.8: The first 1.5 ps of the Diaza GSB and ESA signals show a fast oscillation (left) and their corresponding mode (via FFT) is 260 cm^{-1} (right).

5.1.3 Ultrafast Dynamics of Tetraaza-TIPS-pentacene

Figure 5.9 presents the transient absorption spectra of Tetraaza in toluene. The broad ESA signal is red shifted compared to TIPS-pentacene and Diaza and lies between 500 and 625 nm. The SE band, which is also obscured by the GSB is weak and peaks at 690 nm. The ESA signal experiences a slight blue shift in the first 10 ps, again attributed to vibrational relaxation within the excited state.
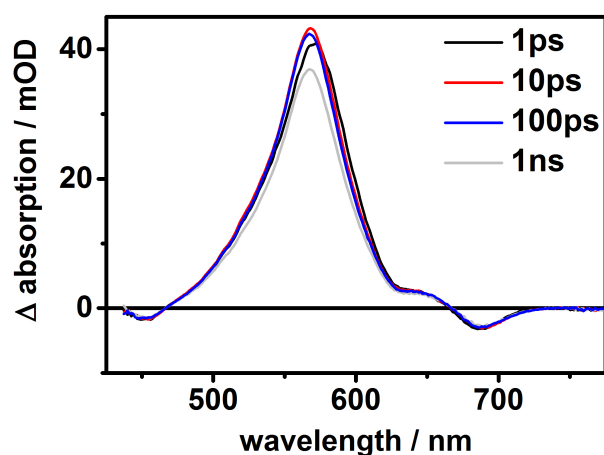
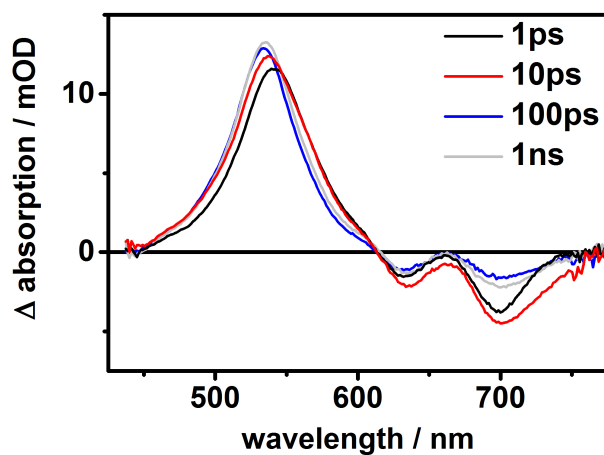**Figure 5.9:** Transient absorption data of Tetraaza in toluene solution at several time delays after excitation at 600 nm.

At 1 ns a decay is visible and the band gets spectral narrower, however, the ground state shows an insignificant recovery, which is illustrated in the transients in Figure 5.10. In the ESA and GSB signals of Tetraaza the low-frequency mode is 270 cm^{-1} (see Figure 5.12) and most distinctive compared to TIPS-pentacene and Diaza, respectively.
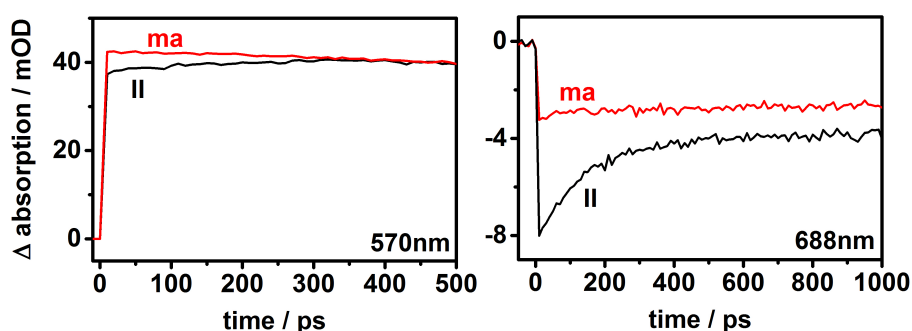
Figure 5.10: Transients at 570 nm=ESA (left) and 688 nm=GSB (right) of Tetraaza in toluene solution with parallel and magic angle polarization.
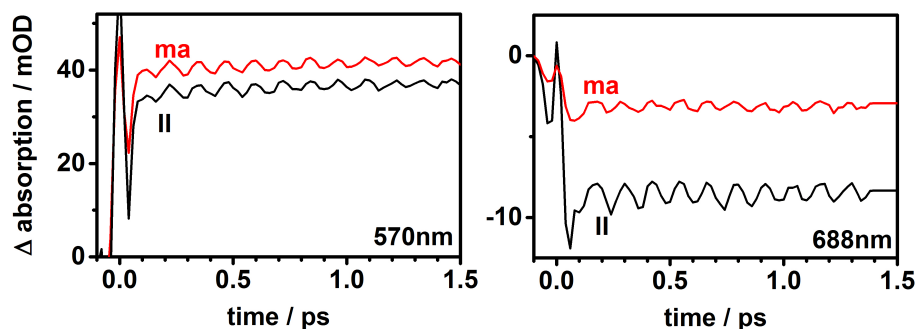
Figure 5.11: First 1.5 ps of the ESA and GSB signals of Tetraaza in toluene solution. Here the oscillations are most pronounced.
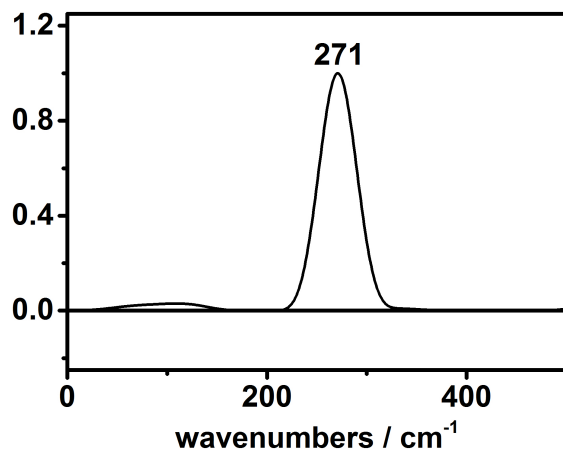
Figure 5.12: Fourier transformation of the GSB signal of Tetraaza gives a vibrational mode of 270 cm^{-1}.

Since there was no vibrational mode observed in Fourier-transform infrared measurements at the frequency range of 260-270 cm^{-1} (see Figure 5.13), it has to be Raman active.
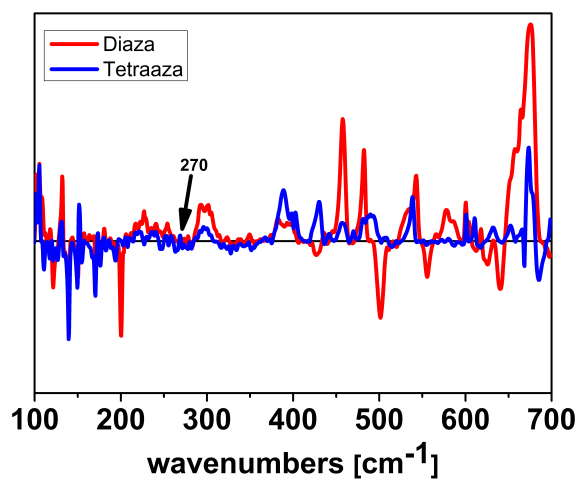
Figure 5.13: FTIR spectrum of Diaza (red) and Tetraaza (blue) in the low-frequency range. There is no mode observable at 270 cm^{-1}. The negative features arise from the analysis of each measurement since difference spectra (pure polymer vs. polymer with material) were taken.

In a recent study on TIPS-pentacene also a strong oscillatory feature at 265 cm^{-1} was identified by means of 2D electronic photon-echo spectroscopy.[103] Della Valle et *al.* stated that all modes above 200 cm^{-1} belong to intramolecular vibrations rather than to a phonon lattice ones.[104] In picene, a vibration of 260 cm^{-1} was assigned to an aromatic breathing mode.[105] In the pentacene radical cation spectrum a totally symmetric normal mode around 260 cm^{-1} was assigned to stem from the excitation from the ground to the excited state.[106]

Striking is the different behavior of TIPS-pentacene in solution after photo excitation compared to the aza-pentacenes. Although the steady state spectra of all compounds look very similar (see section 4.2), the transient absorption data of the heteroacenes show significant deviations compared with TIPS-pentacene. While in TIPS-pentacene the GSB has the highest intensity, Diaza and Tetraaza show almost no bleaching signal and the huge singlet ESA is the most pronounced feature instead. This leads to the assumption that TIPS-pentacene exhibits a larger extinction coefficient for the $S_0 \rightarrow S_1$ transition compared to Diaza and Tetraaza, where the $S_1 \rightarrow S_n$ transition dominates the spectrum. This different behavior after photo excitation demonstrates that the changed electronic structure (substitution of carbon by electron poor nitrogen atoms) influences the excited state dynamics and hence the relaxation network. In order to understand this dramatic change in the photo-induced dynamics of the azaacenes, sophisticated quantum chemical calculations of their excited states would be valuable. The size and multireference character of these systems makes the calculations very costly and challenging[25], however, knowledge about the corresponding energy levels are necessary for the interpretation of the experimental data. The overall excited state dynamics of TIPS-pentacene and its aza-derivatives in solution are summarized in the following scheme (5.14).
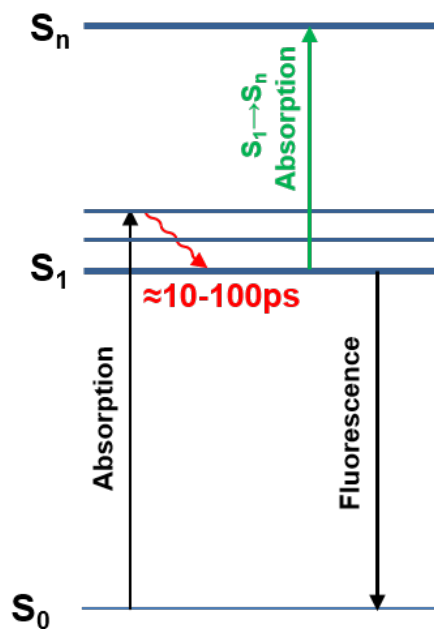
Figure 5.14: Kinetic model of the excited state dynamics of TIPS-pentacene and its aza-derivatives in solution. The vibrational relaxation takes place within 100 ps for Diaza and and within 10 ps for Tetraaza, for TIPS-pentacene there was no vibrational relaxation observed (for both excitation wavelengths).

5.2 Transient Absorption in Thin-Films

5.2.1 Ultrafast Dynamics of TIPS-Pentacene

Figure 5.15: Transient absorption spectra at several probe delay times in the visible and NIR spectral region of TIPS-pentacene.

The transient absorption signal of TIPS-pentacene presented in Figure 5.15 is in accordance with former experiments on the excited state dynamics.[28, 91, 101, 107, 108] They have been described by a decay of the singlet state with a concomitant rise of the triplet species confirming SF as the underlying process. The difference signal in the visible is comprised of a large ESA contribution and only small GSB features can be observed. This indicates a higher extinction coefficient for the $S_1 \rightarrow S_n$ transition compared with the ground state absorption and the GSB is overlaid by the ESA band. Around 700 nm the fast decaying SE is visible, but also superimposed by the GSB signal. The shoulder of the ESA signal around 490 nm decreases within the first 50 fs and the main absorption band (530 nm) rises thereafter. The former is assigned to the $S_1 \rightarrow S_n$ transition and the latter to the triplet ESA $T_1 \rightarrow T_n$, respectively. The decay of the singlet species can be followed at higher energies around 460 nm, where it is more separated from the triplet

band. Fitting single transients at 460 nm (singlet) and 530 nm (triplet) gives a decay and rise time of 155±20 fs (see Figure 5.16). The NIR spectral region shows a broad structureless ESA contribution, which continuously grows in the first 500 fs.

Figure 5.16: Transients at 460 nm (singlet) and 530 nm (triplet) with corresponding fits (monoexponential decay with a time constant of 155 fs and biexponential rise with two time constants of 155 fs and 1 ps). Please note that the dynamics were fitted after the coherent artefact contribution, which results from the overlapping pump and probe beam around delay time zero.

5.2.2 Ultrafast Dynamics of Diaza-TIPS-pentacene

The transient absorption data of Diaza are similar but red shifted (see Figure 5.17). The main absorption band is located at 570 nm and the shoulder at shorter wavelengths is not as pronounced as in TIPS-pentacene. The singlet contribution becomes apparent around 490 nm and decays within the first 30 fs. As for TIPS-pentacene, the main absorption band rises afterwards, proving SF to proceed very rapidly in Diaza.
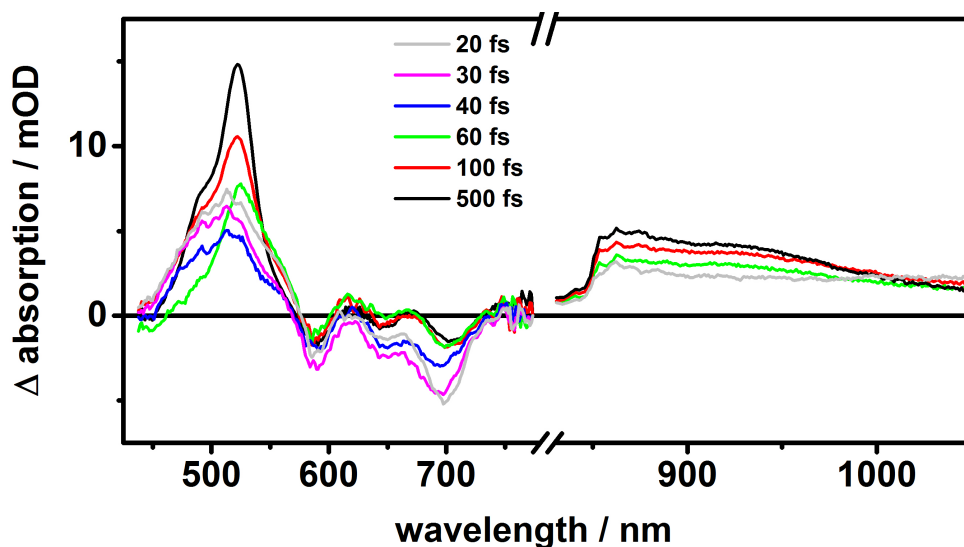
Figure 5.17: Transient absorption spectra at several probe delay times in the visible and NIR spectral region of Diaza.
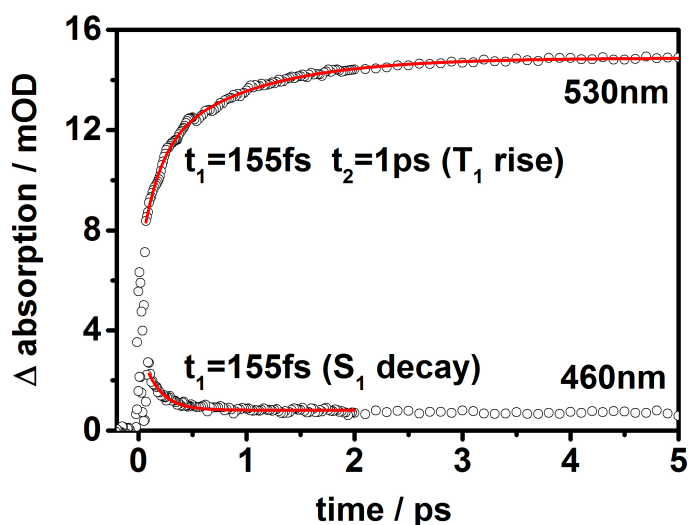

Figure 5.18: Transients at 490 nm (singlet) and 570 nm (triplet) with corresponding fits (monoexponential decay with a time constant of 85 fs and biexponential rise with two time constants of 85 fs and 1 ps). Please note that the dynamics were fitted after the coherent artefact contribution which results from the overlapping pump and probe beam around delay time zero.

In Figure 5.18 a monoexponential fit of the singlet state at 475 nm gives a time constant of 85±20 fs. Accordingly, the rise of the triplet around 570 nm shows a time constant of 85±10 fs and a second component of 1±0.2 ps. Due to the red-shift of the transient signal, a GSB contribution is visible around 460 nm. The relative amplitude between the signal in the visible and NIR spectral region is interesting to note: Diaza features a stronger absorption band in the NIR relative to the band in the visible than TIPS-pentacene.

5.2.3 Ultrafast Dynamics of Tetraaza-TIPS-pentacene

The transient absorption data of Tetraaza, where four carbon atoms are substituted by nitrogen will be discussed in the following. The chemical modification leads to a molecule where the symmetry is conserved, but the electronic properties are different when compared to TIPS-pentacene. This becomes obvious in its excited state dynamics as illustrated in Figure 5.19.
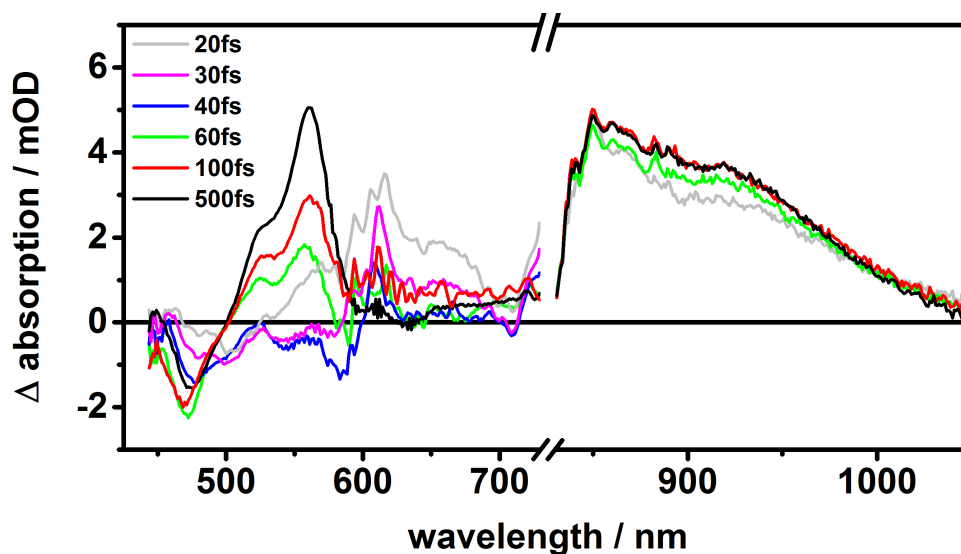
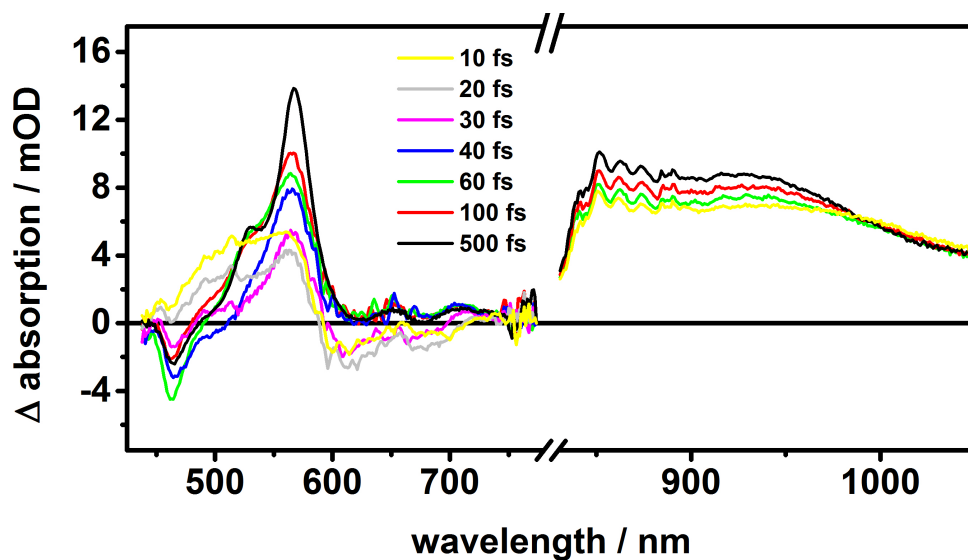**Figure 5.19:** Transient absorption spectra at several probe delay times in the visible and NIR spectral region of Tetraaza.

Here the first detected difference signal is visible at wavelengths around 620 nm and not at higher energies ($\leq$500 nm) as observed for TIPS-pentacene and Diaza. This species decays with a time constant of 100$\pm$20 fs and is assigned to a singlet state with a concomitant rise of the triplet species, which builds up with a biexponential function of 95$\pm$10 fs and 1$\pm$0.2 ps (see Figure 5.20). As for Diaza, a GSB contribution at short wavelengths around 470 nm is detected. Tetraaza exhibits a strong absorption band in the NIR relative to the band in the visible, which might indicate higher quantum efficiencies in this material. The higher noise level around the excitation (600 nm) is due to interference effects occurring between pump pulse scattering with the probe beam.
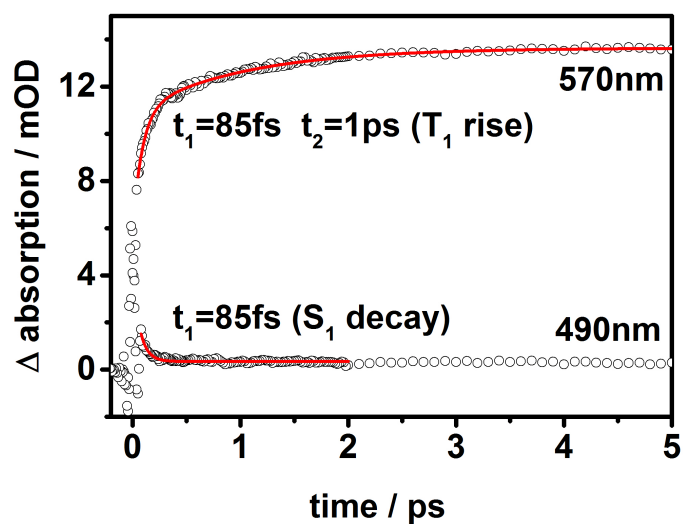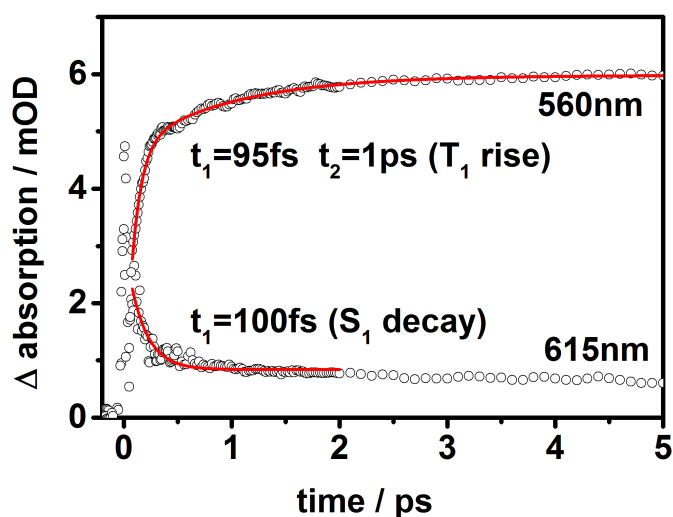

Figure 5.20: Transients at 560 nm (triplet) and 615 nm (singlet) with corresponding fits (monoexponential decay with a time constant of 100 fs and biexponential rise with two time constants of 95 fs and 1 ps). Please note that the dynamics were fitted after the coherent artefact contribution, which results from the overlapping pump and probe beam around delay time zero.

5.2.4   Global Target Analysis

As described before in section 3.3.1 a global target analysis is indispensable to disentangle the spectrally overlapping transient absorption signal and extract the intrinsic dynamics of the investigated systems. Therefore a global fitting routine is carried out to elucidate the relaxation pathways probed in the visible and in the NIR spectral range. A selection of tested models is given in Figure 5.21, the sequential model with three species, a branched model with three species and a mixed model (branched and sequential) with four species.

sequential   **branched**   **mixed**
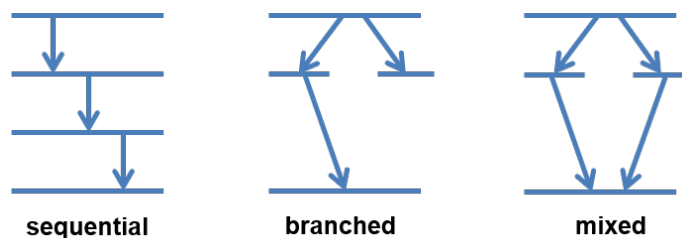
Figure 5.21: Tested kinetic models to describe the ultrafast dynamics of TIPS-pentacene and its aza-derivatives via a global target analysis.

It has been observed that the sequential model describes the data in the most accurate way.[107] Using a branched model, where an initial component can relax into two different channels leads to higher fitting errors. Above all, one arm of the branching exhibits an infinite time constant, i.e. it is unactivated. Hence, a sequential model is independently formed, confirming this as the underlying kinetic model to fit the transient absorption data, which is in line with previous studies on other acenes.[36, 101, 109, 110]

Since all of the pentacene-derivatives show similar excited state dynamics with spectrally shifted bands, a sequential model was used for all three compounds (TIPS-pentacence, Diaza, Tetraaza). The species associated spectra (SAS) gained for TIPS-pentacene in the visible are presented in Figure 5.22. The first species displays a broad spectrum with a contribution in the blue wing of the detection range (450-480 nm), which decays with a time constant of 150 fs. The blue wing is absent in the other SAS and attributed to a species

with singlet character. The second SAS decays with a time constant of 1 ps
and the last species is required to fit the offset, since the time range of the
fit was only 5 ps and the triplet state does not decay within that time. The
GTA of the NIR data set leads to the same picture, however, astonishingly
the first species decays faster compared to the visible spectral region with a
time constant of 120 fs.

Figure 5.22: Species-associated spectra obtained from a global target anal-
ysis using a sequential model for TIPS-pentacene in the visible (left) and in
the NIR (right) spectral range.

Figure 5.23: Species-associated spectra obtained from a global target anal-
ysis using a sequential model for Diaza in the visible (left) and in the NIR
(right) spectral range.

Target analysis for Diaza shows similar results but reveals much shorter initial dynamics as can be seen in Figure 5.23. The singlet species in the blue wing of the spectrum decays with a time constant of 75 fs in the visible. In the NIR, the singlet contribution decays with 55 fs and is more pronounced at higher wavelengths. Hence, the SF dynamics are accelerated by a factor of two in this unsymmetrically substituted heteroacene compared to TIPS-pentacene.

As mentioned above, the transient absorption signal of Tetraaza differs from the other two compounds with regard to the spectral position of the singlet state. This observation is supported by the global fit as shown in Figure 5.24. The first species exhibits a contribution around 620 nm and a negligible feature at shorter wavelengths. Thus, the shoulder at 520 nm observed in the transient absorption signal is not correlated to a contribution of singlet character and the triplet state is more separated when compared to TIPS-pentacene and Diaza. This finding emphasizes the great impact of a small change in the pentacene backbone and the potential of this molecule class to tune their optical properties by chemical modifications. The overall kinetics are similar and the time constant for the triplet formation lies in between the ones found for TIPS-pentacene and Diaza with 100 fs in the visible and 55 fs in the NIR.
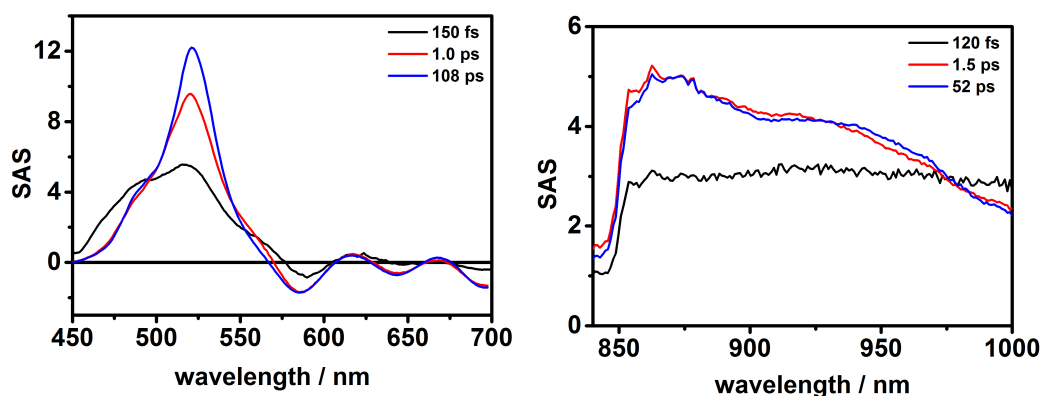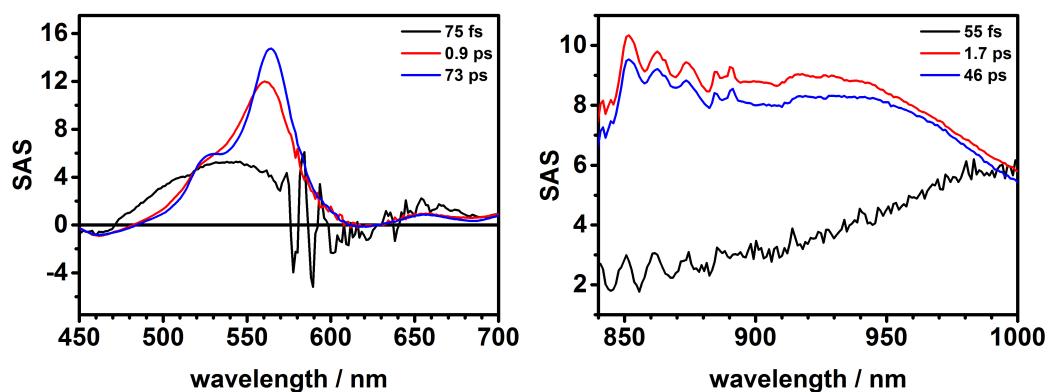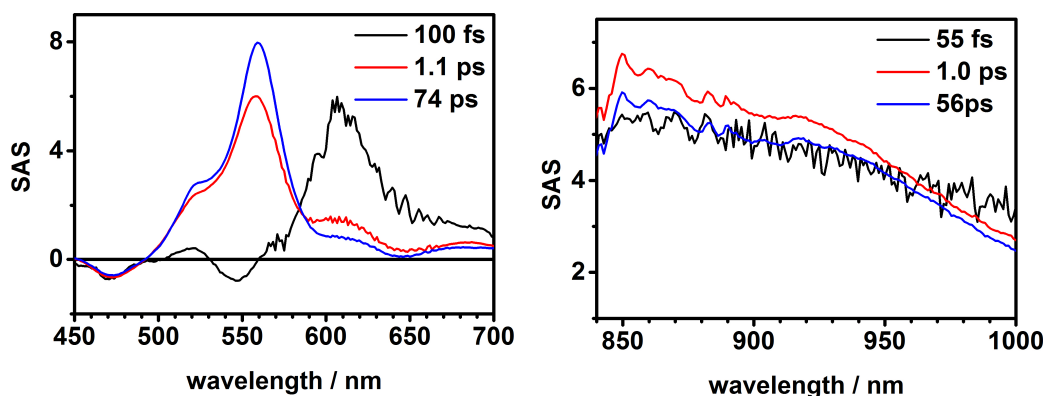

Figure 5.24: Species-associated spectra obtained from a global analysis using a sequential model for Tetraaza in the visible (left) and in the NIR (right) spectral range.

5.2.5   TIPS-pentacene:Diaza-TIPS-pentacene Mixtures

In order to change the morphology of the thin-films and thereby the SF dynamics, mixtures of TIPS-pentacene and Diaza with different concentration ratios were prepared. Since Diaza has lowered energy states, the idea was to first excite both compounds followed by a charge transfer from TIPS-pentacene to Diaza. In that way it may be possible to generate directly triplets via SF in Diaza in the first step and an additional channel populates the triplet manifold after charge transfer from TIPS-pentacene to Diaza. The challenge is though to find the optimal concentration ratio between the compounds in order to get the right composition and morphology to enhance the triplet yield. Polarized microscope images illustrate the different morphology of the films with varying concentrations of TIPS-pentacene and Diaza.
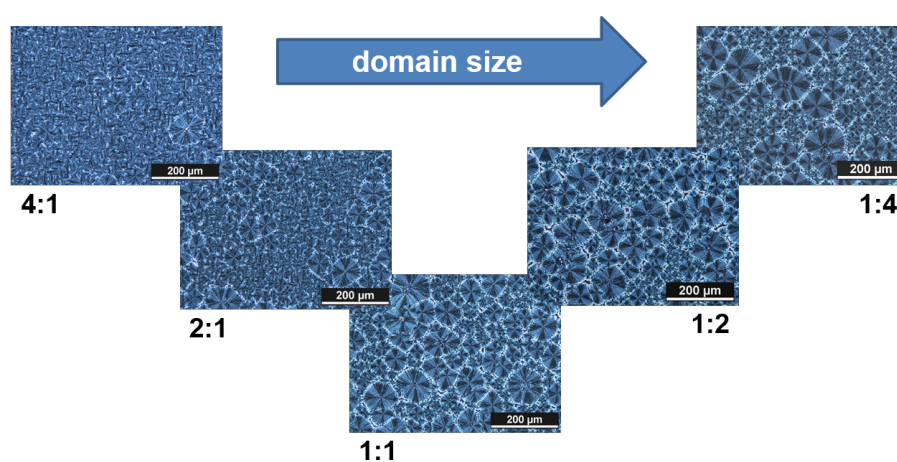
Figure 5.25: Polarized microscope images of thin-films of TIPS and Diaza mixtures with different TIPS:Diaza ratios starting from 4:1 (left) over 2:1 and 1:1 to 1:2 and 1:4 on the right hand side. With an increasing Diaza concentration the domain size is getting larger as indicated by the arrow.

Following the pictures in Figure 5.25 from the left to the right, one can notice the growing domain size with an increasing Diaza concentration. Starting with a TIPS:Diaza ratio of 4:1 on the left, the domain size is small and only isolated spots of larger domains are visible. The amount of larger domains increases at a ratio of 2:1. At a ratio of 1:1 there is already an excess of large

domains observable, indicating Diaza as the abundant species, but always with small domains of TIPS-pentacene in between. Higher concentrations of Diaza result in an even larger domain size, which is visible on the image on the right side of Figure 5.25. The according steady state UV-VIS absorption spectra of the mixtures are shown in Figure 5.26. By increasing the Diaza concentration, a redshift is observable as one would expect. Simultaneously, the band structure becomes more J-aggregate-type as shown previously for the pure Diaza thin-film. Already at a ratio of 1:1 (yellow line in Figure 5.26) the spectral features are dominated by Diaza. The contribution of the band in the UV spectral region is growing, which is also in accordance with the pure spectrum of Diaza when compared with TIPS-pentacene.
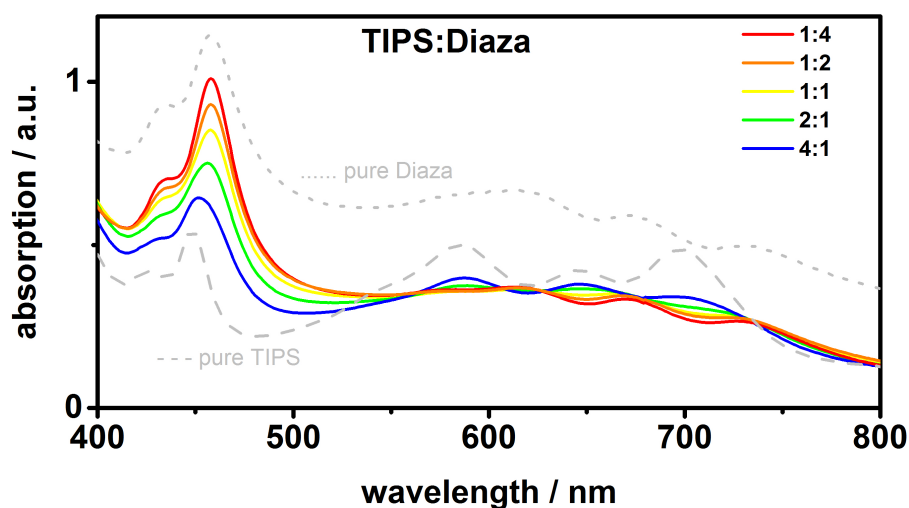
Figure 5.26: Steady state UV-vis absorption spectra of mixtures with different TIPS:Diaza ratios togehter with the pure spectra of TIPS (grey dashed line) and Diaza (grey dotted line).

Both the polarized microscope images as well as the static absorption spectra show, that the theoretical TIPS:Diaza ratio of 1:1 is not reflected in the experimental observations. In other words, the real concentration of the mixture on the thin-film differs from the composition used during the spin-coating procedure. This may be related to a different crystallization of the two compounds. If one material crystallizes first, which means that the sol-

vent evaporates faster, this compound will affect the overall morphology of
the thin-film. The static spectra thus are comprised of both compounds,
which is reflected in a superposition of both absorption bands. Both mate-
rials crystallize in their preferred orientation and no intermediate, such as a
new crystallization pattern is observed. The different surface roughness of
the thin-films can be illustrated in AFM images, which present TIPS:Diaza
ratios of 1:4 and 4:1. There might be an inter layer between the materials,
represented by the smeared domains around the black areas shown in the
AFM image in Figure 5.27 on the right (TIPS:Diaza ratio of 1:4).
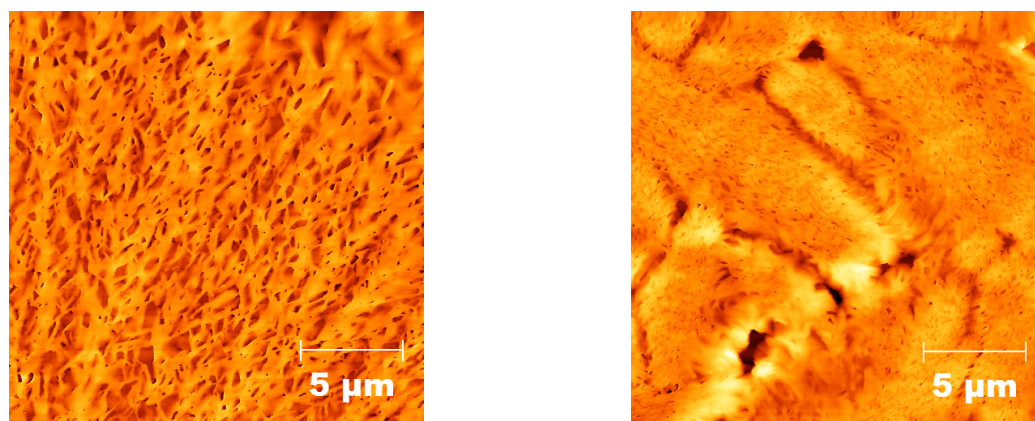
Figure 5.27: AFM images of TIPS:Diaza mixed thin films with ratios of
4:1 (left) and 1:4 (right).

In the following, transient absorption data on these mixtures of Diaza and
TIPS-Pentacene are presented. In Figure 5.28 the data with the highest
concentration differences are shown, where the TIPS:Diaza ratio is 4:1 and
1:4, respectively. On the left side of Figure 5.28 the spectrum is dominated
by the TIPS-pentacene dynamics, however, there is a shoulder observable
at higher wavelengths stemming from Diaza. On the right hand side, the
spectrum is solely comprised of the Diaza dynamics and no features of TIPS-
pentacene are present. The ΔmOD values for the TIPS-pentacene dominated
thin-film are slightly higher compared to the film where Diaza is the abundant
species.
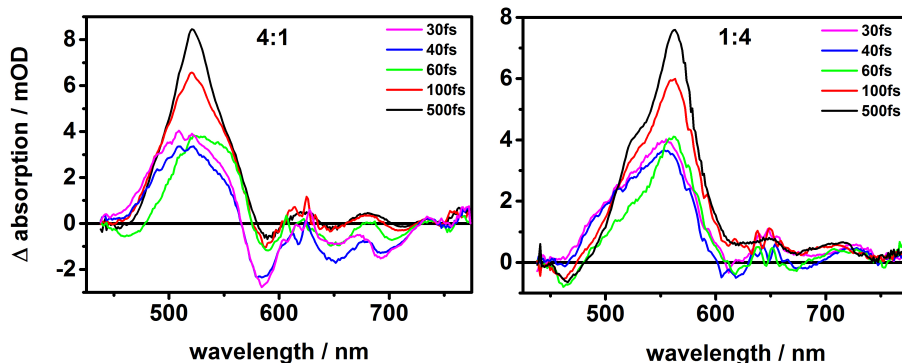
Figure 5.28: Transient absorption data of TIPS:Diaza mixtures with a ratio of 4:1 (left) and 1:4 (right).

At a ratio of 1:1 the ESA is very broad and shows a superposition of the dynamics with a split absorption maximum. Interesting to note is the case where the TIPS:Diaza ratio is 1:2 and the overall dynamics are dominated by Diaza. Here the intensity of the transient signal exceeds the ones from all the other compositions by a more than 20%, as represented in the corresponding ΔmOD values by using the same excitation energy.
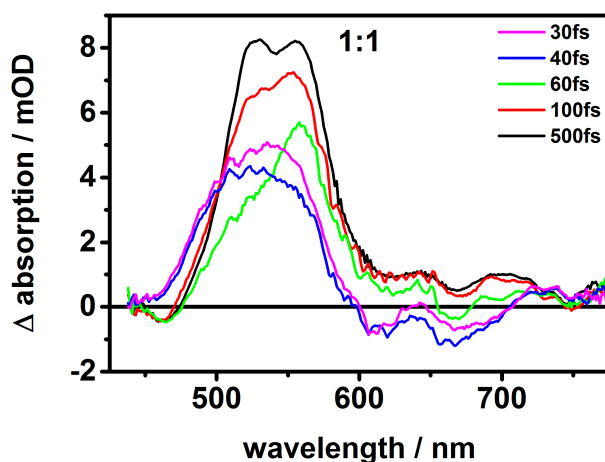
Figure 5.29: Transient absorption data of a TIPS:Diaza mixture with a ratio of 1:1.
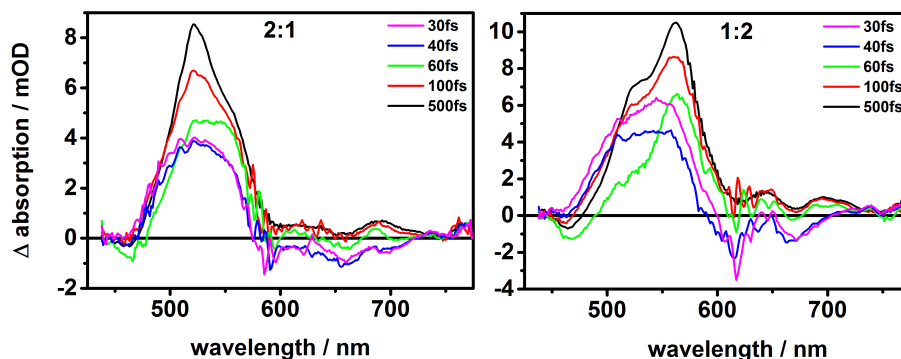
Figure 5.30: Transient absorption data of TIPS:Diaza mixtures with a ratio of 2:1 (left) and 1:2 (right).

Since the signal maximum can be correlated to the generated triplet excitons, this finding suggests a higher quantum yield for a Diaza:TIPS ratio of 1:2 assuming same oscillator strengths for the corresponding transitions. Basically, the sample preparation procedure is very reliable regarding the homogeneity of the thin-films, however, small irregularities in the film structure can lead to an altered dynamics. Therefore, more studies have to be carried out to reproduce and confirm the presented observations. Moreover, the influence of experimental parameters, such as excitation wavelength and pump energy on the dynamics needs to be understood in more detail. One possible next step would be to build a solar cell with these two materials and see if an increased triplet yield leads also to a larger amount of charge carriers.

5.2.6 Energy Dependence and Annihilation

An important matter to be aware of is thermal heating and annihilation.[37, 38, 42, 111–114] Both processes are a result of too high laser intensities during an experiment. Therefore a moderate photon flux has to be maintained that leads to a satisfactory signal-to-noise ratio on the one hand and to linear absorption behavior on the other. Figure 5.31 shows the transient absorption signal evolution of TIPS-pentacene for the first 100 ps when excited

with increasing pulse energies. Following the transients it can be seen that an increased excitation pulse energy leads to a decay behavior instead of a growing signal as observed for low intensities (20 nJ per pulse). This dramatic change in the signal evolution is illustrated in Figure 5.32, where two transients of 20 and 200 nJ per pulse are compared.
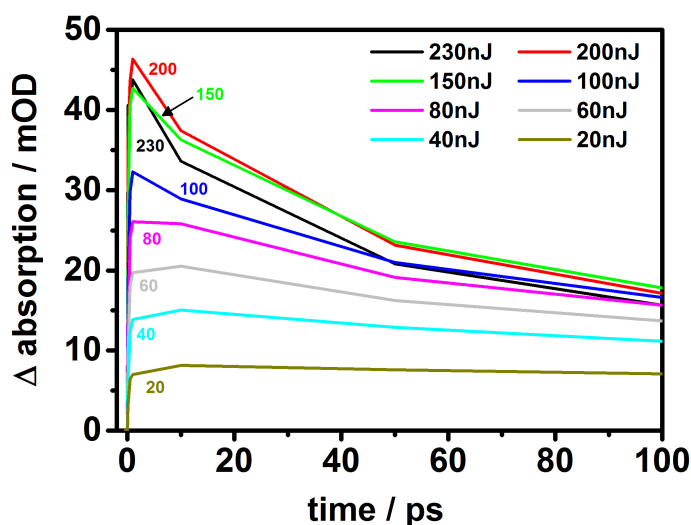
Figure 5.31: Transient absorption signal evolution of TIPS-pentacene at 530 nm for a time delay up to 100 ps using increasing excitation energies.
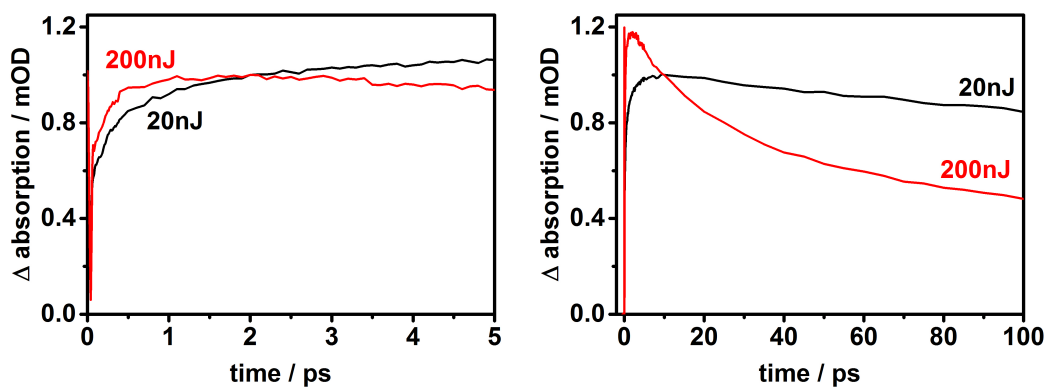
Figure 5.32: Transient absorption signal of TIPS-pentancene at 530 nm with 20 nJ (black curve) and 200 nJ (red curve) excitation energies for a time delay up to 5 ps (left) and up to 100 ps (right).

The decay instead of a triplet rise is a consequence of exciton-exciton or exciton-charge annihilation as explained in the following (see Figure 5.33).[37, 38, 112–114]
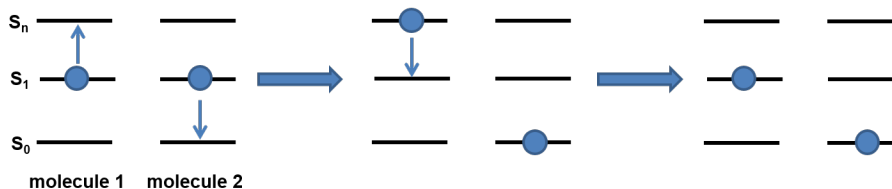
Figure 5.33: Schematic representation of the exciton-exciton annihilation process. Two excited molecules interact with each other creating a higher excited molecule, which subsequently relaxes back to the S_1 state and a molecule in the ground state.

In case of high excitation intensities it may happen that two nearby molecules are excited. Now one excitation is transferred onto an already excited molecule creating a higher excited state S_n followed by rapid internal conversion back to the first excited state, whereas the other molecule relaxes to the ground state. The result of the process is that one excitation gets lost - it is annihilated.
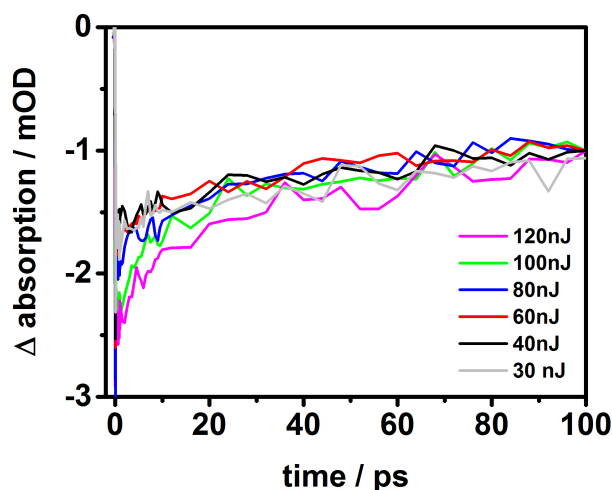
Figure 5.34: Transient absorption signal evolution at 465 nm of Diaza for 100 ps using several excitation energies.

This faster recovery to the ground state can be observed for Diaza (because the excited state dynamics are red shifted), where a GSB signal is detected around 460 nm. Figure 5.34 shows the faster GSB recovery after photoexcitation with higher pulse energies. This is a consequence of annihilation, since one of the two excited molecules relaxes back to the ground state. The decay was fitted by means of a biexponential fit and the gained time constants are plotted against the excitation pulse energy as presented in Figure 5.35. It is demonstrated that the excitation energies have to be kept below 40 nJ per pulse in order to prevent annihilation effects. This observation proofs that the presented dynamics and obtained time constants are not affected by exciton-exciton annihilation effects.
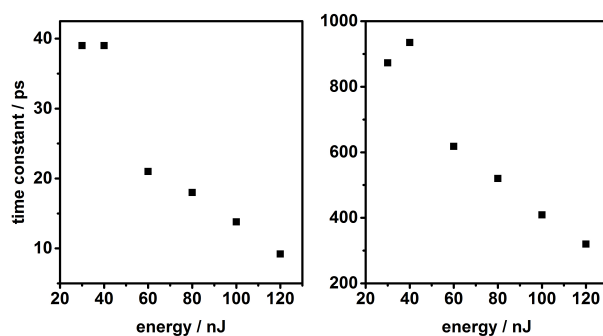
Figure 5.35: Plot of the first (left) and second (right) time constant gained from a biexponential fitting against the increasing excitation energies.

5.2.7 Discussion

The investigation of the ultrafast dynamics of TIPS-pentacene and its aza-derivatives reveals that the carbon to nitrogen substitution results in an acceleration of the overall kinetics. In toluene solution, the fluorescence decays with a time constant of 12 ns for TIPS-pentacene, 7.5 ns for Tetraaza and 5 ns for Diaza. The redshift of the corresponding bands in the absorption and fluorescence spectra increases in the same order. The changed electronic network as a consequence of the different charge distribution over the molecules effectively influences the excited state dynamics, which becomes obvious in

the different transient absorption signal for TIPS-pentacene in solution. A
similar steady state absorption does not necessarily lead to similar excited
state dynamics, i.e. results in dramatic changes of the relaxation network.
The addition of sp^2 nitrogen atoms into the backbone of TIPS-pentacene
also leads to faster kinetics in the solid state, where SF is sped up. As the
efficiency potentially increases with faster dynamics, Tetraaza and especially
Diaza undergo SF in a more efficient way compared with TIPS-pentacene
itself. Stronger intermolecular coupling as a consequence of a smaller $\pi - \pi$
distance in Diaza compared to TIPS-pentacene may explain the accelera-
tion of SF as it was recently stated in a similar study on nitrogen-containing
TIPS-pentacenes.[108] A possible indication of a higher triplet quantum yield
in Diaza and Tetraaza is the stronger $(T_1 \rightarrow T_2)$ signal in the NIR relative to
that in the visible spectral region when compared to TIPS-pentacene, assum-
ing a similar extinction coefficient. Considering the energies of the HOMO
and LUMO, which are more stabilized in the heteroacenes, we would expect
similar effects on the triplet state. In particular if the T_1 state exhibits a
stronger shift, SF should be more exoergic.

A closer look at the results of the GTA reveals fundamental aspects of the
triplet formation in this molecule class. First, the assumption that the NIR
absorption range is free of a singlet contribution as claimed for pentacene[42]
and TIPS-pentacene[28], is not in accordance with our experimental obser-
vations for TIPS-pentacene and its aza-derivatives. There is a very fast
decaying contribution in the NIR spectral region with time constants of 120
fs for TIPS-pentacene and 55 fs for Diaza and Tetraaza. This species cannot
have triplet origin because it is populated directly with the laser interaction.
As for the singlet contribution in the visible spectral region, it is strongly
overlapped with the triplet signal. This finding explains why fitting of the
kinetics is very challenging and hence, pinpointing accurately the triplet state
at one specific wavelength. Second, the formation of triplet species in the
visible and in the NIR takes place with different time constants suggesting
that two different ultrafast channels are involved. For all three investigated
compounds a shorter time constant for the first species is observed in the
NIR spectral region compared to the visible. This raises important ques-

tions regarding the triplet population and relaxation dynamics. If the two transitions in the visible and NIR spectral region would have different origins, i.e. separated initial states, they would not probe the same triplet state T_1. Different initial states could in turn lead to a changed triplet formation in the two spectral ranges. Furthermore, there is no evidence that the population of each transition ends up in the same final excited state. However, if only one triplet state is probed in the two spectral ranges, the triplet transitions should exhibit the same time constants. A possibility to clarify whether the two transitions have the same origin or not, is to perform pump-depletion-probe experiments in this two spectral ranges as shown in the following section 5.3.

A further approach to enhance the quantum efficiency is the creation of a mixture of two materials that show different HOMO and LUMO energies. There SF can first take place directly and then after a charge transfer from the energetically higher lying compound to a lower lying one. Different thin-films with varying concentrations of TIPS-pentacene and Diaza are investigated by transient absorption measurements. Since Diaza has lowered energy states, the idea was to first excite both compounds followed by a charge transfer from TIPS-pentacene to Diaza. In films with a TIPS:Diaza ratio of 1:2 an increased difference signal of more than 20% is observed, which also exceeds the intensity of a TIPS:Diaza film with a 4:1 composition. This is promising with regard to their application as donor and acceptor materials within a solar cell. By using an acceptor that also undergoes SF like the donor material, higher triplet yields could be achieved and thus more charge carriers be generated. However, the studies on mixtures are a first attempt to achieve higher triplet yields and the results need to be confirmed in further investigations. Particular importance has to be paid on the thin-film homogeneity and more experiments have to be carried out to reproduce the observations. This approach of mixing different materials is promising and underlines the potential of aza-derivatives to optimize efficiencies compared with TIPS-pentacene. Additionally, the high resistance against air is a benefit of these new materials for organic electronics applications.

5.3   Pump-Depletion-Probe

In order to gain more insight into the triplet population and relaxation dynamics, femtosecond pump-depletion-probe experiments in the visible as well as in the NIR spectral range were performed.[115] By combining information obtained from the experiment with simulations, a better understanding on how the triplet manifold is populated via the SF mechanism is obtained. Unveiling the origin of the different triplet rise times in the visible and NIR spectral region observed in TIPS-pentacene and its aza-derivatives is the core of this thesis. By studying these new materials, which show similar SF dynamics but spectrally shifted transitions, complementary information on the excited state dynamics is provided. More precisely, due to the spectrally separated singlet contribution in these two systems the triplet formation can be studied independently at the wavelengths chosen for the pump-depletion-probe experiment.

5.3.1   Pump-Depletion-Probe on TIPS-Pentacene

First, the experimental results on TIPS-pentacene are presented. The pump beam centered at 600 nm showed a pulse duration of 14 fs. The experimental setup and details are shown in section 5.3. The depletion pulse around 530 nm with a pulse duration of 18 fs has a bandwidth that nicely matches the triplet ESA of TIPS-pentacene as shown in Figure 5.36. The temporal resolution of the experiments was calculated to be 40 fs in the visible and ca. 100 fs in the NIR (by fitting the curves of the correlated coherent artifacts as shown in chapter 3). As the pump beam is chopped just an effect on the dynamics induced by the pump pulse is observed and the dynamics generated by the depletion pulse ($S_0 \rightarrow S_1$) are not monitored.
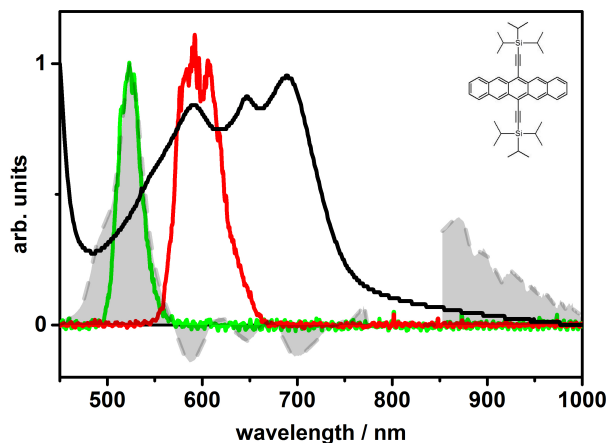
Figure 5.36: UV-vis spectrum of a spin-coated TIPS-pentacene thin-film (black line) together with the excitation spectrum (red), the depletion spectrum (green) and the transient absorption spectrum at a pump-probe delay of 1 ps (grey shaded area).

The pump-depletion experiments probed in the visible as well as in the NIR spectral region are shown in Figure 5.37. The rising dynamics of the triplet species in the visible spectral region are described first. Transients illustrate the evolution of the ESA signals at 530 nm, which are disturbed by the depletion pulse at a selected time T. A loss of signal can be clearly seen when the depletion pulse comes at least 100 fs after the pump pulse (when T=100 fs, 200 fs and 1 ps). The resulting dip feature is sharp and more pronounced at larger T values. The signal recovers after the perturbation, but not all the population comes back when compared to the signal intensity before the depletion pulse arrives. In spite of an experimental response time of approximately 40 fs, the typical dip feature caused by the interaction with the depletion pulse cannot be resolved for T=50 fs (see Figure 5.37 left). The experimental data probed in the NIR look different as shown in Figure 5.37 (right). A loss of signal after depleting the triplet ESA in the visible is clearly observable only for T=1 ps. However, the dip feature is less sharp and builds up with time. No recovery of the signal is measured after the depletion action but a decay behavior can be observed instead, or in other respect, a small rise of the depletion effect. At T=200 fs a depletion effect

can still be detected but the dip feature is much less pronounced and the signal does not recover again. For T values of 100 and 50 fs no dip feature is observed, within the given temporal resolution of approximately 100 fs.
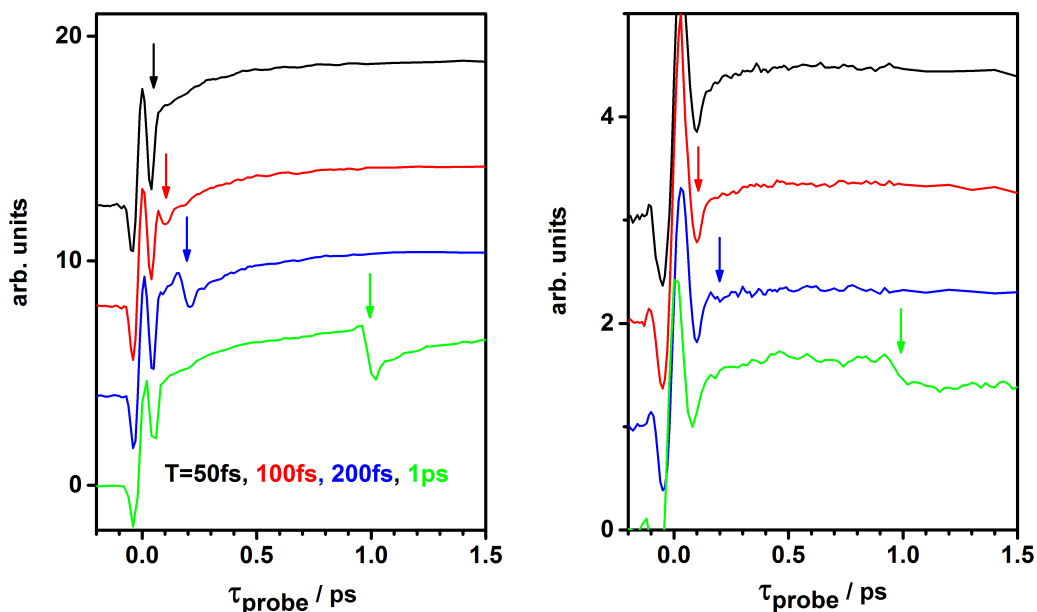
Figure 5.37: Results of the pump-depletion-probe experiments probed in the visible (left) and in the NIR spectral region (right). The probing wavelength of the depicted transients is 530 nm in the visible and an averaged wavelength range from 850 to 860 nm in the NIR. The data sets were vertically shifted in order to clearly illustrate the depletion effect of the single transients. The arrows indicate the arrival time of the depletion pulse.

The experimental results in the visible spectral range are explained as follows. Considering a time constant of 150 fs for the triplet rise (obtained from the global fit), at τ_{probe}=1 ps all the population is already transferred to the triplet state.[107] As the depletion pulse is applied to the triplet ESA, the depletion effect increases with time and is most pronounced at T=1 ps. However, a depletion effect is visible in the transient data at early time delays (τ_{probe}=50-200 fs) when the triplet state has not fully developed. Thus, the observation of a dip feature when the depletion pulse interacts 100 and 200 fs after the pump pulse indicates that also the singlet state ($S_0 \rightarrow S_1$ transition)

is affected by the depletion pulse centered at 530 nm. This finding is related to the broad spectral overlap of the singlet and triplet ESAs in the visible spectral region. Since the depletion pulse is also resonant with the ground state spectrum of TIPS-pentacene it re-excites the S_1 state and decreases the effect of the triplet ESA depletion. The re-excitation of the S_1 state is demonstrated in Figure 5.38, where transients at 475 nm are presented. It shows that the singlet contribution, which has a higher amplitude in this spectral range immediately grows after the depletion pulse is applied.
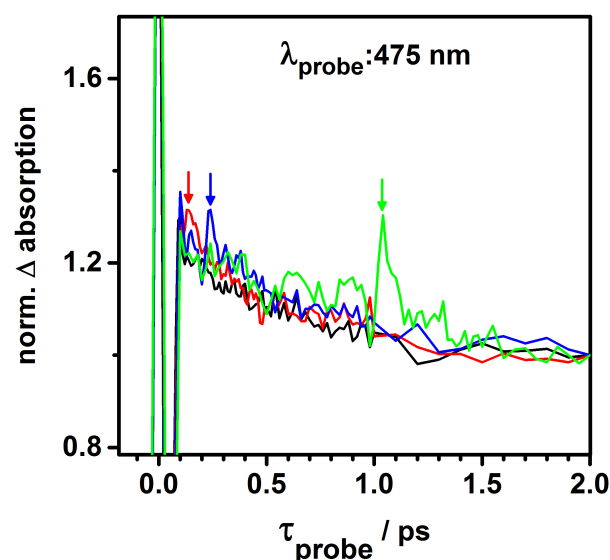
Figure 5.38: Pump-depletion-probe raw data (dashed lines) of TIPS-pentacene probed at 475 nm. The arrows indicate the arrival of the depletion pulse which demonstrates the re-excitation of the S_1 state.

The signal growth (or decay of the depletion effect) after the depletion action in the visible can be explained by this re-excitation, which later re-populates the triplet manifold. The triplet band is shifted to higher wavelengths and located around 530 nm. By looking at the signal before and after the depletion action it can be estimated from the transient probed at 530 nm that approximately one half of the population comes back. The time constants of the recovery are in the same range for all measured transients as shown in Figure 5.39. This means that the triplet signal recovers inden-

pendently from the arrival time of the depletion pulse. However, the time
constants are slightly shorter compared to the triplet rise time obtained from
the conventional pump-probe experiments (155 fs, see section 5.2). This is a
consequence of several effects that are overlapping, i.e. relaxation from higher
excited states back to the T_3 state, direct population of T_3 after exciting the
$S_0 \rightarrow S_1$ transition with the depletion pulse and delayed population after the
S_n state has decayed and relaxes into T_3.
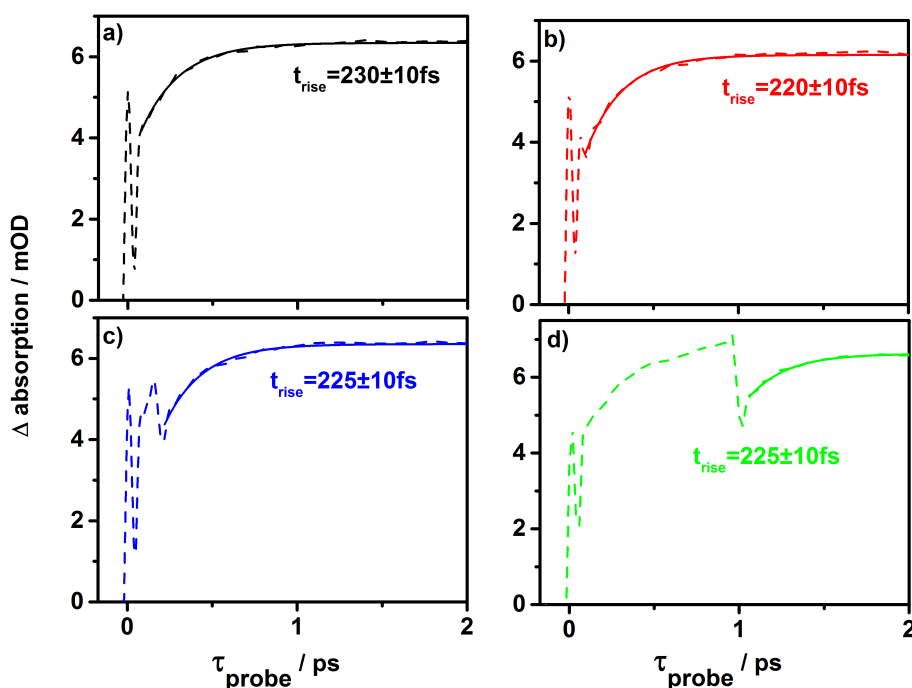
Figure 5.39: Pump-depletion-probe raw data (dashed lines) probed at 530
nm with a corresponding fit (solid line) after arrival of the depletion pulse.
a) T=50 fs, b) T=100 fs, c) T=200 fs, d) T=1 ps

The fact that we do not see a dip feature at T=50 is related to the overlap-
ping coherence spike, resulting from the interaction between the pump and
the probe pulse. In principle, there is a depletion effect from the beginning on
when compared to a transient where no depletion pulse is applied as shown in
Figure 5.40. However, it is challenging to quantify the interaction. A direct
comparison of the signal amplitude of the individual data sets is not possi-

ble since they were taken on different sample spots. This is necessary due to sample degradation which occurs after long time radiation. During the pump-depletion-probe experiment the energy interacts twice with the sample (pump and depletion) leading to a higher photon flux on the sample. The amount of signal that is depleted can therefore not be determined directly.
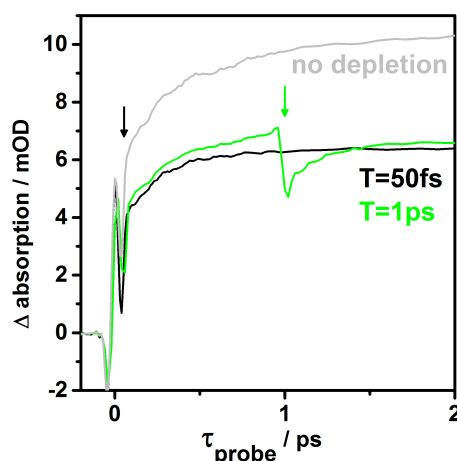
Figure 5.40: Comparison of transient data without (grey) and with depletion pulse at 50 fs (black) and 1ps (green). The arrows indicate the time of the depletion interaction.

In Figure 5.37 it is distinguishable that the triplet ESA probed in the NIR is influenced by the depletion pulse applied in the visible. The different evolution of the signal after applying the depletion pulse at T=1 ps, though, is particularly puzzling (see Figure 5.41). If the transition in the NIR and in the visible would occur from the same state, the depletion pulse should have the same effect on the dynamics, i.e. lead to a sharp dip feature and a signal recovery after the depletion action. In order to observe a signal evolution after the depletion action as experimentally found for the NIR ESA, i.e. a further decay of the signal, a population gain in the excited or a population loss in the initial state is required. In relation to the excited state dynamics of TIPS-pentacene more population in the excited state (T_2) or less population in the T_1 state is required to get the inverted recovery signal. This would either require a decay of the triplet state T_1, what is highly unlikely (and not

97

observed in the visible data) or a population transfer to the T_2 state. A rate model simulation is performed to clarify if the slow increase of the depletion effect (NIR) can be generated by a population gain in the excited state that is probed (T_2) in contrast to the sharp dip feature seen in the visible. The interpretation of the data is only possible, if all the mentioned contributions to the signal are considered and quantified. In other words, the simulation of the depletion signal to extract information from the experimental results becomes essential.
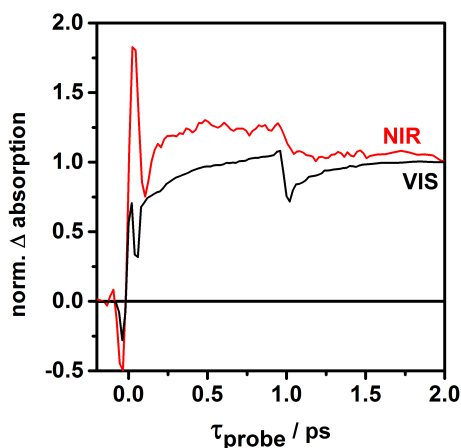
Figure 5.41: Comparison of the depletion effect (depletion at 530 nm, 1 ps after excitation) probed in the visible (530 nm, black curve) and in the near-infrared (850-860 nm, red curve) spectral region for TIPS-pentacene. Data was normalized at τ_{probe}=2 ps.

5.3.2 Rate Model Simulation

The pump-depletion-probe experiments contain a huge amount of information and several contributions account for the observed signal. The interpretation of the data is only possible, if all these contributions to the signal are considered and quantified. The input for the rate model simulation consists of the population of the singlet ground (S_0) and excited state (S_1), the population of the triplet states (T_{hot}, T_1, T_2, T_3) and their connected decay rates according to the respective rate model. In principle, the population of each

state is calculated dependent on the decay rate for every delay time τ_{probe}. At a set time T, the depletion effect is applied. The amount of population that gets depleted can be obtained from the amount of the depletion effect in the experimental data. Furthermore, a certain amount of singlet re-population due to the $S_0 \rightarrow S_1$ excitation by the depletion pulse itself is considered. Since the depletion at 530 nm is resonant with the $T_1 \rightarrow T_3$ transition, the excitation of T_3 is also included. The simulated depletion effect is then again added to the population at time T. This leads to a "new" population including the rise and decay dynamics, the depletion effect on the singlet and triplet states with a certain amount of singlet re-excitation and T_3 excitation. To simulate the signal at a specific wavelength, the relative amplitudes of the singlet and triplet contributions have to be considered. For example, at 530 nm the amount of the triplet ESA contribution relative to the singlet ESA contribution is about 80 %. In order to take the coherence spike into account, Equation 3.3 was included in the simulation. Additionally, we convolute our simulated signal with a Gaussian to take our experimental resolution into account. The results of the pump-depletion-probe experiment were simulated with the following kinetic model (see Figure 5.42).
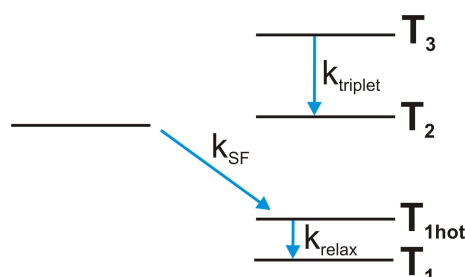
Figure 5.42: Rate model used in the simulation of the pump-depletion-probe signal of TIPS-pentacene in the visible and NIR. The rates of transitions were used as observed in the experiment.
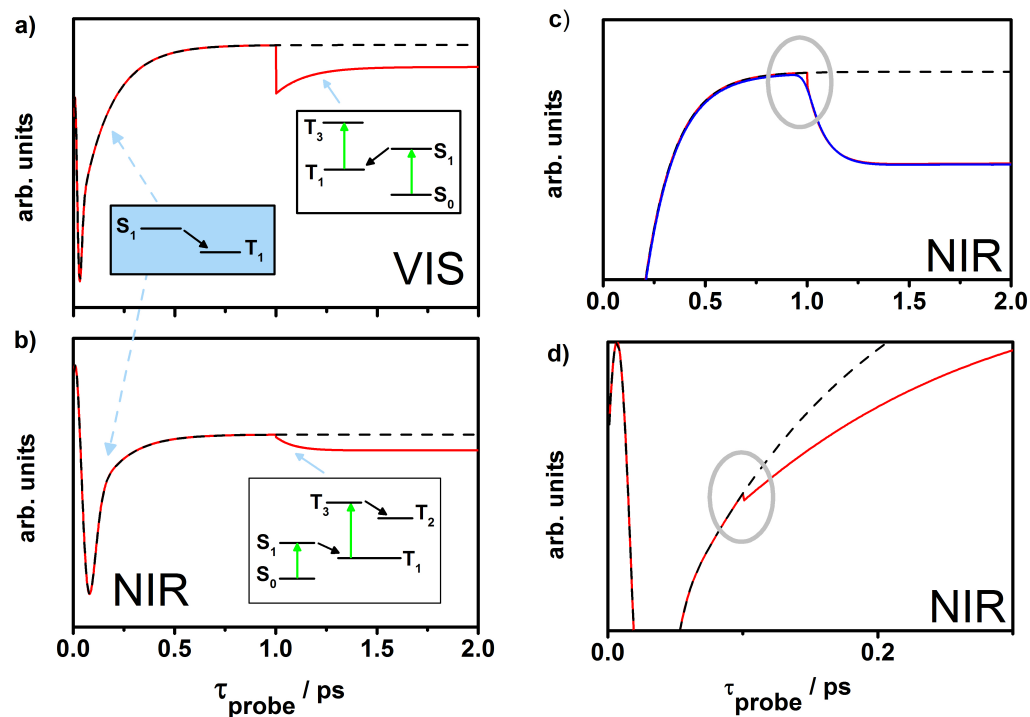
Figure 5.43: Simulation of the pump-depletion-probe signal of TIPS-pentacene. The dashed black line shows the transient dynamics without depletion effect. The red curve demonstrates the dynamics after applying a depletion pulse at 1 ps. a) Dynamics in the visible, b) in the NIR spectral range. The energy diagrams present the underlying processes that cause the signal. c) Zoom into the signal in the NIR of Figure 5.43b), the blue curve takes the experimental response time into account. here, the sharp dip feature cannot resolved. d) Simulated signal, when the depletion pulse arrives 100 fs after the pump pulse with an experimental time resolution of 35 fs. By taking this experimental response time into account, a clear dip feature can be observed when the depletion pulse arrives 100 fs after the pump beam.

Figure 5.43 describes the outcome of the rate model simulation, where the rise of the signal corresponds to the population of the triplet state. At T=1 ps the depletion pulse is applied. The resulting sharp dip feature seen in the experimental data (see Figure 5.37 left) is well reproduced in the simulation. The signal recovery afterwards can be explained by the triplet re-population resulting from the singlet re-excitation as mentioned before. In

correspondence with our experimental settings, the temporal resolution of the simulated NIR data is lower what becomes apparent in the broad coherence spike (see Figure 5.43b). This leads to a temporal broadening of the dip feature in accordance with the experimental observations. As mentioned before, the signal decay after the depletion action instead of a recovery (as found for the visible data) can only occur if the final state of a transition gains population via an additional transfer to the T_2 state. If a population transfer from the T_3 to the T_2 state is included in the rate model simulations, the experimental observations can perfectly be reproduced. This implies, that an additional ultrafast $T_3 \rightarrow T_2$ transition (ca. 90 fs) is required, which seems feasible since the T_3 state lies energetically higher than the T_2 state.[116] The fact that the NIR ESA is affected by the depletion pulse indicates that both transitions (visible and NIR) have their origin in the same initial state T_1. At a first glance one would expect that the same sharp dip feature should be observed also in the NIR. A zoom of the simulation of this depletion action is presented in Figure 5.43c which explains the different shape. The experimental response time in the NIR (blue curve in Figure 5.43c) is much longer so that the depletion effect cannot be resolved. The limited temporal resolution also explains the absence of a dip feature at very early delay times. In order to observe a small dip at a depletion time of T=100 fs, a temporal resolution of about 35 fs is required as shown in the simulation (see Figure 5.43d). By taking the experimental results and the rate model simulation together, it can be stated that the triplet transitions in the visible and NIR probe the same T_1 state. However, in all pump-depletion-probe experiments on TIPS-pentacene the depletion pulse did not only affect the triplet manifold but also the S_1 state was influenced. An independent depletion action on the T_1 state is not feasible in TIPS-pentacene since a depletion pulse around 530 nm is always also resonant with the $S_1 \rightarrow S_n$ transition.

5.3.3   Pump-Depletion-Probe on Tetraaza-TIPS-pentacene

In Tetraaza, the $S_1 \rightarrow S_n$ excitation is well separated and an investigation of the effect of a depletion pulse on the triplet state only is possible because

it does not exhibit a singlet contribution in the region where the depletion
pulse is applied (530 nm). As discussed before, Tetraaza behaves similar to
TIPS-pentacene, however, the singlet species has negligible amplitude at 530
nm where the depletion spectrum is located. Thus, the depletion pulse does
not affect the singlet state ($S_1 \rightarrow S_n$). This can be nicely seen in Figure
5.44. Here, the first and second species associated spectra obtained by the
global target analysis of the transient absorption data of Tetraaza are shown
together with the excitation and depletion spectrum. The first species is
assigned to a state of singlet character and decays with a time constant of
100 fs towards the triplet manifold. It is not overlapping with the depletion
pulse spectrum, whereas the second spectra is correlated with the triplet
species and affected by the depletion pulse.
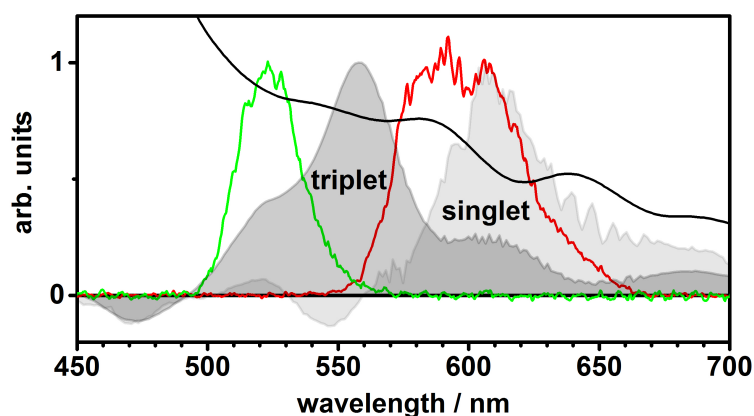
Figure 5.44: UV-vis spectrum of spin-coated Tetraaza thin film (black line)
together with the excitation spectrum (red line) and the depletion spectrum
(green line). The gray areas represent the first (light grey, singlet character)
and the the second (dark gray, triplet character) species associated spectra
obtained from the global target analysis of the transient absorption data.

The results of the pump-depletion-probe experiments probed in the visible
spectral region are shown in Figure 5.45 (left). At early time delays when
the system is still in the excited singlet state, the depletion has no effect
on the dynamics as can be seen for short T values (T=50 and 100 fs). The
dip feature is first observable at T=200 fs when the triplet state has already

developed. A strong depletion effect on the triplet state is visible at T=1 ps. However, compared to the same measurements on TIPS-pentacene, the dip feature is less sharp and only a small amount of population returns to the T_1 state. The signal evolution looks similar to the depletion effect observed for TIPS-pentacene in the NIR (compare Figure 5.37 (right) with 5.45).
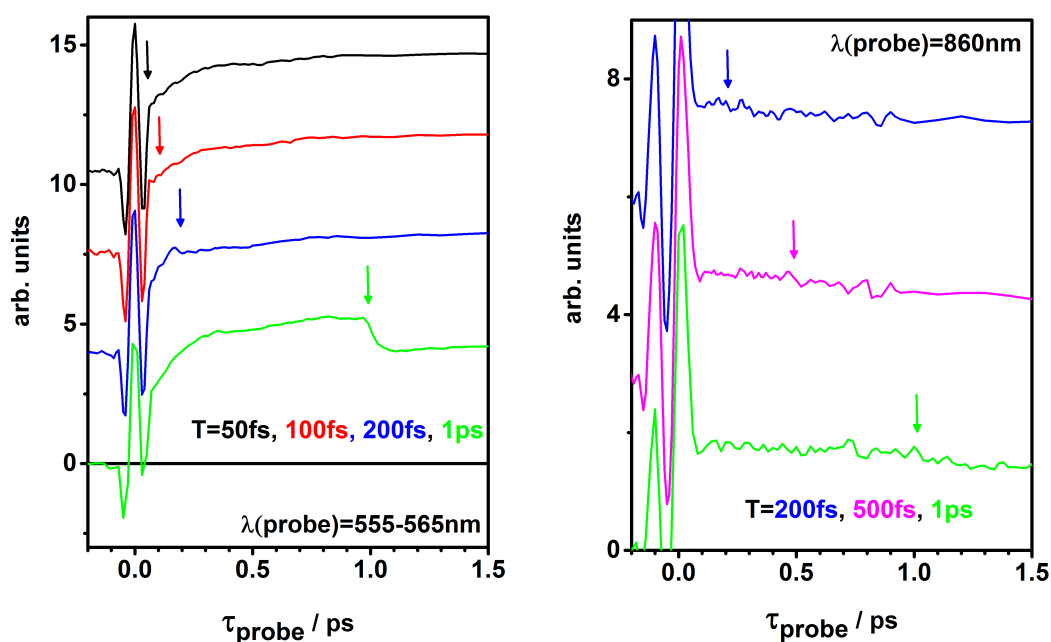
Figure 5.45: Results of the pump-depletion-probe experiments of Tetraaza, pumped at 600 nm, depleted at 530 nm and probed in the visible spectral region (averaged wavelength range from 555 to 565 nm). The arrows indicate the arrival time of the depletion pulse.

In comparison to TIPS-pentacene, though, the triplet $T_1 \rightarrow T_3$ transition is red shifted (around 560 nm) and higher lying vibrational states are addressed by the depletion pulse at 530 nm. The excitation of population, blue shifted with regard to the lowest transition, allows for a detailed discussion of the depletion effect. In Figure 5.46 selected wavelengths are depicted in order to compare the effect of the depletion pulse at 530 nm on the dynamics at different positions in the spectrum. If wavelengths are probed where the depletion pulse acts, intramolecular vibrational energy redistribution (IVR) back to

the lowest vibrational state in T_3 can be monitored directly. Population loss
in the T_{1hot} state (vibrationally excited T_3 state) reduces the depletion effect
when exactly this state is probed. In other respect, population gain of the
lowest vibrational T_1 state results in a further decay of the signal on the time
scale of IVR. Signal recovery resulting from a re-population of the T_3 state
as a consequence of re-exciting S_1 is also not observable when probing higher
vibrational levels in T_3.
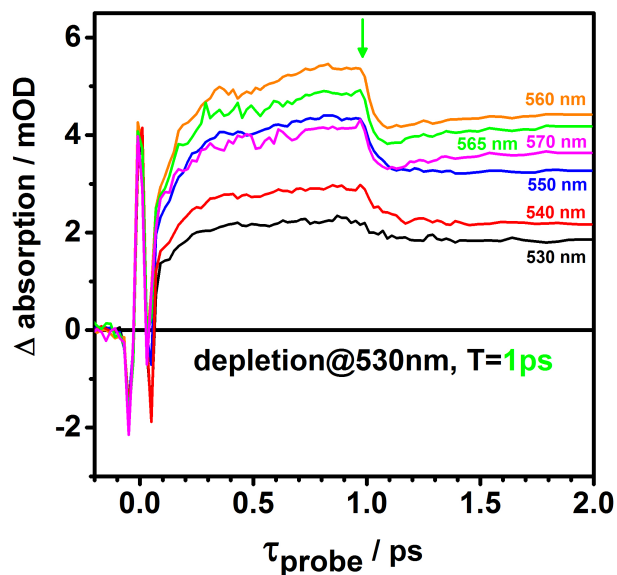
Figure 5.46: Pump-depletion-probe data of Tetraaza after applying the
depletion pulse at 530 nm, 1 ps after the pump pulse at selected probing
wavelengths (530-570 nm).

At higher wavelengths, in this case the maximum of the $T_1 \rightarrow T_3$ absorp-
tion (560 nm), a clear dip feature can be seen, which is slightly delayed. This
is related to the fact that lower vibrational levels in T_3 are probed than orig-
inally excited by the depletion pulse. The depletion effect increases while the
probed state gains population. As confirmed by our rate model simulation,
we can resemble a further decay after the depletion action if a $T_{3hot} \rightarrow T_3$
transition is included (simulation with corresponding model and explanation
of all contributions is shown in Figure 5.47).

104
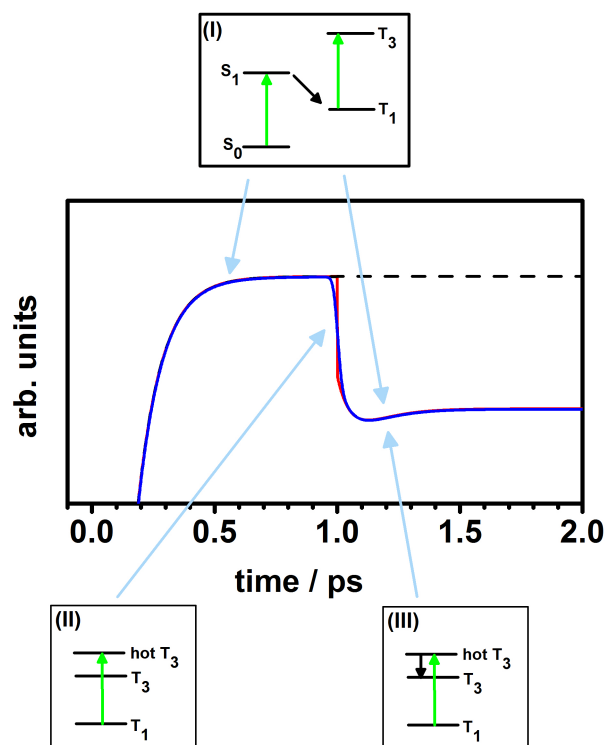
Figure 5.47: Zoom into the simulation of the pump-depletion-probe signal of Tetraaza-TIPS-pentacene. The dashed black line shows the transient dynamics without depletion effect. The red curve demonstrates the dynamics after applying a depletion pulse at 1 ps and the blue curve takes the experimental response time of ca. 40 fs into account (see also Figure 5.43). The energy diagrams present the underlying processes that cause the signal.

(I) represents the population transfer to T_1 followed by the transition to T_3. This signal corresponds to the conventional TA signal.

(II) shows the effect of the depletion pulse. The prompt signal decay results from a depletion of T_1.

(III) illustrates the IVR process in T_3. The depletion effect decreases because the probed state has less population. This signal recovery is also increased due to the fact that the depletion pulse re-excites the S_1 state followed by a population of T_3 (see above (I)).

Also a signal recovery is observed, however, this re-population of T_3 does not possess the same time constant as the initial triplet rise (compare signal evolution before and after the depletion action in Figure 5.46). Both, the

re-population and IVR transfers population into the lowest vibrational T_3 state. Therefore, the signal recovery is reduced since it is compensated by IVR. At intermediate wavelengths (540-550 nm) we observe a behavior that lies in between, where the depletion effect is superimposed by IVR. This leads to a signal evolution which shows a combination of both depending on the amount of each contribution as presented for the transients at 550 nm and 560 nm.

Having shown the data of Tetraaza probed in the visible, the pump-depletion experiment probed in the NIR is discussed in the following. In Figure 5.45 (right) transients are presented when the depletion pulse is applied at T=200 fs, 500 fs and 1 ps after the pump interaction. In principle, the same explanation as given for TIPS-pentacene holds for Tetraaza (ultrafast $T_3 \rightarrow T_2$ population transfer, see subsection 5.3.1) The effect of the elongated decay after the depletion action, though is even more dramatic in Tetraaza compared to TIPS-Pentacene in the NIR. This is intuitive, since T_{3hot} first decays into the relaxed T_3 state via IVR before the $T_2 \rightarrow T_3$ transition can take place.

5.3.4 Pump-Depletion-Probe on Diaza-TIPS-pentacene

Pump-depletion-probe-experiments carried out for Diaza can be interpreted similar to TIPS-pentacene, since it exhibits a singlet transition that is affected by the depletion pulse at 530 nm. This is illustrated in Figure 5.48 where the first (singlet character) and second (triplet character) species associated spectra are shown together with the excitation and depletion spectra. It is obvious that both species are affected by the depletion pulse at 530 nm. In the pump-depletion-probe data (see Figure 5.49) a dip feature is therefore already observable at T=100 fs. This dip feature seems to be delayed, since the depletion pulse is resonant with higher vibrational levels. The result of this T_{3hot} population is discussed in detail for Tetraaza (see above). Due to the restricted experimental response, a depletion effect at T=100 fs could not be detected in the NIR spectral region.
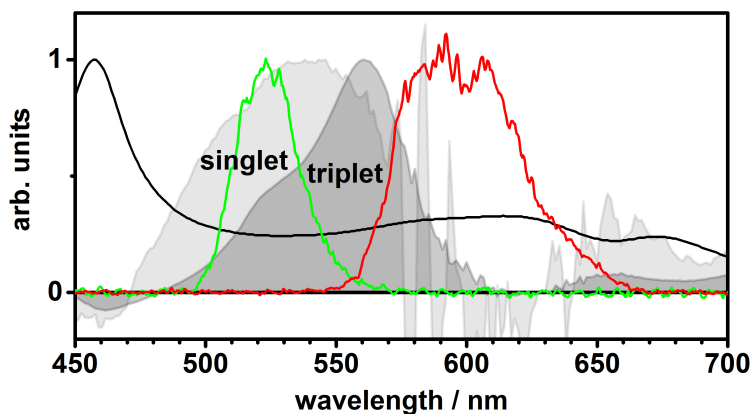
Figure 5.48: UV-vis spectrum of spin-coated Diaza thin-film (black line) together with the excitation spectrum (red line) and the depletion spectrum (green line). The grey areas represent the first (light grey, singlet character) and the second (dark grey, triplet character) species associated spectra obtained from the global target analysis of the transient absorption data.
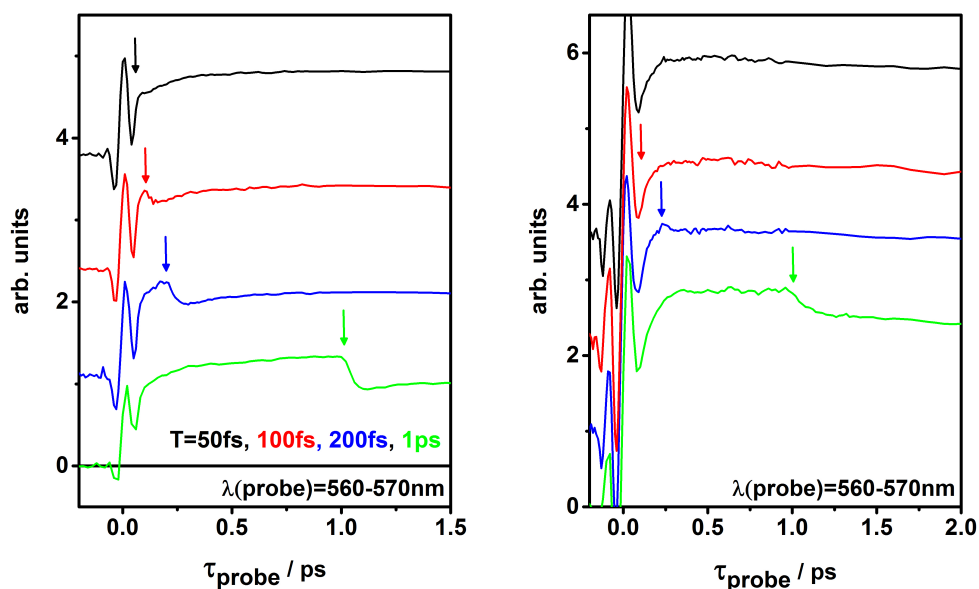
Figure 5.49: Pump-depletion-probe data of Diaza-TIPS-pentacene probed in the visible at a wavelength range between 560-570 nm (left) and in the NIR at a wavelength range of 855-865 nm (right). The arrows indicate the arrival of the depletion pulse.

5.3.5 Assignment of Rise Times

The experimental results and the outcome of the rate model simulation
clearly show that one single triplet state T_1 is populated from the singlet
manifold via SF in all investigated compounds. The observation of two dif-
ferent rise times for the formation of the triplet band in the visible and in
the NIR give access to decipher the entangled dynamics at the initial stages
of SF. There is a general consensus that the formation of free independent
triplets occurs via an intermediate coupled triplet state (^{1}TT, see section
2.4.1).[13, 14, 28, 29, 32, 45, 117, 118] Conservation of angular momentum
requires that this pair of local triplet states is coherently coupled into a
state of pure singlet character. This correlated triplet exciton pair is termed
as multiexciton (ME) state intermediate[33, 103, 118] or optically dark (D)
multiexciton[32], which couples non adiabatically to the bright S_1 state. As
its lifetime is believed to be extremely short, it has been very challenging un-
til now to detect this species by means of conventional transient absorption
measurements due to temporal and spectral overlap of several contributions
at early time delays, e.g. coherent effects, singlet and triplet absorption
bands. By taking ^{1}TT into account and implementing it into the rate model
via a consecutive reaction ($S_1 \rightarrow {}^1TT \rightarrow T_1$) the assignment of the different
experimental triplet rise times in the NIR and visible can now be perfectly
justified (see Figures 5.50-5.52). While the S_1 and T_1 states absorb in the
visible as well as in the NIR (see SAS spectra in Figures 5.22-5.24), the ^{1}TT
state just absorbs in the NIR. This leads to overlapping contributions which
results in slightly different experimental rise times in the visible and NIR.
According to this observation the simulation leads to a time constant of 50 fs
for the rise of the coupled triplet pair state ^{1}TT as shown in Figure 5.50. The
subsequent formation of the T_1 state occurs in 135 fs in the case of TIPS-
pentacene. In the visible a superposition of the two time constants adds up
to 155±10 fs. In the NIR spectral range, however, the situation is different.
In this spectral region also the ^{1}TT species absorbs and the measured signal
exhibits a shorter rise time constant of 120 fs.
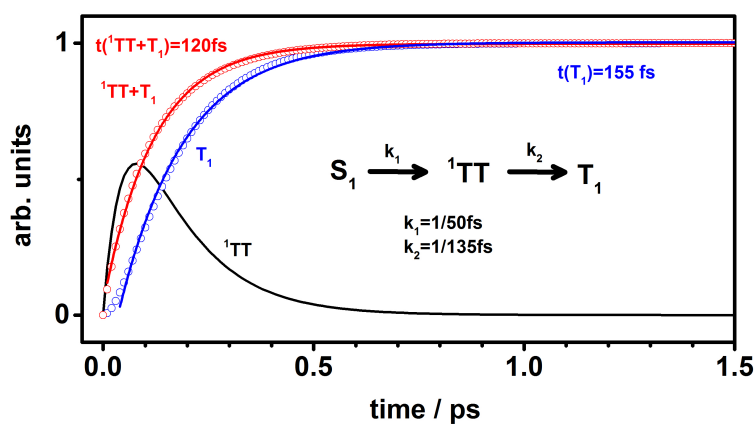
Figure 5.50: Evolution of species in a consecutive reaction with t_1=50 fs and t_2=135 fs reflecting the dynamics of TIPS-pentacene. If the detection pulse probes both states (NIR), a sum of the ^{1}TT and the T_1 state (with equal weighting) can be seen, resulting in a rise time of 120 fs. If the detection is specific only to T_1 (visible), the rise time comes to 155 fs. The fitting is done with a single exponential growth for both curves.
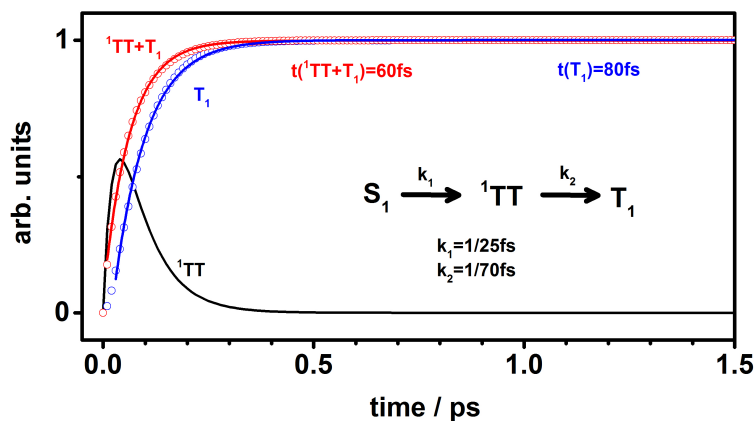
Figure 5.51: Evolution of species in a consecutive reaction with t_1=25 fs and t_2=70 fs reflecting the dynamics of Diaza. If the detection pulse probes both states (NIR), a sum of the ^{1}TT and the T_1 state (with equal weighting) can be seen, resulting in a rise time of 60 fs. If the detection is specific only to T_1 (visible), the rise time comes to 80 fs. The fitting is done with a single exponential growth for both curves.

In the case of TIPS-pentacene the ^{1}TT and T_1 states are equally weighted, which means that both contributions exhibit the same amplitude. This is also the case for Diaza, but the faster dynamics lead to a ^{1}TT formation of 25 fs and a T_1 rise of 70 fs (see Figure 5.51). Thus, it is accelerated by a factor of two compared to TIPS-pentacene confirming the results of the TA experiments. Here, the rise times add up to 80 fs in the visible and 60 fs in the NIR. In Tetraaza the ^{1}TT species builds up with a time constant of 35 fs and has a higher amplitude relative to the T_1 state contribution, which rises with 90 fs (see Figure 5.52). The observed different rise times in the two spectral ranges (visible=100 fs and NIR=60 fs) are perfectly reproduced by taking a weight of 75 % ^{1}TT and 25 % T_1.
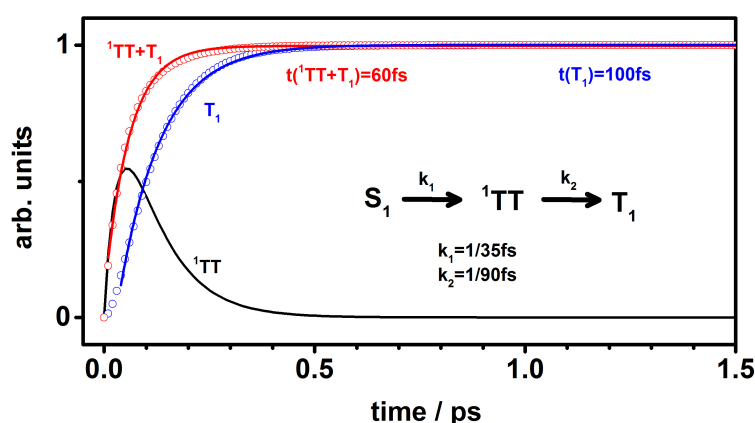
Figure 5.52: Evolution of species in a consecutive reaction with t_1=35 fs and t_2=90 fs reflecting the dynamics of Tetraaza. If the detection pulse probes both states (NIR), a sum of the ^{1}TT and the T_1 state (with a weighting of 75%:25%) can be seen, resulting in a rise time of 60 fs. If the detection is specific only to T_1 (visible), the rise time comes to 100 fs. The fitting is done with a single exponential growth for both curves.

5.3.6   Pump-Depletion-Probe at 800 nm

In order to gain further insight into the dynamics of the triplet states, pump-depletion-probe experiments with depletion pulses at 800 nm were performed. The overall setup directly follows the one described above with excitation

pulses at 600 nm (40 nJ) and white light in the visible and NIR spectral region acting as probe pulses. To guarantee that all the experimental settings are correct, the ESA signal at 800 nm was monitored before the pump-depletion-probe measurements. Interestingly, there was no depletion effect on the $T_1 \rightarrow T_3$ transition in the visible, neither at short nor at long delay times. Also no effect was observed when the NIR ($>$840 nm) spectral region was probed (with both parallel and perpendicular polarization of the pump beam with regard to the probe beam) within our given time resolution. This finding suggests that a singlet state is addressed at 800 nm, which may be the above mentioned coupled triplet pair state ^{1}TT with singlet character. The broad structureless absorption band hypothesizes the interplay between several transitions between states with different multiplicity in the NIR spectral region. The depletion effect on that short-lived ^{1}TT state could not be detected, predominatly due to the restricted experimental response and secondly due to the superposition of the T_1 state at wavelengths between 850 and 950 nm. Therefore, it is not possible to see ^{1}TT directly in transient absorption using probe pulses above 840 nm and experimental response times greater than 20 fs. Very recently, Musser et al. observed that vibrational coherence in the initially excited S_1 is transferred to the triplet state via strong coupling between nuclear and electronic degrees of freedom.[30] Despite of their conclusion that SF is mediated by the formation of the intrinsically intermolecular ^{1}TT state, there is little known about the engergetic levels of this state. Due to its spectral proximity to the first excited singlet state, vibronic coupling between them should be directly observable using multidimensional techniques such as 2D electronic spectroscopy[103, 119] or pump-degenerate four wave mixing[120]. It is important to note that this intermediate state does not influence the dynamics of the depletion effect at 1 ps. Hence, the simulation of the depletion effect shown before is not affected by this new finding.

5.3.7 Summary and Discussion

Combining the information gained from the pump-depletion-probe experiments with simulations, a detailed picture on the relaxation dynamics after photo excitation of TIPS-pentacene and the two aza-derivatives is provided. In Figure 5.53 the derived kinetic model of the excited state dynamics of TIPS-pentacene is shown representatively. Despite of shorter dynamics observed for the aza-derivatives, all investigated compounds follow the same reaction scheme.
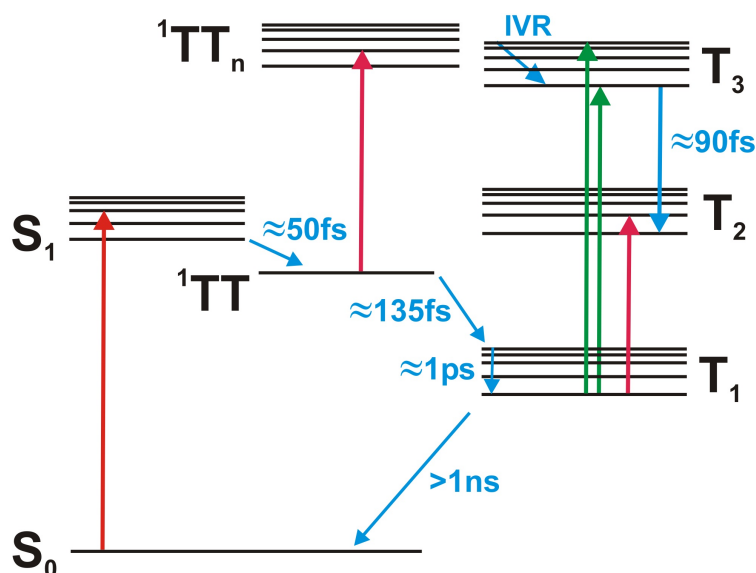
Figure 5.53: Detailed kinetic model for the excited state dynamics of TIPS-pentacene derived from pump-depletion-probe experiments and simulations.

Table 5.1: Time constants of relaxation dynamics of TIPS-pentacene and its aza-derivatives.

	$S_1 \rightarrow^1 TT$	$^1TT \rightarrow T_{1hot}$	$T_{1hot} \rightarrow T_1$	$T_1 \rightarrow S_0$
TIPS-pentacene	≈ 50 fs	≈ 135 fs	≈ 1 ps	> 1 ns
Diaza	≈ 25 fs	≈ 70 fs	≈ 1 ps	> 1 ns
Tetraaza	≈ 35 fs	≈ 90 fs	≈ 1 ps	> 1 ns

Excitation into the first excited state is followed by an ultrafast transition to the coupled triplet pair state ^1TT. This state absorbs in the NIR only (around 800 nm) but cannot be detected directly due to its extremely short lifetime. It decays to the triplet exciton state with a time constant of 135±10 fs in the case of TIPS-pentacene. For comparison the time constants of the aza-derivatives are shown in Table 5.1. In the visible spectral region the $T_1 \rightarrow T_3$ ESA (togehter with the $S_1 \rightarrow S_n$ ESA) is observed, which rises with a time constant resulting from a sum of 50 and 135 fs for TIPS-pentacene. The superposition of the ^1TT and T_1 ESA bands in the NIR leads to an apparent faster triplet rise compared to the visible. The lifetime of T_1 exceeds the observation time of the experiment (1 ns). Furthermore, an additional ultrafast transition of ca. 90 fs from the T_3 to the T_2 state explains the pump-depletion signal probed in the NIR spectral region. For the aza-derivatives not only the formation of the ^1TT state is accelerated but also the build up of the T_1 state. When probing at wavelengths close to the energy of the depletion pulse, which is resonant with higher lying vibrational states, IVR processes in the T_3 state can be monitored directly. This is demonstrated for the aza-pentacenes where the depletion pulse adresses higher vibrational levels in T_3. Its depopulation can be follwed by probing the same level. This additional information is of great relevance regarding the study of loss channels within these materials, since the excess energy is dissipated as heat. By designing materials whose energy levels are close to the ones of the excited donor molecule (as it is the case for the aza-pentacenes compared to TIPS-pentacene), this could reduce the energy losses. In that way the energy is transferred to the acceptor molecule before it can relax back to the lowest vibrational energy level. There are calculations of the singlet and triplet excited states of several nitrogen-containing compounds available using density functional theory and time-dependent density functional theory with the B3LYP functional at 6-31* level.[121] This method is, however, less accurate and multiexcitations are not taken into account. More detailed and accurate calculations of the contributing excited states would be highly beneficial for the understanding of the singlet fission process.

It is now possible to frame these new findings into the existing picture of the excited state dynamics of TIPS-pentacene. In Figure 5.54 the contributions of all relevant excited state transitions of TIPS-pentacene are shown with regard to their spectral occurrence. Former studies on TIPS-pentacene thin-films concordantly showed that the triplet ESA ($T_1 \rightarrow T_3$) is highly superimposed by the singlet ESA in the visible sprectral region, which is in accordance with the results obtained in this thesis.[28, 91, 101, 108] According to calculations performed by Pabst *et al.* there exists another triplet excited state transition ($T_1 \rightarrow T_2$) with a very low transition moment and oscillator strength. This is manifested in the weak absorption band in the NIR that was also observed here.[116]
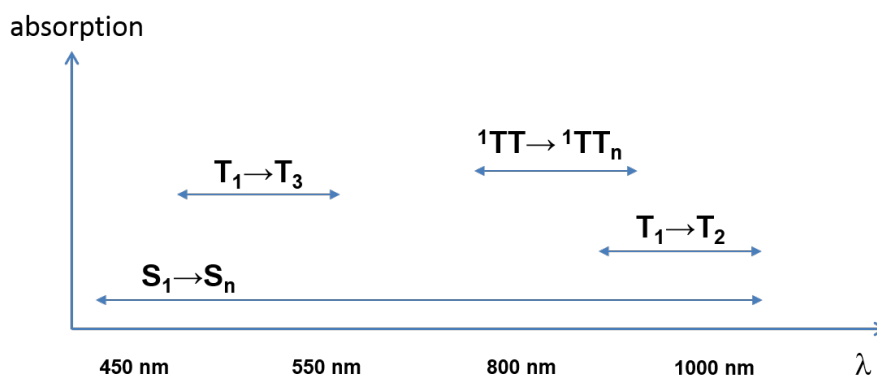
Figure 5.54: A rough estimation of the spectral contributions of the singlet and triplet transitions that are involved in the singlet fission process observed for TIPS-pentacene.

Contrary to investigations on polycrystalline, unsubstituted pentacene [42, 43] and TIPS-pentacene films [28], a singlet ESA contribution was observed over the whole detection range (450-1100 nm). Although a comparison between experiments done in solution is nontrivial, measurements on a high concentrated TIPS-pentacene solution show also a superposition of singlet and triplet contributions in the NIR spectral region.[91] Besides showing that the NIR cannot be investigated independently from a singlet contribution, also the coupled triplet pair state ^{1}TT was assigned to absorb in

that spectral region. The triplet rise times obtained for TIPS-pentacene are varying from 80 fs[30] over 110 fs[28] to 1 ps[101] in the literature. The different observations on the SF kinetics can be explained by an altered thin-film morphology or different conditions during the time-resolved experiments. On the one hand, a different thin-film fabrication critically influences the crystal growth of a material (spin coating procedure, solvent, substrates) and on the other hand, experimental conditions (encapsulated samples, photon flux, excitation and probing wavelengths) might result in changed excited state dynamics. Within this thesis, a time constant of 155 fs was obtained for TIPS-pentacene, which is in the range of the observations by Yost *et al.* (the slightly shorter time constant of 110 fs might be related to the fact that fitting was done only until 700 fs even though the signal rise was not completed). In their study several materials were investigated in order to predict SF performances within a device.[28] The proposed model is based on different intermolecular interactions, depending on the crystal structure, which were correlated to the coupling between the S_1 and ^1TT state. They claim that there is a transition from non-adiabatic to adiabatic energy transfer when the coupling gets stronger. However, their limited model underestimates charge transfer contributions, which in turn rules out the coherent model of SF. Thus, a theoretical description of SF is demanding, most of all due to the multireference character of TIPS-pentacene.[25] Despite of charge transfer contributions, vibronic coupling has also to be considered as shown by Musser *et al.*. They observed that the potential surfaces of S_1 and ^1TT are linked through a conical intersection.[30] Accordingly, in 2D electronic spectroscopy it was found that SF dynamics are based on strong couplings between molecular nuclear and electronic motions[103], which makes a theoretical description of this process expensive.

Chapter 6

Conclusions and Outlook

Within this thesis more light is shed on the relaxation network of TIPS-pentacene and a detailed kinetic model of the initial excited state dynamics is established. Moreover, the influence of nitrogen atoms on the singlet fission process is investigated by means of transient absorption measurements, global target analyses, pump-depletion-probe experiments and rate model simulations. This complementary study on TIPS-pentacene, Diaza and Tetraaza reveals that the formation of a single triplet state occurs via the intermediate coupled triplet pair state ^{1}TT for all three compounds. The nitrogen substitution not only accelerates the formation of this intermediate state with singlet character, but also the creation of the triplet state T_1 via the ^{1}TT state. ^{1}TT builds up within 25 fs for Diaza and within 35 fs for Tetraaza, which is faster than the time constant obtained for TIPS-pentacene (50 fs). Hence, the addition of sp^2 nitrogen atoms into the backbone of TIPS-pentacene results in an acceleration of the singlet fission process up to a factor of two. As the efficiency potentially increases with faster dynamics, the heteroacenes undergo SF more efficiently than TIPS-pentacene itself. A possible indication of a higher triplet quantum yield in the aza-derivatives is the stronger $T_1 \rightarrow T_2$ signal in the NIR relative to that in the visible spectral region when compared to TIPS-pentacene (under the assumption that they exhibit an absorption coefficient similar to TIPS-pentacene). These results underline the potential of aza-derivatives to optimize efficiencies by eliminating loss channels and

thus exceed the triplet quantum yield compared to TIPS-pentacene. The experimental observations furthermore show that ^{1}TT absorbs in the NIR only, while the singlet and triplet absorb in the visible and NIR spectral region. The finding that a singlet species absorbs also in the NIR, which was ruled out before, leads to a detailed picture of the excited state dynamics. It is shown that the superposition of the ^{1}TT and T$_1$ ESA bands in the NIR leads to an apparent faster triplet rise compared to the visible, where only the $T_1 \rightarrow T_3$ ESA is observed. Further knowledge about the interplay between excited states can help in a future step to modify special transitions on a molecular level. In that way, namely by avoiding or activating transitions, the SF process can be optimized. The potential to enhance and direct the SF mechanism by intercepting the normal relaxation dynamics is attractive regarding the design of new materials and their application in organic photovoltaic devices. Additionally the high resistance of azaacenes against air is a potential benefit of these new materials for organic electronics applications.
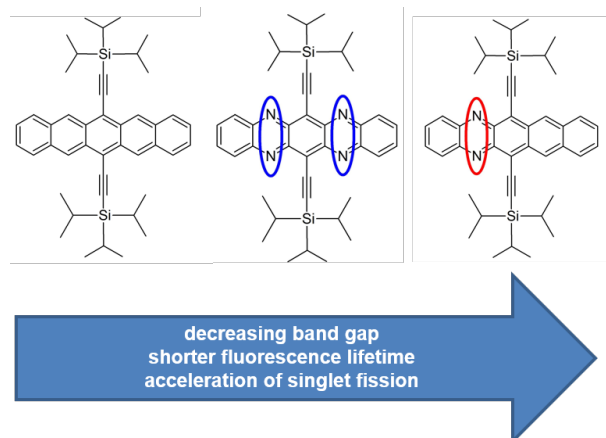
Figure 6.1: Representation of the investigated molecules and their optical properties. By changing the electronic structure of the molecules, the dynamics are changed. The dependence of the energy gap between the HOMO and LUMO, the fluorescence lifetime in solution and the ^{1}TT as well as the triplet rise time via singlet fission in the solid state on the molecular structure is illustrated by the arrow.

It has to be mentioned though, that the investigation of organic materials in the condensed phase poses a big challenge since the performance of a specific compound is highly dependent on the thin-film fabrication procedure itself. In particular, the morphology is influenced by the thin-film processing and even the same starting material can possess different optical properties dependent on its fabrication. For instance, transient absorption measurements on thin-films spin-coated on different substrates lead to slightly changed dynamics. This was discovered by measurements of the pentacene derivatives on pure glass substrates and on polyimide-coated glass substrates, respectively. This approximately 30 nm thick polyimide interlayer was introduced to achieve good wettability of the organic solution and to provide a homogenous film formation and crystallization. The consequence of this change in the thin-film fabrication procedure leads to faster kinetics, hence the SF process speeds up from 200 fs to 155 fs for TIPS-pentacene and from 100 fs to 75 fs in Diaza (triplet absorption in the visible spectral region). It is therefore not surprising that the triplet rise times for TIPS-pentacene, fabricated in different ways reported in literature, are varying. However, the presented observations on TIPS-pentacene and its derivatives within this thesis are based on experiments that were performed under the same conditions, i.e. thin-film fabrication (same solvent and spin-coating parameters) and experimental settings (wavelength, excitation energy, setup geometry). Hence, the given kinetics of the different derivatives can be directly compared with each other. The obtained dynamics of each material could be reproduced in multiple measurements and were not influenced (within the given error) by small possible deviations in the morphology from one procedure to another (even if all parameters and settings are the same, there might occur small deviations). Particular attention has to be paid on the excitation energy of the pump beam within the transient absorption experiment. High pump pulse intensities lead to annihilation processes that superimpose the difference absorption signal. The result of a high photon flux is manifold, since additional features occur and the overall signal evolution can change. Thus, data that are comprised of these annihilation effects are not reliable.

The successful realization of the experiments on thin-films of TIPS-pentacene and two aza-derivatives poses new ideas for future studies in the field of organic electronics that will be discussed in the following. On the one hand, more sophisticated experimental methods are required in order to gain more insight into the initial steps of SF. The extremely short-lived coupled triplet pair state ^{1}TT, that is built up directly after photo-excitation needs to be monitored and studied in more detail, since this state is the precursor of the generated triplets. Deeper knowledge about its electronic properties, vibrational couplings and energetic levels would benefit the understanding of the SF process. Although first multidimensional studies of this state are in progress[103], quantum chemical calculations on the energetic levels of this state are still missing for TIPS-pentacene as well as for the aza-derivatives. Moreover, accurate calculations on the singlet and triplet levels of these compounds are not available until now. The key requirements to resolve the ^{1}TT state within transient absorption measurements depend on the experimental conditions. On the one hand, a higher time resolution has to be maintained by using transform-limited ultrashort excitation and probing pulses. This could be achieved by taking nc-OPA pulses as pump and probe beams that do not exhibit any kind of chirp and thus suppress the coherent artefact. However, the experimental realization of this requirement is very demanding. On the other hand, the film quality has to be improved in order to reduce scattering during the measurements, especially when being close to the temporal overlap between pump and probe. One possible idea would be to measure the sample in reflection instead of transmission and make use of encapsulated samples that are not exposed to air during the measurement. Another important issue is related to the global fitting procedure of the transient absorption data. If a broad white light continuum is used as the probe pulse, a large contribution of the coherent artefact is observed. Until now, the global fitting algorithm does not take the coherent artefact into account and therefore the dynamics around time zero are not included into the fitting procedure. Since this is the region of interest (due to the ultrafast SF mechanism) a global analysis that is also able to fit this coherent contribution would be a great improvement.

The development of new materials with tailored properties plays the key role in the field of organic electronics. Studying structure-function relationships is crucial for the design of the novel architectures that could lead to enhanced efficiencies. Hence, the investigation of photophysical and photochemical qualities is of particular importance in order to make any predictions regarding the optical behavior. Having this feedback, it is now possible to tune the electronic properties of a material to achieve a desired performance. As Diaza shows an accelerated SF, it would be interesting to study if more electronegative substituents speed up the excited state dynamics even more. In Diaza the charge is unsymmetrically distributed over the molecule and new substituents would increase the existing dipole character of the molecule. An acceleration of SF dynamics was also observed for substituted phenazinothiadiazoles[122] when compared with the pure tetracene framework. The aromatic core of this molecules is composed of four rings, however, the tetracene structure is modified to a high extend. There is one pyrazine unit incorporated into the acene backbone and one terminal benzene ring is substituted by a five-membered ring called thiadiazole. Additionally, two TIPS side-groups and four electronegative substituents (fluorine or chlorine, see Figure 6.2 left) are attached. Here, the SF process is about two orders of magnitude faster than in tetracene single crystals (300 fs versus 20-50 ps[36, 39]), which is very promising since the thermal activation barrier can be overcome. (Interestingly, TIPS-tetracene thin-films produced via spin-coating are amorphous and degrade on air within one day.) Accordingly, the investigation of novel phenazinothiadiazoles, such as hetero-tetracenothiadiazoles (four-ring system with an additional thiadiazole ring, see Figure 6.2 right) in terms of their excited state dynamics is auspicious. Pentacene is the first homologue of the acene class where SF is exothermic and ultrafast. Consequently, the higher acenes should undergo SF even faster with respect to their electronic levels. However, in crystalline hexacene this large exothermicity leads to a slower SF performance as a result of multiphonon relaxation in the excited state.[24] Tuning its electronic levels by chemical modification in order to reduce the effect of multiphonon relaxation could provide deeper insights into the relaxation pathways of acenes.
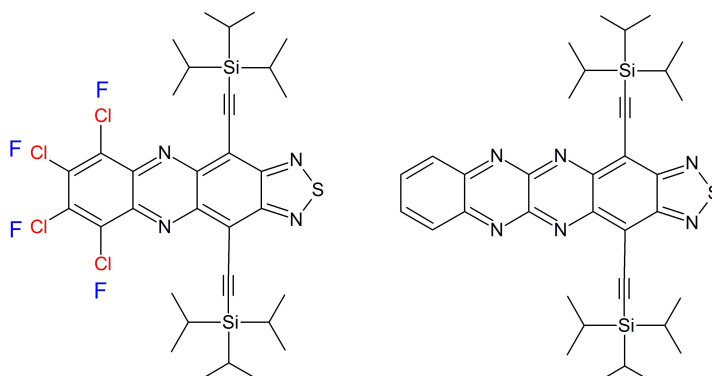
Figure 6.2: Chemical structures of new materials (phenazinothiadiazole (left) and tetracenothiadiazole (right)) interesting to study regarding their SF performances.

By using the zone-casting technique, it is now possible to fabricate films with a specific orientation of the molecules.[123] This new approach allows for the investigation of polarization dependencies (anisotropy) of aligned films within the transient absorption measurement. Additionally, new solvents can be tested in order to change the morphology of the thin-films via the spin-coating procedure. On the other hand, better solubility of the materials could lead to increased film thicknesses that show higher ground state absorption resulting in higher transient absorption signals. Particularly with regard to the recently measured starphene, a higher concentration of molecules would be valuable.

Besides studying the excited state dynamics of one material itself it is also important to consider the interaction within a molecular assembly, i.e. a heterojunction between donor and acceptor. One possibility would be to mix two different acenes in order to create such a heterojunction and study the charge generation process. In particular, experiments that are able to determine the created charge carriers directly would be highly valuable. This means that the usual optical detection has to be extended and also the generated electrons need to be monitored. This is of great relevance when studying not only the materials themselves but also donor-acceptor systems within a specific device, which is the essential next step. By applying an electrical field and

measuring the current between two electrodes, the amount of generated excitons can be directly determined.[124] This gives important information about charge dissociation and diffusion dynamics, which critically determines the performance of material within a device. Additionally, optical pump-push photocurrent probe experiments would provide deeper insight into the dissociation dynamics of the free charges as a complementary study.[125]

The investigation of the excited state dynamics of organic materials on thin-films is a challenging field and will be subject of interesting scientific discussions in the next years. In particular, the process of multiexciton generation via ultrafast SF is going to play a key role in complex spectroscopic experiments and theoretical approaches in the future. The investigation of TIPS-pentacene and two aza-derivatives by means of transient absorption as well as pump-depletion-probe experiments in combination with simulations revealed important insights into the initial photo-induced dynamics in this molecule class. The knowledge about the structure-function relationships obtained within this work paves the way for new studies and especially innovative applications in the field of organic electronics.

Bibliography

[1] John Weier and Robert Cahalan. Solar radiation and climate experiment, 2002. http://eospso.gsfc.nasa.gov/sites/default/files/publications/2002SORCE_SWG.pdf.

[2] Matthias Loster. Total primary energy supply - from sunlight, 2006. http://www.ez2c.de/ml/solar_land_area/.

[3] Martin A. Green, Keith Emery, Yoshihiro Hishikawa, Wilhelm Warta, and Ewan D. Dunlop. Solar cell efficiency tables (version 44). *Progress in Photovoltaics: Research and Applications*, 22(7):701–710, 2014.

[4] Yuhang Liu, Jingbo Zhao, Zhengke Li, Cheng Mu, Wei Ma, Huawei Hu, Kui Jiang, Haoran Lin, Harald Ade, and He Yan. Aggregation and morphology control enables multiple cases of high-efficiency polymer solar cells. *Nature Communications*, 5:5293–5301, 2014.

[5] Chun-Chao Chen, Wei-Hsuan Chang, Ken Yoshimura, Kenichiro Ohya, Jingbi You, Jing Gao, Zirou Hong, and Yang Yang. An efficient triple-junction polymer solar cell having a power conversion efficiency exceeding 11 *Advanced Materials*, 26(32):5670–5677, 2014.

[6] J. E. Anthony. The larger acenes: Versatile organic semiconductors. *Angewandte Chemie International Edition*, 47(3):452–483, 2008.

[7] John E. Anthony. Functionalized acenes and heteroacenes for organic electronics. *Chemical Reviews*, 106(12):5028–5048, 2006.

[8] Jianmin Shi and Ching W. Tang. Anthracene derivatives for stable blue-emitting organic electroluminescence devices. *Applied Physics Letters*, 80(17):3201–3203, 2002.

[9] S. Yoo, B. Domercq, and B. Kippelen. Efficient thin-film organic solar cells based on pentacene/c60 heterojunctions. *Applied Physics Letters*, 85(22):5427–5429, 2004.

[10] Michael Winkler and K. N. Houk. Nitrogen-rich oligoacenes: Candidates for n-channel organic semiconductors. *Journal of the American Chemical Society*, 129(6):1805–1815, 2007.

[11] John E. Anthony, James S. Brooks, David L. Eaton, and Sean R. Parkin. Functionalized pentacene: Improved electronic properties from control of solid-state order. *Journal of the American Chemical Society*, 123(38):9482–9483, 2001.

[12] Shaobin Miao, Anthony L. Appleton, Nancy Berger, Stephen Barlow, Seth R. Marder, Kenneth I. Hardcastle, and Uwe H. F. Bunz. 6,13-diethynyl-5,7,12,14-tetraazapentacene. *Chemistry A European Journal*, 15(20):4990–4993, 2009.

[13] Millicent B. Smith and Josef Michl. Singlet fission. *Chemical Reviews*, 110(11):6891–6936, 2010.

[14] Millicent B. Smith and Josef Michl. Recent advances in singlet fission. *Annual Review of Physical Chemistry*, 64(1):361–386, 2013.

[15] Daniel N. Congreve, Jiye Lee, Nicholas J. Thompson, Eric Hontz, Shane R. Yost, Philip D. Reusswig, Matthias E. Bahlke, Sebastian Reineke, Troy Van Voorhis, and Marc A. Baldo. External quantum efficiency above 100singlet-exciton-fission-based organic photovoltaic cell. *Science*, 340(6130):334–337, 2013.

[16] H. Klauk. *Organic Electronics*. Wiley-VCH, Weinheim, first edition, 2006.

126

[17] F. Cicoira and C. Santato. *Organic Electronics*. Wiley-VHC, Weinheim, first edition, 2013.

[18] W. Brütting and A. Adachi, editors. *Physics of Organic Semiconductors*. Wiley-VCH, Weinheim, second edition, 2012.

[19] Prof. Nir Tessler. Excitons. In *Lecture notes "Organic Semiconductor Devices"*. EE Dept. Technion, http://webee.technion.ac.il/orgelect/Lectures.html, 1999.

[20] A. Köhler and H. Bässler. Triplet states in organic semiconductors. *Materials Science and Engineering: R: Reports*, 66:71–109, 2009.

[21] Nikolas J. Turro, V. Ramamurty, and J.C. Scaiano. *Principles of Molecular Photochemistry - An Introdution*. University Science Books, Sausalito, California, first edition, 2009.

[22] A. Köhler and D. Beljonne. The singlet-triplet exchange energy in conjugated polymers. *Advanced Functional Materials*, 14(1):11–18, 2004.

[23] Mordechai Bixon and Joshua Jortner. Intramolecular radiationless transitions. *The Journal of Chemical Physics*, 48(2):715–726, 1968.

[24] Erik Busby, Timothy C. Berkelbach, Bharat Kumar, Alexey Chernikov, Yu Zhong, Htay Hlaing, X.-Y. Zhu, Tony F. Heinz, Mark S. Hybertsen, Matthew Y. Sfeir, David R. Reichman, Colin Nuckolls, and Omer Yaffe. Multiphonon relaxation slows singlet fission in crystalline hexacene. *Journal of the American Chemical Society*, 136(30):10654–10660, 2014.

[25] Paul M. Zimmerman, Zhiyong Zhang, and Charles B. Musgrave. Singlet fission in pentacene through multi-exciton quantum states. *Nature Chemistry*, 2(8):648–652, 2010.

[26] D. Beljonne, H. Yamagata, J. L. Brédas, F. C. Spano, and Y. Olivier. Charge-transfer excitations steer the davydov splitting and mediate singlet exciton fission in pentacene. *Physical Review Letters*, 110:226402–226405, 2013.

[27] Timothy C. Berkelbach, Mark S. Hybertsen, and David R. Reichman. Microscopic theory of singlet exciton fission. i. general formulation. *The Journal of Chemical Physics*, 138(11):114102–114116, 2013.

[28] Shane R. Yost, Jiye Lee, WilsonMark W. B., Tony Wu, David P. McMahon, Rebecca R. Parkhurst, Nicholas J. Thompson, Daniel N. Congreve, Akshay Rao, Kerr Johnson, Matthew Y. Sfeir, Moungi G. Bawendi, Timothy M. Swager, Richard H. Friend, Marc A. Baldo, and Troy Van Voorhis. A transferable model for singlet-fission kinetics. *Nature Chemistry*, 6(6):492–497, 2014.

[29] Anatoly B. Kolomeisky, Xintian Feng, and Anna I. Krylov. A simple kinetic model for singlet fission: A role of electronic and entropic contributions to macroscopic rates. *The Journal of Physical Chemistry C*, 118(10):5188–5195, 2014.

[30] Andrew J. Musser, Matz Liebel, Christoph Schnedermann, Torsten Wende, Tom B. Kehoe, Akshay Rao, and Philipp Kukura. Evidence for conical intersection dynamics mediating ultrafast singlet exciton fission. *Nature Physics*, 11:352–357, 2015.

[31] Paul M. Zimmerman, Franziska Bell, David Casanova, and Martin Head-Gordon. Mechanism for singlet fission in pentacene and tetracene: From single exciton to two triplets. *Journal of the American Chemical Society*, 133(49):19944–19952, 2011.

[32] Paul M. Zimmerman, Charles B. Musgrave, and Martin Head-Gordon. A correlated electron view of singlet fission. *Accounts of Chemical Research*, 46(6):1339–1347, 2013.

[33] Wai-Lun Chan, Manuel Ligges, Askat Jailaubekov, Loren Kaake, Luis Miaja-Avila, and X.-Y. Zhu. Observing the multiexciton state in singlet fission and ensuing ultrafast multielectron transfer. *Science*, 334(6062):1541–1545, 2011.

[34] S. Singh, W. J. Jones, W. Siebrand, B. P. Stoicheff, and W. G. Schneider. Laser generation of excitons and fluorescence in anthracene crystals. *The Journal of Chemical Physics*, 42(1):330–342, 1965.

[35] Jonathan J. Burdett and Christopher J. Bardeen. The dynamics of singlet fission in crystalline tetracene and covalent analogs. *Accounts of Chemical Research*, 46(6):1312–1320, 2013.

[36] Zephania Birech, Markus Schwoerer, Teresa Schmeiler, Jens Pflaum, and Heinrich Schwoerer. Ultrafast dynamics of excitons in tetracene single crystals. *The Journal of Chemical Physics*, 140(11):114501–114509, 2014.

[37] H. Marciniak, M. Fiebig, M. Huth, S. Schiefer, B. Nickel, F. Selmaier, and S. Lochbrunner. Ultrafast exciton relaxation in microcrystalline pentacene films. *Physical Review Letters*, 99:176402–176406, 2007.

[38] Henning Marciniak, Igor Pugliesi, Bert Nickel, and Stefan Lochbrunner. Ultrafast singlet and triplet dynamics in microcrystalline pentacene films. *Physical Review B*, 79:235318–235326, 2009.

[39] V. K. Thorsmolle, R. D. Averitt, J. Demsar, D. L. Smith, S. Tretiak, R. L. Martin, X. Chi, B. K. Crone, A. P. Ramirez, and A. J. Taylor. Morphology effectively controls singlet-triplet exciton relaxation and charge transport in organic semiconductors. *Physical Review Letters*, 102:017401–017405, 2009.

[40] Thomas S. Kuhlman, Jacob Kongsted, Kurt V. Mikkelsen, Klaus B. Moller, and Theis I. Solling. Interpretation of the ultrafast photoinduced processes in pentacene thin films. *Journal of the American Chemical Society*, 132(10):3431–3439, 2010.

[41] N. Nijegorodov, V. Ramachandran, and D.P. Winkoun. The dependence of the absorption and fluorescence parameters, the intersystem crossing and internal conversion rate constants on the number of rings

in polyacene molecules. *Spectrochimica Acta Part A: Molecular and Biomolecular Spectroscopy*, 53(11):1813–1824, 1997.

[42] Mark W. B. Wilson, Akshay Rao, Jenny Clark, R. Sai Santosh Kumar, Daniele Brida, Giulio Cerullo, and Richard H. Friend. Ultrafast dynamics of exciton fission in polycrystalline pentacene. *Journal of the American Chemical Society*, 133(31):11830–11833, 2011.

[43] Akshay Rao, Mark W. B. Wilson, Justin M. Hodgkiss, Sebastian Albert-Seifried, Heinz Bässler, and Richard H. Friend. Exciton fission and charge generation via triplet excitons in pentacene/c60 bilayers. *Journal of the American Chemical Society*, 132(36):12698–12703, 2010.

[44] Jiye Lee, Matthew J. Bruzek, Nicholas J. Thompson, Matthew Y. Sfeir, John E. Anthony, and Marc A. Baldo. Singlet exciton fission in a hexacene derivative. *Advanced Materials*, 25(10):1445–1448, 2013.

[45] Tao Zeng, Roald Hoffmann, and Nandini Ananth. The low-lying electronic states of pentacene and their roles in singlet fission. *Journal of the American Chemical Society*, 136(15):5755–5764, 2014.

[46] Kolja Kolata, Tobias Breuer, Gregor Witte, and Sangam Chatterjee. Molecular packing determines singlet exciton fission in organic semiconductors. *American Chemical Society Nano*, 8(7):7377–7383, 2014.

[47] C.D. Dimitrakopoulos and P.R.L. Malenfant. Organic thin film transistors for large area electronics. *Advanced Materials*, 14(2):99–117, 2002.

[48] Qian Miao, Thuc-Quyen Nguyen, Takao Someya, Graciela B. Blanchet, and Colin Nuckolls. Synthesis, assembly, and thin film transistors of dihydrodiazapentacene: An isostructural motif for pentacene. *Journal of the American Chemical Society*, 125(34):10284–10287, 2003.

[49] J. Cornil, J.-L. Brédas, J. Zaumseil, and H. Sirringhaus. Ambipolar transport in organic conjugated materials. *Advanced Materials*, 19(14):1791–1799, 2007.

[50] John E. Anthony, David L. Eaton, and Sean R. Parkin. A road map to stable, soluble, easily crystallized pentacene derivatives. *Organic Letters*, 4(1):15–18, 2002.

[51] Oksana Ostroverkhova, Svitlana Shcherbyna, David G. Cooke, Ray F. Egerton, Frank A. Hegmann, Rik R. Tykwinski, Sean R. Parkin, and John E. Anthony. Optical and transient photoconductive properties of pentacene and functionalized pentacene thin films: Dependence on film morphology. *Journal of Applied Physics*, 98(3):033701–033712, 2005.

[52] Olga Lobanova Griffith, John E. Anthony, Adolphus G. Jones, and Dennis L. Lichtenberger. Electronic properties of pentacene versus triisopropylsilylethynyl-substituted pentacene: Environment-dependent effects of the silyl substituent. *Journal of the American Chemical Society*, 132(2):580–586, 2010.

[53] Gaurav Giri, Eric Verploegen, Stefan C. B. Mannsfeld, Sule Atahan-Evrenk, Do Hwan Kim, Sang Yoon Lee, Hector A. Becerril, Alan Aspuru-Guzik, Michael F. Toney, and Zhenan Bao. Tuning charge transport in solution-sheared organic semiconductors using lattice strain. *Nature*, 480(7378):504–508, 2011.

[54] Anthony Lucas Appleton, Scott M. Brombosz, Stephen Barlow, John S. Sears, Jean-Luc Bredas, Seth R. Marder, and Uwe H.F. Bunz. Effects of electronegative substitution on the optical and electronic properties of acenes and diazaacenes. *Nature Communications*, 1:91–97, 2010.

[55] Olena Tverskoy, Frank Rominger, Anastasia Peters, Hans-Jörg Himmel, and Uwe H. F. Bunz. An efficient synthesis of tetraazapentacenes. *Angewandte Chemie International Edition*, 50(15):3557–3560, 2011.

[56] Zhixiong Liang, Qin Tang, Renxin Mao, Danqing Liu, Jianbin Xu, and Qian Miao. The position of nitrogen in n-heteropentacenes matters. *Advanced Materials*, 23(46):5514–5518, 2011.

[57] Zhixiong Liang, Qin Tang, Jianbin Xu, and Qian Miao. Soluble and stable n-heteropentacenes with high field-effect mobility. *Advanced Materials*, 23(13):1535–1539, 2011.

[58] Danqing Liu, Xiaomin Xu, Yaorong Su, Zikai He, Jianbin Xu, and Qian Miao. Self-assembled monolayers of phosphonic acids with enhanced surface energy for high-performance solution-processed n-channel organic thin-film transistors. *Angewandte Chemie International Edition*, 52(24):6222–6227, 2013.

[59] Chengliang Wang, Zhixiong Liang, Yaling Liu, Xiaomu Wang, Ni Zhao, Qian Miao, Wenping Hu, and Jianbin Xu. Single crystal n-channel field effect transistors from solution-processed silylethynylated tetraazapentacene. *Journal of Materials Chemistry*, 21:15201–15204, 2011.

[60] Him Cheng Wong, Zhe Li, Ching Hong Tan, Hongliang Zhong, Zhenggang Huang, Hugo Bronstein, Iain McCulloch, Joao T. Cabral, and James R. Durrant. Morphological stability and performance of polymer-fullerene solar cells under thermal stress: The impact of photoinduced pc60bm oligomerization. *ACS Nano*, 8(2):1297–1308, 2014.

[61] M.C. Scharber and N.S. Sariciftci. Efficiency of bulk-heterojunction organic solar cells. *Progress in Polymer Science*, 38(12):1929–1940, 2013.

[62] Bernhard Ecker. Flexibel, leicht und durchsichtig. *Physik in unserer Zeit*, 44(2):84–91, 2013.

[63] William Shockley and Hans J. Queisser. Detailed balance limit of efficiency of p-n junction solar cells. *Journal of Applied Physics*, 32(3):510–519, 1961.

[64] Ye Huang, Edward J. Kramer, Alan J. Heeger, and Guillermo C. Bazan. Bulk heterojunction solar cells: Morphology and performance relationships. *Chemical Reviews*, 114(14):7006–7043, 2014.

[65] Maxim Tabachnyk, Bruno Ehrler, Sam Bayliss, Richard H. Friend, and Neil C. Greenham. Triplet diffusion in singlet exciton fission sensitized pentacene solar cells. *Applied Physics Letters*, 103(15), 2013.

[66] Bruno Ehrler, Mark W. B. Wilson, Akshay Rao, Richard H. Friend, and Neil C. Greenham. Singlet exciton fission-sensitized infrared quantum dot solar cells. *Nano Letters*, 12(2):1053–1057, 2012.

[67] Bruno Ehrler, Brian J. Walker, Marcus L. Böhm, Mark W.B. Wilson, Yana Vaynzof, Richard H. Friend, and Neil C. Greenham. In situ measurement of exciton energy in hybrid singlet-fission solar cells. *Nature Communications*, 3:1019–1025, 2012.

[68] Le Yang, Maxim Tabachnyk, Sam L. Bayliss, Marcus L. Bohm, Katharina Broch, Neil C. Greenham, Richard H. Friend, and Bruno Ehrler. Solution-processable singlet fission photovoltaic devices. *Nano Letters*, 15(1):354–358, 2015.

[69] Ahmed H. Zewail. *Femtochemistry - Ultrafast Dynamics of the Chemical Bond.* World Scientific Series in 20th Century Chemistry, Vol. 3, 1994.

[70] G. Cerullo, M. Nisoli, S. Stagira, and S. De Silvestri. Sub-8-fs pulses from an ultrabroadband optical parametric amplifier in the visible. *Optics Letters*, 23(16):1283–1285, 1998.

[71] E. Riedle, M. Beutter, S. Lochbrunner, J. Piel, S. Schenkl, S. Spörlein, and W. Zinth. Generation of 10 to 50 fs pulses tunable through all of the visible and the nir. *Applied Physics B*, 71(3):457–465, 2000.

[72] Akira Shirakawa, Isao Sakane, and Takayoshi Kobayashi. Pulse-front-matched optical parametric amplification for sub-10-fs pulse generation

tunable in the visible and near infrared. *Optics Letters*, 23(16):1292–1294, 1998.

[73] G. M. Gale, M. Cavallari, and F. Hache. Femtosecond visible optical parametric oscillator. *Journal of the Optical Society of America B*, 15(2):702–714, 1998.

[74] Nina Gildenhoff, Julia Herz, Kathi Gundermann, Claudia Büchel, and Josef Wachtveitl. The excitation energy transfer in the trimeric fucoxanthin-chlorophyll protein from cyclotella meneghiniana analyzed by polarized transient absorption spectroscopy. *Chemical Physics*, 373(1-2):104–109, 2010.

[75] M. Bradler, P. Baum, and E. Riedle. Femtosecond continuum generation in bulk laser host materials with sub-microjoule pump pulses. *Applied Physics B*, 97(3):561–574, 2009.

[76] M. Lorenc, M. Ziolek, R. Naskrecki, J. Karolczak, J. Kubicki, and A. Maciejewski. Artifacts in femtosecond transient absorption spectroscopy. *Applied Physics B*, 74(1):19–27, 2002.

[77] A. L. Dobryakov, S. A. Kovalenko, and N. P. Ernsting. Coherent and sequential contributions to femtosecond transient absorption spectra of a rhodamine dye in solution. *The Journal of Chemical Physics*, 123(4):044502–044510, 2005.

[78] Wendel Wohlleben, Tiago Buckup, Hideki Hashimoto, Richard J. Cogdell, Jennifer L. Herek, and Marcus Motzkus. Pump-deplete-probe spectroscopy and the puzzle of carotenoid dark states. *The Journal of Physical Chemistry B*, 108(10):3320–3325, 2004.

[79] Tak W. Kee. Femtosecond pump-dump-probe spectroscopy of conjugated polymers: New insight and opportunities. *The Journal of Physical Chemistry Letters*, 5(18):3231–3240, 2014.

[80] Artem A. Bakulin, Akshay Rao, Vlad G. Pavelyev, Paul H. M. van Loosdrecht, Maxim S. Pshenichnikov, Dorota Niedzialek, Jérôme

Cornil, David Beljonne, and Richard H. Friend. The role of driving energy and delocalized states for charge separation in organic semiconductors. *Science*, 335(6074):1340–1344, 2012.

[81] Tiago Buckup, Janne Savolainen, Wendel Wohlleben, Jennifer L. Herek, Hideki Hashimoto, Ricardo R. B. Correia, and Marcus Motzkus. Pump-probe and pump-deplete-probe spectroscopies on carotenoids with n=9-15 conjugated bonds. *The Journal of Chemical Physics*, 125(19):194505–194512, 2006.

[82] H.L. Fragnito, J.-Y. Bigot, P.C. Becker, and C.V. Shank. Evolution of the vibronic absorption spectrum in a molecule following impulsive excitation with a 6 fs optical pulse. *Chemical Physics Letters*, 160(2):101–104, 1989.

[83] Hideki Kandori, Klaus Kemnitz, and Keitaro Yoshihara. Subpicosecond transient absorption study of intermolecular electron transfer between solute and electron-donating solvents. *The Journal of Physical Chemistry*, 96(20):8042–8048, 1992.

[84] Tiago Buckup, Jürgen Hauer, and Marcus Motzkus. On the paradigm of coherent control: the phase-dependent light-matter interaction in the shaping window. *New Journal of Physics*, 11(10):105049–105059, 2009.

[85] D. Zeidler, S. Frey, W. Wohlleben, M. Motzkus, F. Busch, T. Chen, W. Kiefer, and A. Materny. Optimal control of ground-state dynamics in polymers. *The Journal of Chemical Physics*, 116(12):5231–5235, 2002.

[86] Wendel Wohlleben, Tiago Buckup, Jennifer L Herek, Richard J Cogdell, and Marcus Motzkus. Multichannel carotenoid deactivation in photosynthetic light harvesting as identified by an evolutionary target analysis. *Biophysical Journal*, 85(1):442–450, 2003.

[87] Ivo H.M. van Stokkum, Delmar S. Larsen, and Rienk van Grondelle. Global and target analysis of time-resolved spectra. *Biochimica et Biophysica Acta (BBA) - Bioenergetics*, 1657(2-3):82–104, 2004.

[88] Rudi Berera, Rienk van Grondelle, and John T M Kennis. Ultrafast transient absorption spectroscopy: principles and application to photosynthetic systems. *Photosynthesis Research*, 101(2-3):105–118, 2009.

[89] Andrei K. Dioumaev. Evaluation of intrinsic chemical kinetics and transient product spectra from time-resolved spectroscopic data. *Biophysical Chemistry*, 67:1–25, 1997.

[90] Jens U. Engelhart, Benjamin D. Lindner, Olena Tverskoy, Frank Rominger, and Uwe H. F. Bunz. Pd-catalyzed coupling of non-activated dibromoarenes to 2,3-diaminoarenes: Formation of n,n'-dihydropyrazines. *Chemistry A European Journal*, 19(45):15089–15092, 2013.

[91] Brian J. Walker, Andrew J. Musser, David Beljonne, and Richard H. Friend. Singlet exciton fission in solution. *Nature Chemistry*, 5(12):1019–1024, 2013.

[92] Anthony J. Zucchero, Psaras L. McGrier, and Uwe H. F. Bunz. Cross-conjugated cruciform fluorophores. *Accounts of Chemical Research*, 43(3):397–408, 2010.

[93] Uwe H. F. Bunz. The larger linear n-heteroacenes. *Accounts of Chemical Research*, 2015, ASAP.

[94] Frank C. Spano. The spectral signatures of frenkel polarons in h- and j-aggregates. *Accounts of Chemical Research*, 43(3):429–439, 2010.

[95] H. Yamagata, J. Norton, E. Hontz, Y. Olivier, D. Beljonne, J. L. Brédas, R. J. Silbey, and F. C. Spano. The nature of singlet excitons in oligoacene molecular crystals. *The Journal of Chemical Physics*, 134(20):204703–204714, 2011.

[96] Andrew D. Platt, Jonathan Day, Sankar Subramanian, John E. Anthony, and Oksana Ostroverkhova. Optical, fluorescent, and (photo)conductive properties of high-performance functionalized pentacene and anthradithiophene derivatives. *The Journal of Physical Chemistry C*, 113(31):14006–14014, 2009.

[97] J. Cornil, D. Beljonne, J.-P. Calbert, and J.-L. Bredas. Interchain interactions in organic-conjugated materials: Impact on electronic structure, optical response, and charge transport. *Advanced Materials*, 13(14):1053–1067, 2001.

[98] *Fabian Paulus, personal communication, Heidelberg University*, 2015.

[99] Sung Kyu Park, Thomas N. Jackson, John E. Anthony, and Devin A. Mourey. High mobility solution processed 6,13-bis(triisopropyl-silylethynyl) pentacene organic thin film transistors. *Applied Physics Letters*, 91(6):063514–063517, 2007.

[100] Yohann Nicolas, Frédéric Castet, Mélanie Devynck, Pascal Tardy, Lionel Hirsch, Christine Labrugère, Hassan Allouchi, and Thierry Toupance. Tips-triphenodioxazine versus tips-pentacene: Enhanced electron mobility for n-type organic field-effect transistors. *Organic Electronics*, 13(8):1392–1400, 2012.

[101] Charusheela Ramanan, Amanda L. Smeigh, John E. Anthony, Tobin J. Marks, and Michael R. Wasielewski. Competition between singlet fission and charge separation in solution-processed blend films of 6,13-bis(triisopropylsilylethynyl)pentacene with sterically-encumbered perylene-3,4:9,10-bis(dicarboximide)s. *Journal of the American Chemical Society*, 134:386–397, 2012.

[102] J.R. Lakowicz. *Principles of Fluorescence Spectroscopy*. Springer, Berlin, third edition, 2006.

[103] A. Bakulin, S.E. Morgan, J. Alster, D. Egorova, A. Chin, D. Zigmatas, and A. Rao. Vibrational coherence reveals the role of dark multiexci-

ton states in ultrafast singlet exciton fission. In Springer Proceedings in Physics 162, editor, *Ultrafast Phenomena XIX*, volume 19, pages 226–229. Optical Society of America, 2014.

[104] Raffaele Guido Della Valle, Elisabetta Venuti, Luca Farina, Aldo Brillante, Matteo Masino, and Alberto Girlando. Intramolecular and low-frequency intermolecular vibrations of pentacene polymorphs as a function of temperature. *The Journal of Physical Chemistry B*, 108(6):1822–1826, 2004.

[105] Alaska Subedi and Lilia Boeri. Vibrational spectrum and electron-phonon coupling of doped solid picene from first principles. *Physical Review B*, 84:02050–02058, 2011.

[106] Thomas M. Halasinski, Douglas M. Hudgins, Farid Salama, Louis J. Allamandola, and Thomas Bally. Electronic absorption spectra of neutral pentacene (c22h14) and its positive and negative ions in ne, ar, and kr matrices. *The Journal of Physical Chemistry A*, 104(32):7484–7491, 2000.

[107] Julia Herz, Tiago Buckup, Fabian Paulus, Jens Engelhart, Uwe H. F. Bunz, and Marcus Motzkus. Acceleration of singlet fission in an aza-derivative of tips-pentacene. *The Journal of Physical Chemistry Letters*, 5(14):2425–2430, 2014.

[108] Yishi Wu, Ke Liu, Huiying Liu, Yi Zhang, Haoli Zhang, Jiannian Yao, and Hongbing Fu. Impact of intermolecular distance on singlet fission in a series of tips pentacene compounds. *The Journal of Physical Chemistry Letters*, 5(20):3451–3455, 2014.

[109] Sean T. Roberts, R. Eric McAnally, Joseph N. Mastron, David H. Webber, Matthew T. Whited, Richard L. Brutchey, Mark E. Thompson, and Stephen E. Bradforth. Efficient singlet fission discovered in a disordered acene film. *Journal of the American Chemical Society*, 134(14):6388–6400, 2012.

[110] Lin Ma, Keke Zhang, Christian Kloc, Handong Sun, Maria E. Michel-Beyerle, and Gagik G. Gurzadyan. Singlet fission in rubrene single crystal: direct observation by femtosecond pump-probe spectroscopy. *Physical Chemistry Chemical Physics*, 14:8307–8312, 2012.

[111] Akshay Rao, Mark W. B. Wilson, Sebastian Albert-Seifried, Riccardo Di Pietro, and Richard H. Friend. Photophysics of pentacene thin films: The role of exciton fission and heating effects. *Physical Review B*, 84:195411–195419, 2011.

[112] A. Suna. Kinematics of exciton-exciton annihilation in molecular crystals. *Physical Review B*, 1:1716–1739, 1970.

[113] Andrey D. Poletayev, Jenny Clark, Mark W. B. Wilson, Akshay Rao, Yoshitaka Makino, Shu Hotta, and Richard H. Friend. Triplet dynamics in pentacene crystals: Applications to fission-sensitized photovoltaics. *Advanced Materials*, 26(6):919–924, 2014.

[114] Volkhard May. Kinetic theory of exciton-exciton annihilation. *The Journal of Chemical Physics*, 140(5):054103–054110, 2014.

[115] Julia Herz, Tiago Buckup, Fabian Paulus, Jens U. Engelhart, Uwe H. F. Bunz, and Marcus Motzkus. Unveiling singlet fission mediating states in tips-pentacene and its aza-derivatives. *The Journal of Physical Chemistry A*, 2015, just accepted.

[116] Mathias Pabst and Andreas Köhn. Implementation of transition moments between excited states in the approximate coupled-cluster singles and doubles model. *The Journal of Chemical Physics*, 129(21):214101–214112, 2008.

[117] Linjun Wang, Yoann Olivier, Oleg V. Prezhdo, and David Beljonne. Maximizing singlet fission by intermolecular packing. *The Journal of Physical Chemistry Letters*, 5(19):3345–3353, 2014.

[118] Wai-Lun Chan, Timothy C. Berkelbach, Makenzie R. Provorse, Nicholas R. Monahan, John R. Tritsch, Mark S. Hybertsen, David R.

Reichman, Jiali Gao, and X.-Y. Zhu. The quantum coherent mechanism for singlet fission: Experiment and theory. *Accounts of Chemical Research*, 46(6):1321–1329, 2013.

[119] Franz Milota, Valentyn I. Prokhorenko, Tomas Mancal, Hans von Berlepsch, Oliver Bixner, Harald F. Kauffmann, and Jürgen Hauer. Vibronic and vibrational coherences in two-dimensional electronic spectra of supramolecular j-aggregates. *The Journal of Physical Chemistry A*, 117(29):6007–6014, 2013.

[120] Tiago Buckup and Marcus Motzkus. Multidimensional time-resolved spectroscopy of vibrational coherence in biopolyenes. *Annual Review of Physical Chemistry*, 65(1):39–57, 2014.

[121] Yuhan Chen, Li Shen, and Xiyou Li. Effects of heteroatoms of tetracene and pentacene derivatives on their stability and singlet fission. *The Journal of Physical Chemistry A*, 118(30):5700–5708, 2014.

[122] Benjamin D. Lindner, Fabian Paulus, Anthony L. Appleton, Manuel Schaffroth, Jens U. Engelhart, Korwin M. Schelkle, Olena Tverskoy, Frank Rominger, Manuel Hamburger, and Uwe H. F. Bunz. Electron-transporting phenazinothiadiazoles with engineered microstructure. *Journal of Materials Chemistry C*, 2:9609–9612, 2014.

[123] David T. James, Jarvist M. Frost, Jessica Wade, Jenny Nelson, and Ji-Seon Kim. Controlling microstructure of pentacene derivatives by solution processing: Impact of structural anisotropy on optoelectronic properties. *ACS Nano*, 7(9):7983–7991, 2013.

[124] Ajay Ram Srimath Kandada, Annamaria Petrozza, and Guglielmo Lanzani. Ultrafast dissociation of triplets in pentacene induced by an electric field. *Physical Review B*, 90:075310–075315, 2014.

[125] Yana Vaynzof, Artem A. Bakulin, Simon Gélinas, and Richard H. Friend. Direct observation of photoinduced bound charge-pair states at

an organic-inorganic semiconductor interface. *Physical Review Letters*, 108:246605–246610, 2012.

[126] R. W. Boyd. *Nonlinear Optics*. Academic Press, Elsevier, third edition, 2008.

[127] M. Teich B. Saleh. *Grundlagen der Photonik, Lehrbuch der Physik*. Wiley-VHC, Weinheim, 2008.

[128] N. Bloembergen. *Nonlinear Optics*. World Scientific Pub Co Inc, fourth edition, 1996.

[129] F. Träger, editor. *The Springer Handbook of Lasers and Optics*. Springer-Verlag Berlin Heidelberg, second edition, 2012.

Appendix

Nonlinear Optics

In the follwing the basic concepts of nonlinear optics are presented and for further details please refer to literature.[21, 126–129]

Since broadband femtosecond light sources are not tunable over the whole visible spectral region, specific optical processes are required in order to generate wavelengths that are essential for exciting selected absorption bands of conjugated systems. These nonlinear effects can be described by the nonlinear polarization. At high field strengths such as provided by lasers the dielectric polarization, which describes the charge displacements within a media, does not respond linearly to the electric field. Therefore higher order terms of the dielectric polarization have to be considered, which gives rise to new frequencies. The nonlinear polarization is defined as:

$$\vec{P} = \epsilon_0 \sum_n \chi^{(n)} \vec{E}^n = \epsilon_0 \left[\chi^{(1)} \vec{E} + \chi^{(2)} \vec{E}^2 + \chi^{(3)} \vec{E}^3 + ... \right] \qquad (6.1)$$

where ϵ_0 is the electric field constant, $\vec{E}$ the electrical field of the wave and $\chi^{(n)}$ are the nth order susceptibilities.

In the following, nonlinear optical phenomena, which are fundamental for the realization of time resolved experiments, are described in more detail. To begin with, in all nonlinear processes conservation of energy has to be fulfilled, according to:

$$\sum \omega_{in} = \sum \omega_{out} \qquad (6.2)$$

143

Likewise also the spatial dependence of the incoming and created waves have to be considered. The momentum of a photon is given by its wave vector $\vec{k}$. The nonlinear process is most efficient if there is constructive interference between the waves (waves have to be in phase while propagating through the media). The resulting phase matching condition is given by:

$$\Delta\vec{k} = \sum \vec{k}_{out} - \sum \vec{k}_{in} = 0 \tag{6.3}$$
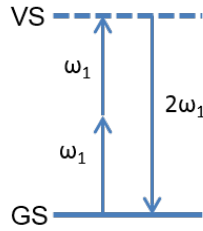
Second Harmonic Generation (SHG)

Figure A1: Schematic representation of the second order nonlinear effect SHG. GS=ground state, VS=virtual state

In SHG, a pump wave of the frequency ω generates a signal with twice the frequency 2ω as it propagates through a nonlinear medium. Since all even-order susceptibilities cancel out in centrosymmetric media, SHG as a second order nonlinear effect can only occur in materials without inversion symmetry. The phase matching condition represents conservation of momentum for the SHG process, when the two photons travel at the same velocity. Since all materials are dispersive, the waves actually travel with different velocities corresponding to different refractive indices n(ω). In other words, $\Delta\vec{k} = 2k_1 - k_2$ is the wave-vector mismatch for the SHG process. A way to circumvent this phase matching problem is the use of birefringent nonlinear crystals, in this case *beta*-Barium-borate (BBO), which can compensate for dispersion. In an uniaxial crystal like BBO the values of the refractive indices depend differently on the directions of the waves relative to the optical axis.

144

By choosing the right angle between the optical axis and propagation of the wave, phase-matching can be achieved, what is illustrated in Figure A2.
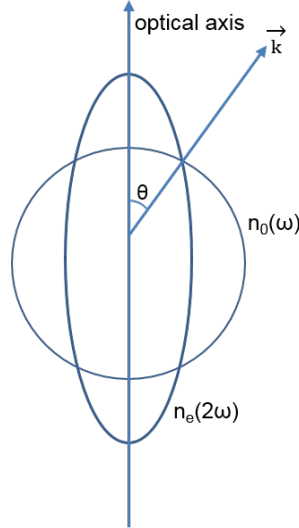

Figure A2: Phase-matching in SHG in a birefringent crystal. Due to dispersion, the in- and outgoing waves exhibit different indices of refraction. At the angle θ, the dispersion is exactly compensated and the phase-machting condition is fullfilled.

In type I SHG, as used within this work, the pump wave has ordinary polarization with respect to the crystal, while the outgoing wave at the frequency of the second harmonic exhibits extraordinary polarization. The circle in Figure A2 represents the cross section of the refractive-index sphere $n_0(\omega)$ for an ordinary wave at the pump frequency ω and accordingly, n_0 is independent of the direction of propagation of the wave. The ellipse is the cross section of the refractive-index ellipsoid $n_e(2\omega)$ for an extraordinary wave at the frequency of the second harmonic 2ω, which is dependent on the direction of propagation of the wave. Phase-matching is achieved when $n_0(\omega)=n_e(2\omega)$, corresponding to an angle θ with respect to the optical axis of the crystal. By tuning the crystal orientation relative to the incoming beam, the optimal efficiency of SHG can be achieved. The SHG intensity grows as a function of the length L of the nonlinear medium, as long as it remains much less than the pump intensity. The entire pump energy can be transferred to the SHG

145

and as the pump field becomes depleted, the SHG field is saturated. Due to fact that the waves travel with different velocities through the crystal (walk-off between pump and SHG), group velocity mismatch becomes apparent when the length of the crystals exceeds this walk-off, which is dependent on the pulse width of the pump field. When L is a lot larger than the walk-off, the SHG pulse width scales linearly with the the length of the crystal and becomes independent of the pump pulse width.

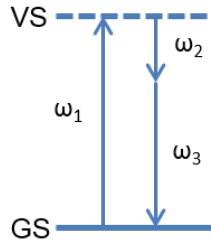## Noncollinear Optical Parametric Amplifier (nc-OPA)

Figure A3: Schematic representation of the optical parametric amplification. GS=ground state, VS=virtual state

The OPA process allows for the amplification of a seed beam by overlapping it with a strong pump field within a nonlinear crystal in order to create specific wavelengths at adequate intensities. In a general picture (see Figure A3), a pump pulse excites the crystal into a virtual level and the instantaneous decay back to the ground state results in two beams of lower frequencies with the requirement $\omega_1 = \omega_2 + \omega_3$. A weak input field referred to as signal field ω_2 becomes amplified by a nonlinear interaction with a powerful pump field ω_1. Additionally, an idler wave ω_3 with complementary wavelength is created, according to conservation of energy. In OPA, the signal and idler photons usually travel collinearly through a nonlinear optical crystal and phase-matching is required for the process to work well. Since the refractive indices of signal and idler are different, the phase-matching condition cannot be achieved by the crystal angle only. Noncollinear OPAs (nc-OPAs) have

been developed to have an additional degree of freedom and phase-matching is also determined by the angle between the two beams.[70–73] Optimal amplification is achieved when $\Delta \vec{k}$ is close to zero and group velocity mismatch is minimal. This process allows for ultrashort pulses to be amplified at high intensities and is of particular significance as it offers the possibility to generate intense coherent radiation in the infrared range. Signal and idler can cover a wide wavelength range and thus they find application as pump and probe beams in time-resolved techniques.
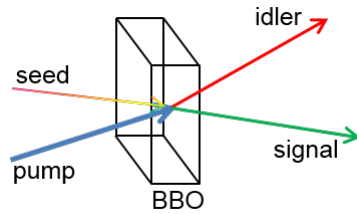

Figure A4: Schematic representation of the nc-OPA process using a BBO crystal. The pump beam has a specific angle with respect to the seed beam, which is a white light continuum. The direction of the signal beam is determined by the seed-pulse. If the signal beam is generated in the visible spectral range using a 400 nm pump pulse, the respective idler beam is in the infrared region in order to fulfill energy conservation.

As shown in Figure A4, the pump field is superimposed by a seed field in the BBO crystal and thus, the seed gets amplified. Within this work, a white light continuum is used as seed field in order to generate broadband pulses. After passing the BBO crystal of the nc-OPA, the created beam is lengthened and possesses a positive (red precedes blue wavelengths) chirp, that is mostly linear due to the white light. Linear chirp can be compensated by means of a prism compressor, reducing the pulse length to its original. This is based on the fact that angular dispersion introduces negative chirp, hence it can compensate for positive chirp. The beam travels in total four times through the material, to eliminate all other spatio-temporal distortions (see Figure A5). Within this work, a two-prism compressor was used with a mirror, which sends the beam exactly the same way back in order to simplify the alignment.

The chirp of a special wavelength can be compensated by moving the prism into or out of the beam, i.e. introducing more or less glass. Additionally, the distance between the two prisms can be changed. Higher order chirp cannot be compensated by a prism compressor and more sophisticated methods are required involving, for example spatial light modulators.
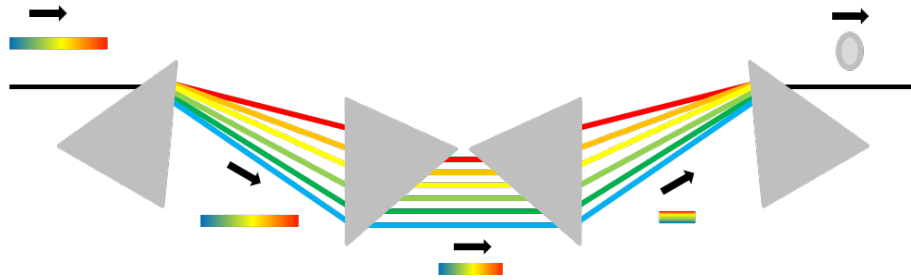

Figure A5: Principle of a prism compressor to compensate positive chirp. In total, the beam has to travel four times through the prisms to compensate all distortions. Please note that within this study, a two prism-compressor in combination with a mirror is used.

Cross-Phase Modulation (XPM)

XPM is a third-order nonlinear process and a result of an optical interaction of at least two physically distinguishable light pulses with, for example different frequencies. This effect is based on the fact that one pulse (probe pulse) experiences a phase modulation due to the change in the refractive index n of a material induced by an intensive second pulse (pump pulse). The cross-action of the pump with ω_1 on a probe pulse with ω_2 leads to a nonlinear phase shift of the latter. This phase shift causes a frequency shift of the probe pulse. The leading edge shifts to lower frequencies while the trailing edge shifts to higher frequencies as a function of the change in pump intensity. This effect is similar to self-phase modulation, where the change of the refractive index is induced by the beam itself as a result of the optical Kerr effect (as the pump beam in XPM). The generated frequencies broaden the spectrum leading to higher spectral bandwidths, which is the key condition for the generation of a supercontinuum. In experiments dispersion

effects appear, which means that not all of the wavelengths have the same velocity while traveling through a medium. In glass substrates, for example, the lower frequencies have a higher velocity than the counterparts of higher energy referred to as positive chirp. The front of the pulse moves faster than the back and accordingly the spectrum is broadened in time. XPM becomes higher with increasing chirp of the probe pulse, which is manifested in the large coherent spike in the transient absorption data.

Danksagung

Mein besonderer Dank richtet sich an Prof. Dr. Marcus Motzkus, der mir die Möglichkeit zu einer Dissertation in seiner Arbeitsgruppe gab. Nur durch sein mir entgegengebrachtes Vertrauen konnte ich das Themengebiet der organischen Elektronik vorantreiben und darüber hinaus neue, spannende Einblicke in den Bereich der organischen Solarzellen gewinnen. Ich konnte stets auf seine wissenschaftliche Erfahrung bauen und über die Teilnahme an der Gordon Tagung in der Toscana, die mir große Freude bereitete, bin ich sehr dankbar. Außerdem möchte ich mich für die hervorrangende experimentelle Ausstattung in den Laboren bedanken, die mich schon von Anfang an stark beeindruckte. Die während meiner Doktorarbeit erlernten Fähigkeiten gehen weit über das Fachliche hinaus und werden auch meine persönliche Zukunft bereichern.

Weiterhin möchte ich Herrn Prof. Dr. Uwe H.F. Bunz nicht nur für die Übernahme des Zweitgutachtens, sondern auch für seine immer ehrliche, lustige und überaus menschliche Art danken. Hierdurch konnte ich sehen, wie vielfältig sich Laborleben abspielen können. Ich konnte mich immer auf seine kritische Meinung verlassen und darüber hinaus auf seine Unterstützung bezüglich neuer Proben.

Für die wissenschaftliche Unterstützung dieser Arbeit möchte ich besonders Herrn Dr. Tiago Buckup danken. Er hatte stets neue Ideen und seine Tür stand für Diskussionen immer offen. Ich konnte mich auf seine Hilfe verlassen, sei es im Labor mit der Elektronik oder beim Verfassen von Publikationen.

Dr. Jens Engelhart möchte ich für seine Synthesekunst danken und Fabian Paulus für die zahlreichen Filme. Wann immer ich anrief, lief der spincoater quasi schon warm. Vielen Dank für die gute Zusammenarbeit, es hat mir großen Spaß gemacht, mit euch zu kollaborieren!

Prof. Yana Yaynzof danke ich für die tolle Kooperation, die schon erste Früchte trägt. Ich bin froh, dass ich in diesem interessanten Themengebiet mitwirken konnte. An dieser Stelle möchte ich auch meine Bachelorstudenten Jannis Koch und Maximilian Krings erwähnen, die mit vollem Einsatz an meiner Forschung mitwirkten.

Für die freundliche Aufnahme in die Arbeitsgruppe möchte ich Dr. Alexander Wipfler, Dr. Jean Rehbinder, Dr. Christoph Pohling, Dr. Jan-Philip Kraack, Dzmitry Starukhin, Dr. Marie Krause und Dr. Jens Möhring danken. Hieraus sind Freundschaften entstanden, die ich nicht mehr missen möchte. Es freut mich sehr, dass uns die teilweise großen Entfernungen nichts anhaben können. Bei Marie, Dzmitry und Philip möchte ich mich für die experimentelle Hilfe im Labor 152 zu Beginn meiner Zeit in Heidelberg bedanken. Besonders danke ich Alex, mit dem ich die ersten zwei Jahre das Büro teilen durfte und der mir bei einigen LabVIEW-Problemen brereitwillig zur Seite stand. Vielen Dank für die schöne Zeit bei diversen Heißgetränken, lehrreichen Gesprächen und vielen lustigen, auch musikalischen Abenden.

Die Veränderung der Arbeitsgruppe mit Takeshi Miki, Lukas Brückner, Jiang Man, Elisabeth Brühl und Ellen Bruce sorgte für frischen Wind und viele neue Forschungsprojekte. Jj, dir danke ich für dein wunderbares Wesen und die vielen ernsten, aber auch witzigen Gespräche neben dem Laboralltag. Ich bin mir sicher, dass Du eine hervorragende Arbeit abgeben wirst. Takeshi möchte ich für seine große Hilfsbereitschaft, Ehrlichkeit und sein positives Gemüt danken und dafür, dass das Chemielabor stets mit allem ausgestattet war. Elisabeth ist eine große Bereicherung für die Arbeitsgruppe und man kann sich immer auf sie und ihre konstruktiven Einfälle verlassen.

Lukas danke ich für seinen unermüdlichen Humor und seine grandiosen Sprüche, die leider nicht jeder versteht. Auch danke ich ihm für seinen Scharfsinn, seine pragmatische Art und sein gewinnendes Wesen, das es immer wieder schafft, mich zu erden.

Prof. Dr. Hans-Robert Volpp möchte ich für seine Hilfsbereitschaft danken, sei es im wissenschaftlichen Sinne, oder während des Bewerbungsprozesses. Auch danke ich ihm für seine Ausgelassenheit und seinen unschlagbaren Frohsinn, der so einige Party bereichert hat. Dr. Thomas Kriesche danke ich für diverse AFM Messungen, ich sage nur "du mit deinen furchtbaren Proben" und "das habe ich in fünf Jahren nicht geschafft".

Sylvia Boganski danke ich für ihre Unterstützung, sowohl auf persönlicher Ebene als auch bezüglich meines Doktorandenvertrags. Ihre Hilfsbereitschaft und außerordentliche Organisationsfähigkeit schätzte ich während meiner gesamten Zeit in Heidelberg sehr und unsere Diskussionen über "fleischfressende Ungeheuer" werde ich vermissen!

Der feinmechanischen Werkstatt danke ich für die gute Zusammenarbeit. Die Konstruktion der rotierbaren Halterung mit Herrn Schmitt und seinem Team war mir eine große Freude.

Meinen sehr guten Freunden Dr. Mirka-Kristin Neumann-Verhoefen, Dr. Karsten Neumann, Dr. Nina Scheich und Dr. Heike Staudt aus Frankfurter Unizeiten danke ich von ganzem Herzen für ihre Unterstützung. Ihr habt mich in die Wissenschaft geleitet und ich wäre heute nicht dort, wo ich jetzt bin. Ich bin sehr froh, dass es euch gibt!

Meiner Familie danke ich für die vielseite Unterstützung während meiner kompletten Studienzeit. Meine Mutter hielt mir stets den Rücken frei, versorgte mich mit mehr als nötig war und vertraute in mich und meine Fähigkeiten. Die Erweiterung unserer Familie mit Tom und Pia erfüllt mich mit größter Freude und ich bin überglücklich, wann immer ich sie um mich habe.

Eidesstattliche Erklärung

Bei der vorliegenden Dissertation handelt es sich um meine eigenständig erbrachte Leistung. Ich habe nur die angegebenen Quellen und Hilfsmittel benutzt und mich keiner unzulässigen Hilfe Dritter bedient. Insbesondere habe ich wörtlich oder sinngemäß aus anderen Werken übernommene Inhalte als solche kenntlich gemacht.

Heidelberg, den 11. Juni 2015

Julia Herz